Univerzita Karlova v Praze
Matematicko-fyzikální fakulta

# DIPLOMOVÁ PRÁCE

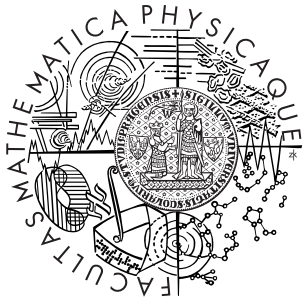


Miroslav Frost

## Elastické vlastnosti cévy vyztužené mechanickou cévní náhradou

Matematický ústav UK

Vedoucí diplomové práce: Prof. Ing. František Maršík, DrSc.

Studijní program: Matematika, matematické a počítačové modelování ve fyzice a v technice

2007

V důsledku naléhavé potřeby řešit problémy související s modelováním elastických vlastností materiálů s tvarovou pamětí dříve, než se přistoupí k aplikacím, soustředí se tato práce na popis a modelování elastických a paměťových vlastností těchto materiálů. Vedle výstuhy cévních náhrad jsou materiály s tvarovou pamětí využívány např. jako prvky aktivního tlumení lopatek větrných elektráren. Větší část práce byla vypracována ve spolupráci s Ústavem termomechniky AV ČR, v.v.i., kde je jak problematika termomechanických vlastností materiálů s tvarovou pamětí tak i jejich aplikací řešena v rámci mezinárodního projektu MULTIMAT a projektů GA ČR a MŠMT ČR.

Rád bych poděkoval svému vedoucímu, Prof. Ing. Františku Maršíkovi, DrSc., a konzultantovi, Ing. Petru Sedlákovi, za rady a připomínky, které výrazně přispěly k výsledné podobě této práce. Druhému jmenovanému také děkuji za poskytnutí výsledků srovnání modelu s experimenty. Tyto experimenty provedli Ing. Jan Pilch a Audrey Kujawa – i jim patří můj dík. V neposlední řadě bych též rád poděkoval své rodině a přátelům za podporu, které se mi dostávalo po celou dobu studia.

Prohlašuji, že jsem svou diplomovou práci napsal samostatně a výhradně s použitím citovaných pramenů. Souhlasím se zapůjčováním práce a jejím zveřejňováním.

V Praze dne 10. srpna 2007 Miroslav Frost

# Contents

Název práce: Elastické vlastnosti cévy vyztužené mechanickou cévní náhradou
Autor: Miroslav Frost
Katedra: Matematický ústav Univerzity Karlovy
Vedoucí diplomové práce: Prof. Ing. František Maršík, DrSc.
E-mail vedoucího: marsik@it.cas.cz

Abstrakt: Předložená práce se zabývá modelováním chování NiTiNOLového drátu podrobeného jednoosému tepelně-mechanickému namáhání. NiTiNOL, patřící díky reverzibilní martenzitické fázové transformaci (MT) mezi materiály s tvarovou pamětí, je ve formě tenkých drátů používán v mnoha aplikacích (mj. jako výstuha cévních náhrad).

MT je studována z hlediska rozšířené nerovnovážné termodynamiky směsí a je pro ni odvozena Clausiova-Clapeyronova rovnice. Matematicky je formulován nový fenomenologický model iRLOOP vyvinutý v AV ČR, který simuluje chování drátu z NiTiNOLu při tepelně-mechanickém zatěžování. Pro fitovací funkce v navrženém hysterezním mechanizmu jsou odvozena omezení plynoucí ze druhého zákona termodynamiky. Pro superelastickou variantu modelu je ukázána existence a jednoznačnost řešení počáteční úlohy. Numerická implementace do programovacího prostředí MATLAB umožnila porovnat výsledky modelu s experimenty.

Klíčová slova: materiály s tvarovou pamětí; modelování jevů tvarové paměti; rozšířená nerovnovážná termodynamika; martenzitická fázová transformace.

Title: Elastic properties of blood veins with a scaffold
Author: Miroslav Frost
Department: Mathematical Institute of Charles University
Supervisor: Prof. Ing. František Maršík, DrSc.
Supervisor's e-mail address: marsik@it.cas.cz

Abstract: Presented master's thesis deals with modeling of a NiTiNOL wire under thermal and uniaxial mechanical loading. NiTiNOL can undergo reversible martensitic phase transformation and thus belongs among shape memory alloys. In the form of a thin wire it is used in many applications (e.g. as a reinforcement for veins).

MT is studied with respect to the extended non-equilibrium thermomechanics of mixtures and the Clusius-Clapeyron equation is derived for it. A new phenomenological model iRLOOP, developed at AS CR, simulating thermomechanical behavior of a NiTiNOL wire is mathematically formulated. Restrictions on fitting functions in proposed hysteresis mechanism are derived from the second law of thermodynamics. The existence and uniqueness of the solution of an initial problem are proven for the superelasticity model. Experiments are compared with results modeled by numerical implementation of iRLOOP.

Keywords: Shape Memory Alloys; Modelling of Shape Memory Effects; Extended Non-Equilibrium Thermodynamics; Martensitic Phase Transformation.

# Chapter 1

# Introduction

Shape memory alloys (SMAs) have the unusual material property of being able to sustain and recover large strains (of the order of 10%) without inducing irreversible plastic deformation and to "remember" a previous configuration and return to it with a temperature change. These interesting material characteristics arise due to distinctive internal crystalline phase transformations with temperature and/or applied stress, thus can be studied within the extended non-equilibrium thermodynamics frame. The increasing number of investigations of SMAs in the past two decades reflects growing global interest in this type of material, which is promising from the wide range of possible applications point of view. The natural result is that modeling of shape memory effects (SMEs) is attractive both for physicists, who are interested in confirmation of proposed explanation of experimental results, and for engineers, demanding accurate prediction of SMAs behavior needed in new products development, and even for mathematicians, who often try to employ advanced mathematical tools to predict SMA behavior *ab initio*. This work deals with SMEs phenomenological modeling taking principles of thermodynamics into account.

In the next chapter the martensitic phase transition is introduced and shape memory effects extensively described. Some specific properties of NiTiNOL are also mentioned.

In the third chapter the basics of extended non-equilibrium thermodynamics with respect to martensitic phase transformation are formulated. The second law of thermodynamics is employed to obtain non-equilibrium entropy of mixtures and a constitutive relation for homogenous isotropic thermo-visco-elastic material is derived. Also, the Clausius-Clapeyron equation for a solid-to-solid martensitic phase transition is derived.

In the fourth chapter a brief overview of shape memory effects modelling approaches and the general thermodynamic framework for thermodynamics based models can be found. Some types of one-dimensional SMEs models and of models for hysteresis are also reviewed.

In the fifth chapter a new phenomenological model developed at the Academy of Sciences of the Czech Republic and called iRLOOP is introduced and mathematically formulated. The model was constructed gradually, each stage expanded the previous one.

First, superelastic behavior with R-phase contribution and return point memory effect were introduced to the "superelasticity model". Detailed description of computational mechanism is followed by derivation of restrictions on functions forming the major hysteresis loop (fitting functions of the model) in involved extended Duhem-Madelung model of hysteresis. These restrictions result from the second law of thermodynamics. Employing Picard-Lindelöf theorem the existence and uniqueness of the solution of an initial problem are proven for this model, too.

Next, pseudoplasticity, reorientation process and thus also one-way SME in tension were added to establish "pseudoplasticity model". The new features of this model and possible fitting procedure for material parameters are described and experimental results are compared with results of "pseudoplasticity model" implemented to MATLAB programming language.

So far the last stage – "thermomechanical model" – connects all previous effects and their interaction to complex tension-compression algorithm. This algorithm is just sketched, since it is still under construction.

In the last chapter conclusions of this thesis can be found.

# Chapter 2

# Basic Properties of Shape Memory Alloys

## 2.1 Martensitic Transformation

Intermetallic alloys exhibiting the unique shape memory effects (SMEs) are known as shape memory alloys (SMAs). Although these effects were firstly observed at Au-Cd alloy in 1951, the research has intensified after 1963, when the commercially most successful Ni-Ti-based shape memory alloys were discovered.

The key physical process for understanding of all shape memory effects, which are described in more detail in the next section, is the *martensitic phase transition* (MT). This first-order solid-to-solid phase transition from the parent phase, which is referred to as *austenite*, to the less-ordered product phase, *martensite*, is a typical example of so called *military transformation*. The mechanism of this type of transformation consists of a regular rearrangement of the lattice in such way that relative displacement of neighboring atoms does not exceed the interatomic distances and the atoms do not interchange places. This "shearing of the parent lattice into the product" is sometimes referred as *lattice-distortive* transition. The name emphasizes the analogy between the coordinated motion of atoms crossing the glissile interface between the parent and product phases and that of soldiers moving in ranks on the parade ground. (In contrast, the uncoordinated transfer of atoms across a non-glissile interface results in what is known as a civilian transformation.) That is why the interface between austenitic and martensitic phases reaches almost the speed of sound in the solid.

The martensitic transformation in most cases is nucleated heterogeneously by formation of thin plates of parent/product phase in the matrix of product/parent phase, at special defect sites in a SMA material, forming a two-phase austenite-martensite zone. The defects induce a strain field that facilitates the initiation of the transformation (lowers the energy barrier for nucleation). In a SMA polycrystalline body, the mechanism of martensite phase transformation is complicated by interaction of the walls of growing or shrinking martensite plates with the grain boundaries of the austenite matrix. The two principles determining MT were established by Kurdjumov [1]:

1. A martensitic transformation is a strain transformation, i.e. the lattice strain (also called self-strain) is a transformation parameter which determines physical state of an initial phase and a product phase. The self-strain in a more general case can include, in addition to the homogeneous strain, some kind of rearrangement or shuffling of lattice sites, provided that this shuffling is unambiguously related to the strain. (The free energy as a function of an uniform transformation strain is then a primary quantitative characteristic of martensitic transition determining its thermodynamics and kinetics.)

2. The coherency of a two-phase structure determines its evolution from an initial phase to a product phase.

Let us recall here the first-order phase transitions exhibit a discontinuity in the first derivative of the thermodynamic potential (e.g. free energy) with respect to the thermodynamic variable, e.g. a discontinuity in strain, in entropy (which is connected with the latent heat), etc.

In general, the martensitic transformation is *diffusionless* and *athermal*. It means the amount of martensite formed is a function only of the temperature and not of the length of time at which the alloy is held at that temperature. Athermal transformations start at well-defined temperatures, which are usually insensitive to rate-effects. Furthermore, in the case of SMA the MT is of *thermoelastic* type (in contrast to ferrous materials), which indicates:

1. The thermodynamic driving force for the phase transformation is rather small.

2. The domain walls are very mobile (small internal friction) and their motion is reversible.

3. The product phase stays coherent with the parent phase (the displacement field is continuous).

These properties imply that no plastic flow is generated during the transformation, the transformation is fully reversible – therefore SMA products can undergo a great number of transformation cycles almost without any fatigue – and dissipation of energy during transformation is quite small. Energy dissipation, although small, is responsible for *hysteretic properties* of SMA and therefore plays an important role in the process of transformation. The essential contributions to the energy dissipation are associated with interfacial friction, defect production and acoustic emission caused by nucleation and growth of martensite plates and interactions between them during transformation [2]. Further metallurgical aspects of MT (as detailed description of martensite nucleation and growth or stabilization) can be found, for instance, in [3].

The MT can be driven by temperature or by changing external stresses or by simultaneous change of stresses and temperature. The temperature induced transformation proceeds by formation, expansion and migration of a two-phase zone from cooled or heated boundaries. In a SMA polycrystalline body the stress induced transformation

can be driven by shear loading or by tension or compression, since even a simple uniaxial loading induces a complex 3-D microstress field with nonzero shear component in individual grains of polycrystalline body due to its inhomogeneous structure. The shift of the two-phase equilibrium under stress results not only in the change of quantity of a martensite phase but also in the change of the variant fractions in it.

If there is no preferred direction for the occurrence of the transformation, the martensite takes advantage of the existence of different possible ordering, forming a series of crystallographically equivalent variants. The product phase growing to a platelet shape is then termed *multiple-variant martensite* and is characterized by a twinned microstructure, which minimizes the misfit between the martensite and surrounding austenite. On the other hand, if there is a preferred direction for the occurrence of transformation (e.g. imposed stress), all the martensitic crystals tend to be formed to the most favorable variant. The product phase is termed *fully oriented martensite*[1] and is characterized by a *detwinned* structure, which again minimizes the misfit between the martensite and the surrounding austenite. Moreover, the conversion of each variant of martensite into different single variant is possible. Such process is known as *reorientation process*. Two effects determine the change of the martensitic variants fraction during stress induced processes:

- selection of martensite plates with preferable orientation with respect to the external stress,
- increase of fraction of the preferable variants in a martensite plates.

From a crystallographic point of view, in general SMA parent phases have superlattice body-centered cubic structures and are classified as $\beta$-phase alloys. The martensite crystals obtained from $\beta$-phase austenite are indicated as $\beta'$ and have periodic stacking order structures. Since in the martensite atoms of different radii are packed without any symmetry, the super-lattice structure tends to deform slightly, resulting in a typical monoclinic configuration. Depending on alloy, upon cooling and before the formation of martensite, slight crystallographic changes, such a small lattice distortion, might be observed. These intermediate phases are often termed *pre-martensitic phases*. In some SMAs, structure of the martensitic lattice can slightly change when changing temperature or stress which leads to forming *intermartensitic phases*. Usually, the maximum amount of recoverable strain and the hysteresis loop in these cases are small compared to the ones associated with the full martensitic transition.

In the last decade the magnetic shape memory alloys, where MT is induced by temperature, stress and even external magnetic field change, were developed and intensively studied. Probably the most promising are Ni-Mn-Ga-based magnetic SMAs (see e.g. [4]).

[1] more often, but less precise termed *single-variant martensite* in the literature

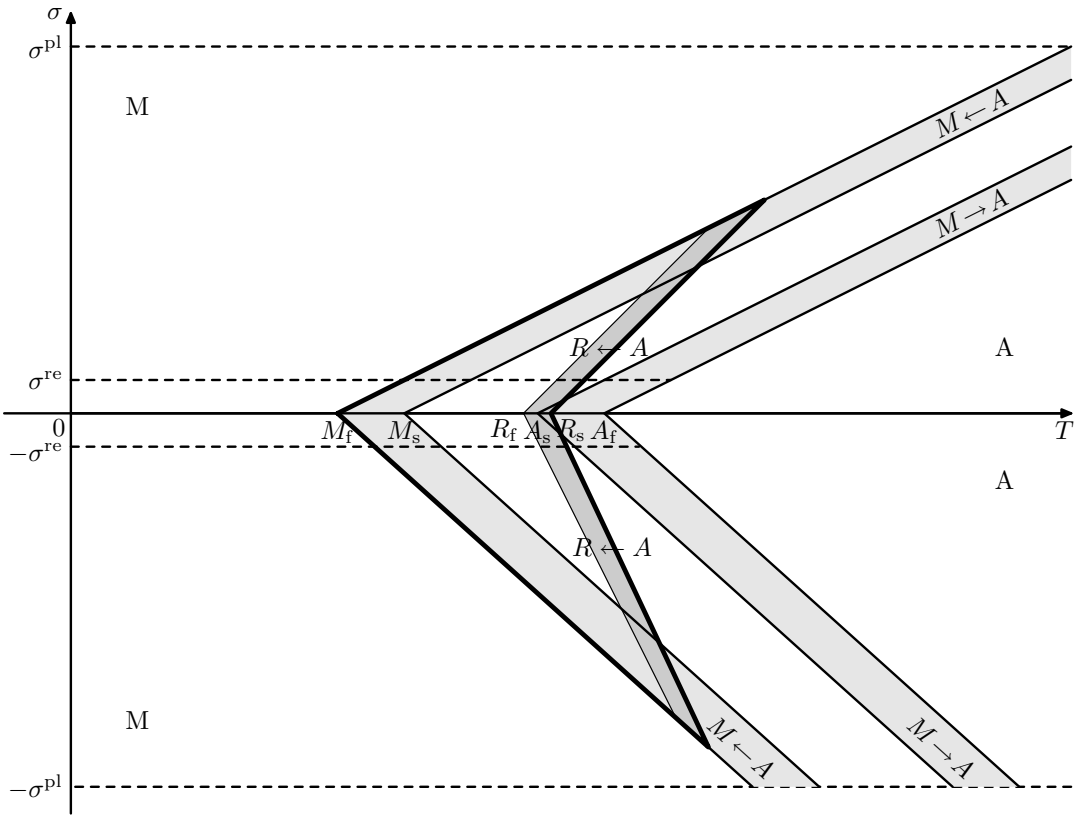


Figure 2.1: Stress-temperature space. Area where austenite/martensite exists denoted by 'A'/'M', area where R-phase can occur contoured with thick line, transformation strips marked with grey color.

## 2.2 Shape Memory Effects

For better understanding of shape memory effects, let us restrict ourselves to complex thermal and one-dimensional mechanical loading of a SMA specimen, which has been very well experimentally examined and explained in many previous works (for NiTiNOL see the comprehensive paper [5] and the references cited therein, for instance) and is sufficient with respect to one-dimensional thin wires modelling studied in this work.

The activation of martensitic transformation occurs due to the presence of driving forces, either thermal or kinetic. To initiate a transformation, the chemical free energy difference between the parent and product phases must be greater than the necessary free energy barriers, such as transformational strain energy or interface energy. For the determination of when transformations initiate, the space parameterized by stress, $\sigma$, and temperature, $T$, is commonly used, since the thermodynamic driving force depends only on stress and temperature in a very good approximation. The stress-temperature ($\sigma$-$T$) space is referred to as the phase space and is depicted in figure 2.1.

In the figure the transformation temperatures $M_s$, $M_f$, $A_s$ and $A_f$ indicate the start and finish temperatures at zero stress for martensite and austenite production, respectively. $\sigma^{re}$ and $-\sigma^{re}$ denote the critical finish stresses of martensite reorientation processes, $\sigma^{pl}$ ($-\sigma^{pl}$) indicate the values of stress above (under) which plastic slip will occur.

Depending upon the path taken within the phase space, certain characteristic features of the stress-strain response will manifest themselves. If austenite is cooled from above $A_f$ to below $M_f$ at zero stress, the resulting effect will be the creation of a self-accommodating (or twinned) microstructure. This process begins at $M_s$ and completes at $M_f$. The ensuing multiple variants, which form, tend to average the overall deformation to a net zero change in shape on the macroscopic scale (neglecting thermal expansion). If this material is subsequently mechanically stressed, the multiple variants will coalesce into one variant in the preferred direction of loading, in a process of *reorientation* (also known as detwinning). This process finishes at $\sigma^{re}$. Upon removal of the mechanical load, a permanent deformation is retained in the specimen. (Preferential variants are stable until the loading direction is reversed, i.e. from tension to compression or vice versa.) This is sometimes called *pseudoplasticity* or *quasiplasticity*. If the material is now heated above the critical temperature $A_f$, it reverts to austenite and completely recovers its original shape – i.e. the so-called *one-way shape memory effect*. The recovery process begins at $A_s$ and completes at $A_f$, see a schema of the process in the temperature-strain-stress space, figure 2.2.

When the temperature is above the finish temperature $A_f$ and the specimen is loaded mechanically above a critical stress level given by Clausius-Clapeyron equation (see section 3.4) and marked as two diagonals (one for tension, one for compression) starting at $M_s$ in figure 2.1, austenite will start to transform into a martensite with respect to the direction of loading, accompanied by a large macroscopic strain (so called *transformation strain* $\varepsilon^{tr}$). The transformation is finished by crossing the diagonals starting form $M_f$. The strain is recovered upon removal of the mechanical load in a reverse process, since martensite is not stable at low stress and high temperatures and it transforms into austenite in the stripe of $\sigma$-$T$ plane bounded by parallel lines starting in $A_s$ and $A_f$ temperatures. Typically, this type of process is called *superelasticity* (or *pseudoelasticity*), since the behavior is such that the material returns to its initial configuration upon removal of the loading. Let us recall this processes are possible due to reversibility of MT, which is specific for SMAs.

In a typical loading-unloading experiment under tension and compression where the stress level is assumed to be smaller than the plastic yield stress the *tension-compression asymmetry* will demonstrate itself. When martensite plates grow, different preferential crystallographic variants are favorable for tension or compression loading and thus different internal martensitic structure is established. As a result, the transformation strain induced by phase transformation under compression is smaller and the absolute value of stress level required to start the forward phase transformation under compression is higher than that of the tension experiment. Experimentally, a wider hysteresis

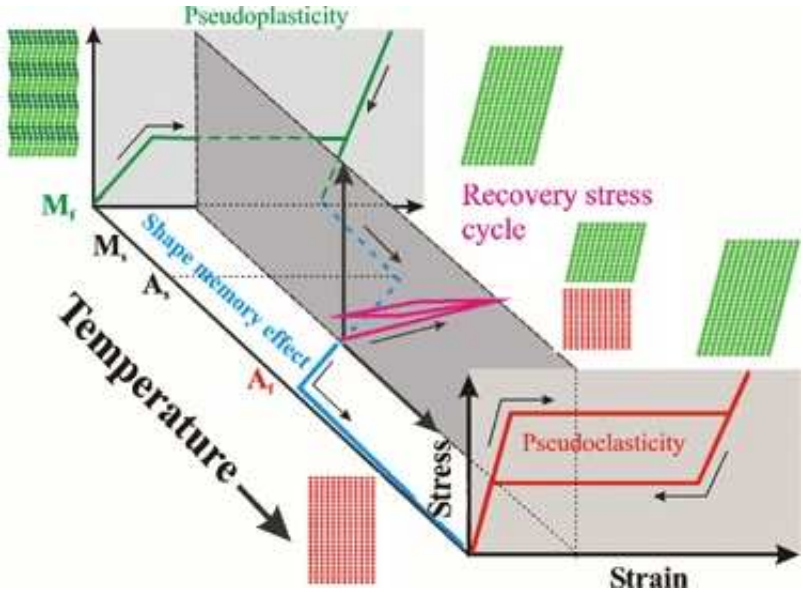


Figure 2.2: Stress-strain-temperature space. Some important shape memory effects are sketched.

loop along the stress axis is observed under compression and the size of the stress-strain hysteresis along the strain axis is considerably smaller under compression. The explanation of different critical stress level for MT in tension and compression at fixed temperature (see figure 2.1) is based on Clausius-Clapeyron equation and it is given in the next chapter.

When changing the direction of stress under $M_s$ (tension to compression or vice versa), martensite variant tend to arrange themselves in the preferred direction of loading. This process of *reorientation* of inappropriately oriented variants also finishes at (approximately temperature-independent) values $\sigma^{re}$ and $-\sigma^{re}$ for tension and compression, respectively, and it is analogous to detwinning. This process contributes to change of the total strain of specimen. In this work martensite created at positive values of stress is referred *"tensile martensite"*, martensite created at negative values of stress is referred *"compressive martensite"*. This artificial classification simplifies the complexity of internal structure, but it is useful for brief description.

Since the response of the system depends not only on the current values of stress and temperature but also on their previous values ("direction of evolution"), hysteresis is a manifestation of "memory" in the system. An interesting property of hysteresis in SMAs is the *return point memory* (RPM), global memory of the system. After a cyclic variation of the driving, the system follows exactly the same trajectory that it would have followed if the cyclic variation had not taken place. In this way, a hierarchy of loops within loops is formed, each *internal subloop* being characterized by the point at which it was initiated – *return point* – i.e. by the point, where the direction of lading

is changed. Results of RPM experiments can be summarized by the following [6].

- The path resulting from complete forward transformation and complete reverse transformation sets the boundaries of the two-phase region, where RPs may occur. The transformation path followed by the system in this two-phase region depends on its previous history through the ensemble of return points in the path.

- The influence of a return point on the evolution of a transformation path disappears when the transformation path reaches the return point again. At the same time the influence of previous return point, constituting the same internal subloop, also disappears and system evolutes as the subloop has never been formed. This phenomena is called *wiping out property*.

- The RPM in SMA is very well established in polycrystals and very often found in single crystals, in both thermally and stress-induced transformations, although differing behaviors have also been reported in the last case.

Different behavior mentioned in the last item refer to experimental results, in which the memory of the return points evolve with time. Some observations also show the hysteresis loop is sensitive to the transformation rate. Both abnormalities are related and rigorously, they would be in contradiction with the basic physical assumption of *reversible athermal* MT. But they can be easily explained by the progressive difficulty in evacuating or absorbing the transformation latent heat at high strain rates (the latent heat not absorbed by environment increases the temperature of specimen, which changes transformation conditions) or irreversible internal evolution of microstructure SMA (e.g. ageing). If the loading is quasistatic and the ambient temperature is kept constant, the hysteresis loops tend asymptotically to be independent on the strain rate.

Since hysteresis in present even in martensite reorientation, the process of reverse transformation from tensile martensite to austenite occurs also in negative stresses between the lines starting at points $A_\mathrm{s}, A_\mathrm{f}$ prolonged from $\sigma \geq 0$ half space (and similarly for compressive martensite) (see [7]).

*Partial (transformation) cycle* is another often referred term connected with hysteretic behavior. By partial cycle we mean a thermomechanical cycle, at which the initial and the final state of material are the same pure phase (martensite or austenite), the phase transition is initiated but, due to one abrupt reversion of driving during the cycle, it is not completed.

SMAs, when constrained, can develop very large macroscopic stress upon heating commonly called the *recovery stress* (see [8], for instance). It has to be necessarily measured and simulated in multistage thermomechanical load, in the former stage of which the SMA element transforms with no restriction on the macroscopic strain. In the latter stage (when a part of material has transformed), an external constraint on macroscopic strain is imposed and the element is loaded thermally. The stress evolving in the latter stage, when thermally induced transformation proceeds, is called recovery stress. It can be shown experimentally, that the recovery stress may increase or decrease

depending on the history and material parameters of the alloy, test limits or on the constraint.

Reaching the $\sigma^{pl}$ stress level in tension or $-\sigma^{pl}$ stress level in compression, the processes determined by plastic deformation as plastic slip or creep will occur. Neither these, neither other plastic changes induced by permanent load or long-term cycling (two-way shape memory effect) are concerned in this work, thus not described herein. (Details can be found elsewhere in the literature.)

## 2.3 NiTiNOL

Many alloys exhibiting SMEs have been discovered since 1950s. Due to type of the martensitic crystallographic lattice, we can distinguish these groups of SMAs (number of crystallographic variants and some examples are given):

- tetragonal lattice (3) – InTl, $Ni_2MnGa$, NiAl, FePt
- orthorhombic lattice (6) – AuCd, CuNiAl
- monoclinic lattice (12) – CuZn, CuAlZn, NiTi

Only some of these can be produced and manufactured at reasonable price and hence are useful for commercial applications. At the present time, most of the SMA products are based on NiTi alloy.

Ni-Ti-based SMA were discovered in 1963 at the Naval Ordnance Laboratory (NOL), hence the usually referred acronym NiTiNOL. In NiTiNOL, as like in other SMA, the diffusionless MT is from one ordered structure to another and effectively enables the alloy to be deformed by a thermoelastic (non-plastic) shear mechanism, i.e. the transformation is *reversible*. Although the reversibility essentially involves an alloy of nominally stoichiometric composition, small additional increase in Ni can be tolerated. This increase in Ni content has an important effect of decreasing the martensite start temperature (content change within range of 1% implies $M_s$ change of more 100K; see [3], page 436).

For the full MT the recoverable memory strain in NiTiNOL is of the order 8%, while the hysteresis width is typically 30–50 K. The martensite-like intermediate transformation is called *R-phase transformation* in NiTiNOL. For R-phase transition the recoverable memory strain is up to 1% and the corresponding hysteresis width is of 1–2 K, but R-phase structure only occurs for specific compositions and annealing temperatures [9]. In figure 2.1 the transformation temperatures of R-phase transition are denoted $R_s, R_f$ (hysteresis neglected). Note steep slopes of critical transformation stress lines in this case. The area of $\sigma$-$T$ space where R-phase can occur is marked with thick line.

The combination of cold-working and subsequent annealing has been explored as a way to improve NiTiNOL characteristics. Depending on the composition and on the

heat treatment, it is possible to obtain Ni-Ti alloy for which the properties associated with transition stabilize after few training cycles. This stability of the material properties is important for the cyclic applications. NiTiNOL has excellent corrosion-resistance and fulfil severe biocompatibility requirements, too.

The unique properties of SMAs are used in such applications as self-erecting space antennae, helicopter blades, surgical tools, reinforcement for arteries and veins, self-locking rivets, actuators, etc. SMAs are convenient for many dynamic applications, but at higher frequencies rate-independence of transition can be affected by retarded heat transfer. The remarkable features of SMAs that make them especially suitable for active elements in actuators are their capacity for high forces, high displacements and reliability with temperature control. In contrast to actuators based on piezoelectric or magnetostrictive materials, SMA actuators offer the advantage that they can exert large repeatable displacements at zero or constant load.

Many applications use SMAs in wire form, since it is generally the least expensive and most readily available form. Thin NiTiNOL wires as basic structural components have several advantages over bulk elements — they are stronger, show enhanced functional properties, the structures made of them are less prone to failure and able to be actuated with higher frequencies (cooling and heating is faster).

# Chapter 3

# Thermodynamics of Shape Memory Alloys

## 3.1 Conception of Continuum Thermodynamics

An elementary term of the theory of continuum is a *material point*, which is not a single atom or molecule, but enough small elementary particle of solid or fluid, whose state represents the local state of material. Position and temperature are the fundamental physical quantities describing a material point developing in time.

The other fundamental physical quantities are defined by balance laws (which will be formulated next) and following physical axioms, which help to complete the system of variables and equations [10]:

1. causality – evolution of the system results from evolution of position and temperature of its material points
2. determinism – all parameters of a material point at thermodynamic equilibrium are determined by history of motion and temperature of all other material points of the system
3. equipresence – all constitutive relations are assumed to be dependent on the same variables, but any of these variables can be excluded due to another axiom
4. objectivity – coordinates transformation invariance
5. material invariance – constitutive relations have to respect material symmetries
6. influence of vicinity – evolution of any material point can be influenced by evolution of any other material point, but usually the influence is decreasing with increasing distance of these points
7. memory of material – influence of history of material to its future development
8. time irreversibility – second law of thermodynamics

9. maximum probability – the system tends to reach the most probable state

Moreover, for mixtures we assume following conditions:

- all properties of a mixture result from properties of its components, but new properties can occur due to their mutual interactions
- in the special case of one substance in a mixture, form of all laws for the mixture is identical with form of these laws for pure substance

Physical and mathematical formulation of maximum probability axiom at instability of systems is difficult and not satisfactorily solved so far. Non-equilibrium thermodynamics focuses on such unstable systems, i.e. chemical reactions, phase transformations or systems at critical states. The constitutive relations are supposed to be dependent on both usual quantities (internal energy, deformation) and, moreover, on dissipative processes (especially heat flux, diffusion flux and dissipative part of stress tensor).

In the following sections, first variables are introduced and balance laws are formulated. After that the second law of thermodynamics is employed to obtain non-equilibrium entropy of mixtures and a constitutive relation for homogenous isotropic thermo-vicso-elastic material is derived. Also, standard definition of chemical potential is extended to the case of finite deformations and Clausius-Clapeyron equation for solid-to-solid phase transition is derived. Finally, hysteresis is introduced as a dissipative process.

We further assume the elementary notions of thermodynamics (temperature, energy, entropy) are well-known (for precise introduction see [10], for instance). The considered functions are supposed to be smooth. Vectors and tensors are in **bold** type or denoted by (Roman alphabet) components. We use Einstein summation convention for *Roman alphabet* subscripts and superscripts. The summation symbol without bounds of summation ($\sum$) is used to denote summation $\sum_{\alpha=1}^{r}$, i.e. sum for all $\alpha = 1, 2, \ldots, r$.

## 3.2 Elements of Continuum Mechanics

Material point corresponds to pure substance in a reference configuration. We suppose there are $r$ pure components $C_\alpha, \alpha = 1, 2, \ldots, r$ in the mixture, each in a reference state at the beginning of studied process. A pure component is not a chemical substance only, but it can be a different crystalline modification or phase. The initial reference state at time $t = 0$ is given by the position

$$\mathbf{X}_\alpha = (X^1_\alpha, X^2_\alpha, X^3_\alpha) \in V_{0,\alpha}, \quad \alpha = 1, 2, \ldots, r \tag{3.1}$$

of each material point $\mathbf{X}_\alpha$ with temperature $T_\alpha(\mathbf{X}_\alpha)$, $V_{0,\alpha}$ is reference volume of component $\alpha$.

The mixture of the chemical components or phases $C_\alpha$ is created by "mixing process", after which each material point of mixture

$$\mathbf{X} = (X^1, X^2, X^3) \in V_0, \tag{3.2}$$

is composed from all components ($V_0$ is reference volume).

Position of material point $\mathbf{X}_\alpha$ at time $t$ is represented by (vector) function

$$\mathbf{x} = \mathbf{x}_\alpha(\mathbf{X}_\alpha, t), \quad \text{i.e.} \quad x^i = x^i_\alpha(X^I_\alpha, t),\ i = 1, 2, 3 \tag{3.3}$$

and temperature of substance $\alpha$ of material point $\mathbf{X}_\alpha$ is represented by function

$$T_\alpha(\mathbf{X}_\alpha, t) = T_\alpha(\mathbf{x}, t), \quad \text{i.e.} \quad T_\alpha(X^I_\alpha, t) = T_\alpha(x^i, t). \tag{3.4}$$

In following text we assume the system is spatially isothermal, i.e. $T_\alpha(\mathbf{x}, t) = T(t),\ \alpha = 1, 2, \ldots, r$. Then there is a unique correspondence between *reference configuration* $X$ at time $t = 0$ and *actual configuration* $x$ at arbitrary time $t$ represented by function (3.3). This function has to be continuous in the first derivatives with respect to $X^I, I = 1, 2, 3$, for all times $t$ and Jacobian determinant $\iota_\alpha$ has to be non-zero, i.e.

$$\iota_\alpha = \det \left| \frac{\partial x^i_\alpha}{\partial X^I_\alpha} \right| \neq 0, \quad \text{for} \quad i, I = 1, 2, 3;\ \alpha = 1, 2, \ldots, r. \tag{3.5}$$

(Relations between elements of volume and area in reference and actual configuration are determined by $\iota_\alpha$.)

Velocity of material point $\mathbf{X}_\alpha$ is defined as follows

$$\mathbf{v}_\alpha(\mathbf{X}_\alpha, t) := \left. \frac{\partial \mathbf{x}_\alpha(\mathbf{X}_\alpha, t)}{\partial t} \right|_{\mathbf{X}_\alpha} = \dot{\mathbf{x}}_\alpha(\mathbf{X}_\alpha, t), \tag{3.6}$$

or in the subscript notation

$$v^i_\alpha(X^I_\alpha, t) := \left. \frac{\partial x^i_\alpha(X^I_\alpha, t)}{\partial t} \right|_{X^I_\alpha} = \dot{x}^i_\alpha(X^I_\alpha, t). \tag{3.7}$$

Acceleration of material point $\mathbf{X}_\alpha$ is defined as follows

$$\mathbf{a}_\alpha(\mathbf{X}_\alpha, t) := \left. \frac{\partial^2 \mathbf{x}_\alpha(\mathbf{X}_\alpha, t)}{\partial t^2} \right|_{\mathbf{X}_\alpha}, \quad \text{i.e.} \quad a^i_\alpha(X^I_\alpha, t) := \left. \frac{\partial^2 x^i_\alpha(X^I_\alpha, t)}{\partial t^2} \right|_{X^I_\alpha} = \dot{v}^i_\alpha(X^I_\alpha, t) \tag{3.8}$$

If velocity is considered as a function of actual coordinates, i.e. $\mathbf{v}_\alpha(\mathbf{x}, t)$, then

$$\begin{aligned} \dot{v}^i_\alpha(x^j, t) &= \frac{\partial v^i_\alpha(x^j, t)}{\partial t} + \left. \frac{\partial v^i_\alpha(x^j, t)}{\partial x^l} \, \frac{\partial x^l(X^L_\alpha, t)}{\partial t} \right|_{X^L_\alpha} \\ &= \frac{\partial v^i_\alpha(x^j, t)}{\partial t} + v^l_\alpha(X^L_\alpha, t) \frac{\partial v^i_\alpha(x^j, t)}{\partial x^l} \end{aligned} \tag{3.9}$$

From now on we suppose the quantities are expressed in actual configuration implicitly and we do not denote it explicitly, i.e. for quantities $o, \mathbf{O}$

$$o \equiv o(\mathbf{x}, t) \quad \text{or} \quad \mathbf{O} \equiv \mathbf{O}(\mathbf{x}, t), \quad \text{i.e.} \quad O^i \equiv O^i(\mathbf{x}, t),\ i = 1, 2, 3. \tag{3.10}$$

The mass center point trajectory is defined implicitly in the vicinity of $\mathbf{x}$ point and the mass center velocity $\mathbf{v}$ is defined as follows

$$\mathbf{v} := \frac{1}{\rho}\sum \rho_\alpha \mathbf{v}_\alpha \quad \text{i.e.} \quad v^i := \frac{1}{\rho}\sum \rho_\alpha v^i_\alpha. \tag{3.11}$$

As a consequence of mass center velocity we introduce diffusion velocity of substance $\alpha$

$$\mathbf{v}_{\mathrm{D}\alpha} := \mathbf{v}_\alpha - \mathbf{v}, \quad \text{i.e.} \quad v^i_{\mathrm{D}\alpha} := v^i_\alpha - v^i, \tag{3.12}$$

and diffusion flux of substance $\alpha$ with respect to the mass center point

$$\mathbf{j}_{\mathrm{D}\alpha} := \rho_\alpha \mathbf{v}_{\mathrm{D}\alpha}, \quad \text{i.e.} \quad j^i_{\mathrm{D}\alpha} := \rho_\alpha v^i_{\mathrm{D}\alpha}. \tag{3.13}$$

Now it is clear

$$\sum \mathbf{j}_{D\alpha} = 0. \tag{3.14}$$

Let $\vartheta_\alpha$ be a smooth scalar function. We distinguish two different material derivatives:

- Material derivative with respect to the trajectory $\mathbf{x}_\alpha$ of component $C_\alpha$ (already introduced and denoted with `):

$$\grave{\vartheta}_\alpha = \left.\frac{\partial \vartheta_\alpha(\mathbf{x},t)}{\partial t}\right|_{\mathbf{X}_\alpha} = \frac{\partial \vartheta_\alpha(x^j,t)}{\partial t} + \frac{\partial \vartheta_\alpha(x^j,t)}{\partial x^l}\left.\frac{\partial x^l(X^L_\alpha,t)}{\partial t}\right|_{X^L_\alpha} = \frac{\partial \vartheta_\alpha}{\partial t} + v^l_\alpha \frac{\partial \vartheta_\alpha}{\partial t}. \tag{3.15}$$

  (We assume the trajectory $\mathbf{x}_\alpha$ coincides with the geometrical point $\mathbf{x}$.)

- Material derivative with respect to the trajectory $\mathbf{x}$ of mass center of the mixture (denoted with ˙):

$$\dot{\vartheta}_\alpha = \left.\frac{\partial \vartheta_\alpha(\mathbf{x},t)}{\partial t}\right|_{\mathbf{X}} = \frac{\partial \vartheta_\alpha(x^j,t)}{\partial t} + \frac{\partial \vartheta_\alpha(x^j,t)}{\partial x^l}\left.\frac{\partial x^l(X^L,t)}{\partial t}\right|_{X^L} = \frac{\partial \vartheta_\alpha}{\partial t} + v^l \frac{\partial \vartheta_\alpha}{\partial t}. \tag{3.16}$$

Following important relations between material derivative of $\vartheta_\alpha(\mathbf{x},t)$ with respect to pure substance and with respect to mixture (velocity of mass center) are clear from previous definitions:

$$\dot{\vartheta_\alpha} = \grave{\vartheta}_\alpha - v^l_{\mathrm{D}\alpha}\frac{\partial \vartheta_\alpha}{\partial x^l} \tag{3.17}$$

$$\rho_\alpha \dot{\vartheta}_\alpha = \rho_\alpha \grave{\vartheta}_\alpha - j^l_{\mathrm{D}\alpha}\frac{\partial \vartheta_\alpha}{\partial x^l} \tag{3.18}$$

Let us assume following system of chemical reactions (or phase transitions) involved in our thermodynamical system:

$$\sum \nu_{\beta\alpha} C_\alpha \rightleftharpoons \sum \nu'_{\beta\alpha} C_\alpha \quad \nu_{\beta\alpha}, \nu'_{\beta\alpha} \in \mathbb{N}, \quad \beta = 1,2,\ldots,\kappa \tag{3.19}$$

where $\kappa$ is the number of all substances (components) concerned in reactions (transitions) and $\nu_{\beta\alpha}, \nu'_{\beta\alpha}$ are stoichiometric coefficients.

To characterize the chemical (or phase) composition we introduce following variables (in actual configuration; for clarity, [SI units] of quantities stated):

| | | |
|---|---|---|
| $n_\alpha$ | [mol] | molar amount of substance $\alpha$ |
| $n$ | [mol] | molar amount of mixture |
| $\rho_\alpha$ | [kg/m$^3$] | (mass) density of substance $\alpha$ |
| $\rho$ | [kg/m$^3$] | (mass) density of mixture |
| $m_\alpha$ | [kg] | partial mass of substance $\alpha$ |
| $m$ | [kg] | total mass of mixture |
| $V_{m\alpha}$ | [m$^3$/mol] | molar volume of substance $\alpha$ |
| $M_\alpha$ | [kg/mol] | molar mass of substance $\alpha$ |
| $c_\alpha$ | [mol/m$^3$] | molar concentration of substance $\alpha$ |
| $c$ | [mol/m$^3$] | molar concentration of mixture |
| $x_\alpha := \frac{n_\alpha}{n}$ | [1] | molar fraction of substance $\alpha$ |
| $w_\alpha := \frac{\rho_\alpha}{\rho}$ | [1] | mass fraction of substance $\alpha$ |
| $\xi_\alpha := V_{m\alpha} c_\alpha$ | [1] | volume fraction |

Identities following from previous definitions:

$$n = \sum n_\alpha, \quad \rho = \sum \rho_\alpha, \quad m = \sum m_\alpha, \quad c = \sum c_\alpha, \tag{3.20}$$

$$\sum x_\alpha = 1, \quad \sum w_\alpha = 1, \quad \sum \xi_\alpha = 1, \tag{3.21}$$

And moreover,

$$\rho_\alpha = M_\alpha c_\alpha, \quad c_\alpha = \rho \frac{w_\alpha}{M_\alpha}, \quad w_\alpha = \frac{M_\alpha}{\rho V_{m\alpha}} \xi_\alpha. \tag{3.22}$$

Now, we can formulate general form of balance laws. Let $\vartheta$ is an intensive quantity of a mixture and $\vartheta_\alpha$ an intensive quantity for substance $\alpha$. We assume the following equations hold

$$\rho\vartheta = \sum \rho_\alpha \vartheta_\alpha. \tag{3.23}$$

$$\mathbf{j}(\vartheta) = \sum \mathbf{j}(\vartheta_\alpha), \tag{3.24}$$

$$\sigma(\vartheta) = \sum \sigma(\vartheta_\alpha). \tag{3.25}$$

where $\mathbf{j}(\vartheta)$ is flux of quantity $\vartheta$ through the boundary of an elementary volume and $\sigma(\vartheta)$ is production the same quantity in the elementary volume.

Balance law for substance $\alpha$ in global form:

$$\overline{\int_V \rho_\alpha \vartheta_\alpha \,\mathrm{d}v} = \int_{\partial V} j^l_\alpha(\vartheta_\alpha) \,\mathrm{d}a_l + \int_V \sigma_\alpha(\vartheta_\alpha) \,\mathrm{d}v, \tag{3.26}$$

where the left term describes the total increment of quantity $\vartheta$ in a volume $V$, first term on the right stands for flux of the quantity through boundary of $V$ and the last term is

production of quantity in the volume $V$. Local form of balance law for each component $\alpha$ can be found by standard procedures (Gauss theorem, principle of locality):

$$\frac{\partial(\rho_\alpha \vartheta_\alpha)}{\partial t} + \frac{\partial(\rho_\alpha \vartheta_\alpha v^l)}{\partial x^l} + \frac{\partial[\vartheta_\alpha j^l_{D\alpha} - j^l_\alpha(\vartheta_\alpha)]}{\partial x^l} - \sigma_\alpha(\vartheta_\alpha) = 0, \tag{3.27}$$

Adding the equations (3.26) for all components $\alpha = 1, 2, \ldots, r$ with respect to (3.23)–(3.25) we obtain global balance law for mixture

$$\overset{\cdot}{\overline{\int_V \rho\vartheta \,\mathrm{d}v}} = \int_{\partial V} j^l(\vartheta)\,\mathrm{d}a_l + \int_V \sigma(\vartheta)\,\mathrm{d}v. \tag{3.28}$$

The expected local form of balance law for mixture is

$$\frac{\partial(\rho\vartheta)}{\partial t} + \frac{\partial(\rho\vartheta v^l)}{\partial x^l} - \frac{\partial j^l(\vartheta)}{\partial x^l} - \sigma(\vartheta) = 0, \tag{3.29}$$

if we require

$$\sum \vartheta_\alpha \mathbf{j}_{D\alpha} = 0. \tag{3.30}$$

This physical constraint ensures there is no transport of quantity $\vartheta$ due to self-diffusion.

By special choice of variable $\vartheta_\alpha$ ($u_\alpha$ denotes internal energy)

$$\vartheta_\alpha \in \left\{1, v^i_\alpha, \frac{(v^i_\alpha)^2}{2}, u_\alpha, u_\alpha + \frac{(v^i_\alpha)^2}{2}\right\} \tag{3.31}$$

we can obtain conservation laws for each substance $\alpha = 1, 2, ..., r$. Their specific form can be found elsewhere (see [11], for instance). Similarly, the conservation law of mass, momentum and kinetic, internal ($u$) and total energy for mixture in usual form can be obtained when

$$\vartheta \in \left\{1, v^i, \frac{(v^i)^2}{2}, u, u + \frac{(v^i)^2}{2}\right\}. \tag{3.32}$$

Balance law for entropy is deeply discussed in the next section.

For future reference let us recall two conservation laws for mixture. First, introducing $\omega_\beta$ as velocity of reaction $\beta$, the production of mass of substance $\alpha$ in the system is

$$\sum_{\beta=1}^{\kappa} M_\alpha(\nu'_{\beta\alpha} - \nu_{\beta\alpha})\omega_\beta. \tag{3.33}$$

As a result the conservation of mass has the form

$$\rho\dot{w}_\alpha + \frac{\partial j^l_{\mathrm{D}\alpha}}{\partial x^l} = \sum_{\beta=1}^{\kappa} M_\alpha(\nu'_{\beta\alpha} - \nu_{\beta\alpha})\omega_\beta. \tag{3.34}$$

Conservation of internal energy $u$ when production of mechanical energy due to gradients of velocity field is neglected in the system:

$$\frac{\partial(\rho u)}{\partial t} + \frac{\partial(\rho u v^l)}{\partial x^l} + \frac{\partial}{\partial x^l}\left(q^l + \sum u_\alpha j^l_{\mathrm{D}\alpha}\right) = t^{li}\frac{\partial v^i}{\partial x^l} + \sum\left(t^{li}_\alpha \frac{\partial v^i_{\mathrm{D}\alpha}}{\partial x^l} + j^i_{\mathrm{D}\alpha} b^i_\alpha\right), \tag{3.35}$$

where $\mathbf{b}_\alpha$ are external volume forces, $\mathbf{q}$ stands for heat flux and $\mathbf{t}$ is stress tensor (see also section 3.3). Let us recall the conservation of angular momentum implies the stress tensor $\mathbf{t}$ is symmetric.

Deformation of continuum is usually described by deformation gradient $\mathbf{F}_\alpha$, which is defined as follows

$$F^i_{I,\alpha} = \frac{\partial x^i(X^k_\alpha, t)}{\partial X^I_\alpha}, \tag{3.36}$$

and Cauchy tensor (related to actual configuration)

$$\mathbf{c}_\alpha = \mathbf{F}_\alpha^{-\mathrm{T}}\mathbf{F}_\alpha^{-1}, \quad \text{i.e.} \quad c_{kl,\alpha} = \frac{\partial X^I_\alpha}{\partial x^k}\frac{\partial X^I_\alpha}{\partial x^l}. \tag{3.37}$$

Relative deformation is described by Euler tensor

$$\mathbf{e}_\alpha = \frac{1}{2}(\mathbf{I} - \mathbf{c}_\alpha), \quad \text{i.e.} \quad e_{kl,\alpha} = \frac{1}{2}\left(\delta_{kl} - c_{kl,\alpha}\right). \tag{3.38}$$

Next, let us assume the Amagade conception, where volume is equal to sum of volumes of substances and thus deformation is equal to sum of deformations of substances, i.e.

$$\mathbf{e} = \sum \mathbf{e}_\alpha, \quad \text{and} \quad e_{ij,\alpha} = \xi_\alpha e_{ij}. \tag{3.39}$$

For description of deformation dynamics material derivative of deformation tensors are used. Velocity gradient $\mathbf{l}$ is defined by equation

$$l^{ij} = \frac{\partial v^i}{\partial x^j}. \tag{3.40}$$

and can be decomposed into symmetric deformation rate tensor $\mathbf{D}$,

$$d^{ij} = \frac{1}{2}\left(\frac{\partial v^i}{\partial x^j} + \frac{\partial v^j}{\partial x^i}\right), \tag{3.41}$$

and antisymmetric spin tensor $\mathbf{W}$,

$$w^{ij} = \frac{1}{2}\left(\frac{\partial v^i}{\partial x^j} - \frac{\partial v^j}{\partial x^i}\right). \tag{3.42}$$

Thus

$$\mathbf{l} = \mathbf{D} + \mathbf{W}, \quad \text{i.e.} \quad l^{ij} = d^{ij} + w^{ij}. \tag{3.43}$$

Similarly, we define deformation rate tensor $\mathbf{D}_\alpha$ for component $\alpha$

$$d^{ij}_\alpha = \frac{1}{2}\left(\frac{\partial v^i_\alpha}{\partial x^j} + \frac{\partial v^j_\alpha}{\partial x^i}\right). \tag{3.44}$$

An important identity can be obtained by several computations

$$\dot{e}_{ij,\alpha} = d_{ij,\alpha} - e_{lj,\alpha}\frac{\partial v^l}{\partial x^i} - e_{il,\alpha}\frac{\partial v^l}{\partial x^j}, \tag{3.45}$$

i.e.

$$\dot{e}_{ij,\alpha} = d_{ij,\alpha} - e_{lj,\alpha} l^{li} - e_{il,\alpha} l^{lj}. \tag{3.46}$$

Similarly for mixture

$$\dot{e}_{ij} = d_{ij} - e_{lj} l^{li} - e_{il} l^{lj}. \tag{3.47}$$

With respect to (3.39) and (3.45) it follows

$$\dot{e}_{ij} = \sum (\xi_\alpha \dot{e}_{ij,\alpha} + e_{ij,\alpha} \dot{\xi}_\alpha) = \sum \left[ \xi_\alpha \left( d_{ij,\alpha} - e_{lj,\alpha} \frac{\partial v^l}{\partial x^i} - e_{il,\alpha} \frac{\partial v^l}{\partial x^j} \right) + e_{ij,\alpha} \dot{\xi}_\alpha \right]. \tag{3.48}$$

Comparing (3.47) and (3.48) we obtain relation

$$d_{ij} = \sum (\xi_\alpha d_{ij,\alpha} + e_{ij,\alpha} \dot{\xi}_\alpha). \tag{3.49}$$

## 3.3 Extended Non-Equilibrium Thermodynamics of Mixtures

Following the axiom of determinism, we assume values of all quantities of material point are determined by values of following independent variables ($\alpha = 1, 2, \ldots, r$) at thermodynamic equilibrium ([SI units] of quantities stated):

| | | |
|---|---|---|
| $u_\alpha$ | $[\mathrm{J \cdot kg^{-1}}]$ | internal energy of component $\alpha$ |
| $w_\alpha$ | [1] | mass concentration of component $\alpha$ |
| $\mathbf{j}_{D\alpha}$ | $[\mathrm{kg \cdot m^{-2} \cdot s^{-1}}]$ | diffusion flux vector of component $\alpha$ |
| $\mathbf{q}_\alpha$ | $[\mathrm{J \cdot m^{-2} \cdot s^{-1}}]$ | heat flux vector of component $\alpha$ |
| $\mathbf{e}_\alpha$ | [1] | Euler deformation tensor of component $\alpha$ |
| $\mathbf{t}_{\mathrm{dis}}$ | $[\mathrm{J \cdot m^{-3}}]$ | dissipative part of stress tensor |

for which we suppose (3.14),(3.21) and

$$\rho u = \sum \rho_\alpha u_\alpha, \quad u = \sum w_\alpha u_\alpha, \quad q^i = \sum q^i_\alpha, \quad i = 1, 2, 3,$$

$$e^{ij} = \sum e^{ij}_\alpha, \quad t^{ij}_{\mathrm{dis}} = \sum t^{ij}_{\mathrm{dis}\alpha}, \quad i, j = 1, 2, 3, \tag{3.50}$$

The symmetric stress tensor $\mathbf{t}$ is assumed to be composed of elastic and dissipative part:

$$\mathbf{t} = \mathbf{t}_{\mathrm{el}} + \mathbf{t}_{\mathrm{dis}} \tag{3.51}$$

and the dissipative part is further considered to be independent variable.

Specific entropy of material

$$s(u, w_\alpha, \mathbf{j}_{\mathrm{D}\alpha}, \mathbf{q}, \mathbf{e}, \mathbf{t}_{\mathrm{dis}}) = \sum w_\alpha s_\alpha(u_\alpha, w_\alpha, \mathbf{e}_\alpha, \mathbf{t}_{\mathrm{dis}\alpha}, \mathbf{j}_{\mathrm{D}\alpha}, \mathbf{q}_\alpha) \tag{3.52}$$

is defined by entropy balance law

$$\rho \dot{s} - \frac{\partial j^l(s)}{\partial x^l} = \sigma(s) \geq 0 \tag{3.53}$$

where the non-equality is an expression of the second law of thermodynamics (and the time irreversibility axiom). A specific form of entropy production, $\sigma(s)$, arise from balance laws for other extensive quantities; resulting forms of entropy, $s$, and its flux, $\mathbf{j}(s)$, are revealed by entropy balance law.

First, let us assume the entropy change is due to heat conduction only. Then entropy flux density is defined as follows:

$$\mathbf{j}(s) = \frac{\mathbf{q}}{T}, \quad \text{i.e.} \quad j^i = \frac{q^i}{T}, \tag{3.54}$$

and (3.53) implies

$$\sigma(s) = \rho\dot{s} + q^i \frac{\partial}{\partial x^i}\left(\frac{1}{T}\right) + \frac{1}{T}\frac{\partial q^i}{\partial x^i} \geq 0. \tag{3.55}$$

Using balance law for internal energy in the form of equation (3.35) we obtain

$$\begin{aligned} \sigma(s) &= \rho\left(\dot{s} - \frac{\dot{u}}{T}\right) + q^i \frac{\partial}{\partial x^i}\left(\frac{1}{T}\right) + \frac{1}{T} t^{li}\frac{\partial v^i}{\partial x^l} - \\ &\quad \frac{1}{T}\frac{\partial}{\partial x^l}\left(\sum u_\alpha j^l_{\mathrm{D}\alpha}\right) + \frac{1}{T}\sum t^{li}_\alpha \frac{\partial v^i_{\mathrm{D}\alpha}}{\partial x^l} + \frac{1}{T}\sum j^i_{\mathrm{D}\alpha} b^i_\alpha \geq 0. \end{aligned} \tag{3.56}$$

Let us expand material derivative of specific entropy $s$

$$\begin{aligned} \dot{s} &= \left(\frac{\partial s}{\partial u}\right)\dot{u} + \left(\frac{\partial s}{\partial e^{ij}}\right)\dot{\overline{e^{ij}}} + \sum\left(\frac{\partial s}{\partial w_\alpha}\right)\dot{w_\alpha} + \\ &\quad \left(\frac{\partial s}{\partial t^{ij}_{\mathrm{dis}}}\right)\dot{\overline{t^{ij}_{\mathrm{dis}}}} + \sum\left(\frac{\partial s}{\partial j^i_{\mathrm{D}\alpha}}\right)\dot{\overline{j^i_{\mathrm{D}\alpha}}} + \left(\frac{\partial s}{\partial q^i}\right)\dot{q^i}, \end{aligned} \tag{3.57}$$

decompose the stress tensor to dissipative and elastic part (3.51), recall definition (3.40) and decomposition (3.43). Next, employing (3.47) and recalling the scalar product of a symmetric and an antisymmetric tensor is equal to zero, we obtain fairly complex term for entropy production:

$$\begin{aligned} \sigma(s) &= \rho\left[\frac{\partial s}{\partial u} - \frac{1}{T}\right]\dot{u} + \rho\left[\frac{\partial s}{\partial e_{ij}} - \frac{\partial s}{\partial e_{il}}e_{lj} - \frac{\partial s}{\partial e_{lj}}e_{il} + \frac{t^{ij}_{\mathrm{el}}}{\rho T}\right] d_{ij} + \\ &\quad \rho\frac{\partial s}{\partial t^{ij}_{\mathrm{dis}}}\dot{\overline{t^{ij}_{\mathrm{dis}}}} + \frac{t^{ij}_{\mathrm{dis}}}{T}d_{ij} + \frac{1}{T}\sum(t^{li}_{\mathrm{el}\alpha} + t^{li}_{\mathrm{dis}\alpha})\frac{\partial v^i_{\mathrm{D}\alpha}}{\partial x^l} + \\ &\quad \rho\frac{\partial s}{\partial q^i}\dot{q^i} + q^i\frac{\partial}{\partial x^i}\left(\frac{1}{T}\right) + \sum\left[\rho\left(\frac{\partial s}{\partial j^i_{\mathrm{D}\alpha}}\dot{\overline{j^i_{\mathrm{D}\alpha}}}\right) - \frac{1}{T}\frac{\partial(u_\alpha j^l_{\mathrm{D}\alpha})}{\partial x^l}\right] \\ &\quad \sum\left[\rho\frac{\partial s}{\partial w_\alpha}\dot{w_\alpha} + \frac{j^i_{\mathrm{D}\alpha}b^i_\alpha}{T}\right] \geq 0. \end{aligned} \tag{3.58}$$

It is clear that

$$-\frac{1}{T}\frac{\partial(u_\alpha j^l_{\mathrm{D}\alpha})}{\partial x^l} = -\frac{\partial}{\partial x^l}\left(\frac{u_\alpha j^l_{\mathrm{D}\alpha}}{T}\right) + u_\alpha j^l_{\mathrm{D}\alpha}\frac{\partial}{\partial x^l}\left(\frac{1}{T}\right). \tag{3.59}$$

Conservation of mass in form (3.34) helps to convert:

$$\begin{aligned}\sum \rho\frac{\partial s}{\partial w_\alpha}\dot{w}_\alpha &= \sum \frac{\partial s}{\partial w_\alpha}\left(\sum M_\alpha(\nu_{\beta\alpha}-\nu'_{\beta\alpha})\omega_\beta - \frac{\partial j^l_{\mathrm{D}\alpha}}{\partial x^l}\right)\\ &= \sum \frac{\partial s}{\partial w_\alpha}\left(\sum M_\alpha(\nu_{\beta\alpha}-\nu'_{\beta\alpha})\omega_\beta\right)\\ &\quad -\sum \frac{\partial}{\partial x^l}\left(\frac{\partial s}{\partial w_\alpha}j^l_{\mathrm{D}\alpha}\right)+\sum j^l_{\mathrm{D}\alpha}\frac{\partial}{\partial x^l}\frac{\partial s}{\partial w_\alpha}. \end{aligned} \tag{3.60}$$

Taking into account both previous equations we have

$$\begin{aligned}\frac{1}{T}\frac{\partial(u_\alpha j^l_{\mathrm{D}\alpha})}{\partial x^l}+\sum \rho\frac{\partial s}{\partial w_\alpha}\dot{w}_\alpha &= \sum \frac{\partial}{\partial x^l}\left(\frac{u_\alpha j^l_{\mathrm{D}\alpha}}{T}+\frac{\partial s}{\partial w_\alpha}j^l_{\mathrm{D}\alpha}\right)+\\ &\quad \sum j^l_{\mathrm{D}\alpha}\left[u_\alpha j^l_{\mathrm{D}\alpha}\frac{\partial}{\partial x^l}\left(\frac{1}{T}\right)+\frac{\partial}{\partial x^l}\frac{\partial s}{\partial w_\alpha}\right]+\\ &\quad \sum \frac{\partial s}{\partial w_\alpha}\left(\sum M_\alpha(\nu_{\beta\alpha}-\nu'_{\beta\alpha})\omega_\beta\right). \end{aligned} \tag{3.61}$$

The first term on the right is divergence of additional entropy flux, thus we redefine (3.54) as follows

$$j^i(s)=\frac{q^i}{T}+\sum \frac{\partial}{\partial x^l}\left(\frac{u_\alpha j^l_{\mathrm{D}\alpha}}{T}+\frac{\partial s}{\partial w_\alpha}j^l_{\mathrm{D}\alpha}\right). \tag{3.62}$$

and thus diffusion is included.

Hence, inequality (3.58) in the new form:

$$\begin{aligned}\sigma(s) &= \rho\left[\frac{\partial s}{\partial u}-\frac{1}{T}\right]\dot{u}+\rho\left[\frac{\partial s}{\partial e_{ij}}-\frac{\partial s}{\partial e_{il}}e_{lj}-\frac{\partial s}{\partial e_{lj}}e_{il}+\frac{t^{ij}_{\mathrm{el}}}{\rho T}\right]d_{ij}+\\ &\quad \sum \frac{\partial s}{\partial w_\alpha}M_\alpha(\nu'_{\beta\alpha}-\nu_{\beta\alpha})\omega_\beta+\\ &\quad \rho\frac{\partial s}{\partial t^{ij}_{\mathrm{dis}}}\dot{\overline{t^{ij}_{\mathrm{dis}}}}+\frac{t^{ij}_{\mathrm{dis}}}{T}d_{ij}+\frac{1}{T}\sum t^{ij}_{\mathrm{dis}\alpha}L^{ij}_{\mathrm{D}\alpha}+\\ &\quad \rho\frac{\partial s}{\partial q^i}\dot{q}^i+q^i\frac{\partial}{\partial x^i}\left(\frac{1}{T}\right)+\sum u_\alpha j^i_{\mathrm{D}\alpha}\frac{\partial}{\partial x^i}\left(\frac{1}{T}\right)+\\ &\quad \sum\left[\rho\frac{\partial s}{\partial j^i_{\mathrm{D}\alpha}}\dot{\overline{j^i_{\mathrm{D}\alpha}}}+j^i_{\mathrm{D}\alpha}\frac{\partial}{\partial x^i}\frac{\partial s}{\partial w_\alpha}+\frac{j^i_{\mathrm{D}\alpha}b^i_\alpha}{T}\right]\geq 0. \end{aligned} \tag{3.63}$$

The fundamental restriction of non-negative entropy production in (3.63) is fulfilled if and only if (see [11] or [12], for instance) following 6 equations hold:

$$\frac{\partial s}{\partial u} = \frac{1}{T}, \tag{3.64}$$

$$\frac{\partial s}{\partial e_{ij}}-\frac{\partial s}{\partial e_{il}}e_{lj}-\frac{\partial s}{\partial e_{lj}}e_{il} = -\frac{t^{ij}_{\mathrm{el}}}{\rho T}, \tag{3.65}$$

$$\frac{\partial s}{\partial w_\alpha} = -\frac{\mu_\alpha}{T}, \tag{3.66}$$

$$\frac{\partial s}{\partial j^i_{\mathrm{D}\alpha}} = -\frac{\tau_{\mathrm{D}\alpha}}{\rho}\frac{\partial}{\partial x^i}\left(\frac{\mu_\alpha}{T}\right), \tag{3.67}$$

$$\frac{\partial s}{\partial q^i} = \frac{\tau_T}{\rho}\frac{\partial}{\partial x^i}\left(\frac{1}{T}\right), \tag{3.68}$$

$$\frac{\partial s}{\partial t^{ij}_{\mathrm{dis}}} = \frac{\tau_p}{\rho}\frac{d^{ij}}{T}, \tag{3.69}$$

and thus, material derivative of entropy (3.57) has the form

$$\dot{s} = \frac{\dot{u}}{T} - \frac{t^{ij}_{\mathrm{el}}}{\rho}\frac{d^{ij}}{T} - \sum\frac{\mu_\alpha}{T}\dot{w}_\alpha + \underbrace{\frac{\tau_{\mathrm{p}}}{\rho}\frac{d^{ij}}{T}\overset{\cdot}{\overline{t^{ij}_{\mathrm{dis}}}} + \frac{\tau_T}{\rho}\frac{\partial}{\partial x^i}\left(\frac{1}{T}\right)\dot{q}^i - \sum\frac{\tau_{\mathrm{D}\alpha}}{\rho}\frac{\partial}{\partial x^i}\left(\frac{\mu_\alpha}{T}\right)\overset{\cdot}{\overline{j^i_{\mathrm{D}\alpha}}}}_{\dot{s}_{\mathrm{N}}}. \tag{3.70}$$

We have introduced time derivative of non-equilibrium entropy $\dot{s}_{\mathrm{N}}$ (it manifest itself at rapid processes only), times of relaxation of non-equilibrium processes

- $\tau_{\mathrm{p}}$ relaxation time of plastic flow
- $\tau_{\mathrm{D}\alpha}$ relaxation time of diffusion waves
- $\tau_T$ relaxation time of temperature waves

and a new parameter $\mu_\alpha$, chemical potential, which is further described in the next section.

For $\tau_{\mathrm{p}} = \tau_{\mathrm{D}\alpha} = \tau_T = 0$ we get usual Gibbs definition of entropy for solid body:

$$\dot{s} = \frac{\dot{u}}{T} - \frac{t^{ij}_{\mathrm{el}}d^{ij}}{\rho T} - \sum\frac{\mu_\alpha\dot{w}_\alpha}{T} \tag{3.71}$$

Another useful quantity is affinity of chemical reaction

$$A_\beta = -M_\alpha(\nu'_{\beta\alpha} - \nu_{\beta\alpha})\mu_\beta, \quad \beta = 1, 2, \ldots, \kappa. \tag{3.72}$$

Considering this definition and equations (3.64)–(3.69), the final form of entropy production is

$$\sigma(s) = \left(\tau_{\mathrm{p}}\overset{\cdot}{\overline{t^{ij}_{\mathrm{dis}}}} + t^{ij}_{\mathrm{dis}}\right)\frac{d^{ij}}{T} + \left[\tau_T\dot{q}^i + \left(q^i + \sum u_\alpha j^i_{\mathrm{D}\alpha}\right)\right]\frac{\partial}{\partial x^i}\left(\frac{1}{T}\right) + \sum_{\beta=1}^{\kappa}\frac{A_\beta\omega_\beta}{T}$$
$$- \sum\left(\tau_{\mathrm{D}\alpha}\overset{\cdot}{\overline{j^i_{\mathrm{D}\alpha}}} + j^i_{\mathrm{D}\alpha}\right)\frac{\partial}{\partial x^i}\left(\frac{\mu_\alpha}{T}\right) + \frac{1}{T}\sum\left(t^{ij}_\alpha\frac{\partial v^i_{\mathrm{D}\alpha}}{\partial x^j} + j^i_{\mathrm{D}\alpha}b^i_\alpha\right) \geq 0. \tag{3.73}$$

For an arbitrary 3-dimensional tensor (of rank 2), $\mathbf{T}$, let us define its trace

$$T_{(1)} := T^{ij}\delta^{ij} \tag{3.74}$$

and its deviatoric part

$$T^{ij}_{(0)} := T^{ij} - \frac{\delta^{ij}}{3}T_{(1)}, \tag{3.75}$$

where $\delta^{ij}$ represents Kronecker delta symbol:

$$\delta^{ij} := \begin{cases} 1 & i = j, \\ 0 & i \neq j. \end{cases} \tag{3.76}$$

Then sufficient conditions for non-negative production of entropy can be written as follows:

$$\tau_{\mathrm{p}} \overset{\cdot}{\overline{t^{ij}_{\mathrm{dis}(0)}}} + t^{ij}_{\mathrm{dis}(0)} = L_{\mu} d^{ij}_{(0)}, \tag{3.77}$$

$$\tau_{\mathrm{p}} \overset{\cdot}{\overline{t_{\mathrm{dis}(1)}}} + t_{\mathrm{dis}(1)} = L_{\mu v} d_{(1)} + \sum_{\beta=1}^{\kappa} L_{\mu\beta} A_{\beta}, \tag{3.78}$$

$$\tau_T \dot{q}^i + q^i + \sum \mu_{\alpha} j^i_{\mathrm{D}\alpha} = L_q \frac{\partial}{\partial x^i}\left(\frac{1}{T}\right) + L_{q,\mathrm{D}\alpha} \frac{\partial}{\partial x^i}\left(\frac{\mu_{\alpha}}{T}\right), \tag{3.79}$$

$$\tau_{\mathrm{D}\alpha} \overset{\cdot}{\overline{j^i_{\mathrm{D}\alpha}}} + j^i_{\mathrm{D}\alpha} = -L_{\mathrm{D}\alpha} \frac{\partial}{\partial x^i}\left(\frac{\mu_{\alpha}}{T}\right) + L_{\mathrm{D}\alpha,q} \frac{\partial}{\partial x^i}\left(\frac{1}{T}\right), \tag{3.80}$$

$$\omega_{\beta} = L_{\beta} A_{\beta} + L_{\beta\mu} d_{(1)}. \tag{3.81}$$

where the equations describe subsequently viscoplasticity, volume viscosity, heat conductivity, diffusion and velocity of chemical reaction and processes connected with introduced coefficients are ($\alpha = 1, 2, \ldots, r;\ \beta = 1, 2, \ldots, \kappa$):

| | |
|---|---|
| $L_{\mu}$ | shear viscosity |
| $L_q$ | heat conductivity |
| $L_{\mathrm{D}\alpha}$ | diffusion |
| $L_{\mu v}$ | volume viscosity |
| $L_{\beta}$ | velocity of chemical reaction |
| $L_{q,\mathrm{D}\alpha}$ | thermal transfer by diffusion |
| $L_{\mathrm{D}\alpha,q}$ | thermodiffusion |
| $L_{\mu\beta}$ | mechanical stress induced by chemical reactions |
| $L_{\beta\mu}$ | velocity of chemical reactions induced by mechanical stress |

Let us neglect the last term on the left-hand side of inequality (3.73) and employ phenomenological relations (3.77)–(3.81). The production of entropy represented by the left-hand side of the inequality is then a quadratic form of variables

$$d^{ij}_{(0)}, \frac{\partial}{\partial x^i}\left(\frac{1}{T}\right), \frac{\partial}{\partial x^i}\left(\frac{\mu_{\alpha}}{T}\right), d_{(1)}, A_{\beta} \tag{3.82}$$

where $i, j = 1, 2, 3;\ \alpha = 1, 2, \ldots, r;\ \beta = 1, 2, \ldots, \kappa$. If we further assume

$$L_{q,\mathrm{D}\alpha} = L_{\mathrm{D}\alpha,q}, \quad L_{\mu\beta} = L_{\beta\mu}, \quad \alpha = 1, 2, \ldots, r;\ \beta = 1, 2, \ldots, \kappa, \tag{3.83}$$

then this quadratic form is positive-definite, if the well-known Sylvester criterion is met. This further restricts values of phenomenological coefficients $L_{\mu}, L_q, L_{\mathrm{D}\alpha}, L_{\mu v}, L_{\beta}$ and $L_{q,\mathrm{D}\alpha}, L_{\mathrm{D}\alpha,q}, L_{\mu\beta}, L_{\beta\mu}$.

As an example let us consider homogenous isotropic thermo-visco-elastic material of Hookean type. Then elastic part of stress tensor is given by the Hook's law

$$t^{ij}_{\mathrm{el}} = K e_{(1)} \delta^{ij} + 2G e^{ij}_{(0)} \tag{3.84}$$

where $K$ is the bulk modulus and $G$ is the shear modulus. Employing (3.51), (3.65), (3.77), (3.78) and (3.84) we finally get constitutive relation for homogenous isotropic thermo-visco-elastic material following the Hook's law:

$$\begin{aligned} \tau_{\mathrm{p}} \overset{\cdot}{\overline{t^{ij}}} + t^{ij} &= \tau_{\mathrm{p}} \overset{\cdot}{\overline{t^{ij}_{\mathrm{el}}}} + t^{ij}_{\mathrm{el}} + \tau_{\mathrm{p}} \overset{\cdot}{\overline{t^{ij}_{\mathrm{dis}}}} + t^{ij}_{\mathrm{dis}} \\ &= K \left( e_{(1)} + \tau_{\mathrm{p}} \dot{e}_{(1)} \right) + 2G \left( e^{ij}_{(0)} + \tau_{\mathrm{p}} \overset{\cdot}{\overline{e^{ij}_{(0)}}} \right) + \\ &\quad \frac{\delta^{ij}}{3} \left( L_{\mu} d^{ij} + \sum L_{\mu\beta} A_{\beta} \right) + L_{\mu v} d^{ij}_{(0)}. \end{aligned} \tag{3.85}$$

By experimental methods we usually obtain Young modulus, $E$, and Poisson's ratio, $\upsilon$. Relations between them and parameters $K, G$ are following:

$$E = \frac{9GK}{3K + G}, \tag{3.86}$$

$$\upsilon = \frac{3K - 2G}{2(3K + G)}. \tag{3.87}$$

## 3.4 Chemical Potential of Solids; Clausius-Clapeyron Equation

The relation between the specific entropy of the mixture, $s$, and the specific entropy of each component, $s_\alpha$ ($\alpha = 1, 2, \ldots, r$), can be expressed

$$s = \sum w_\alpha s_\alpha \quad \text{or} \quad \rho s = \sum \rho_\alpha s_\alpha, \tag{3.88}$$

because of

$$w_\alpha := \frac{\rho_\alpha}{\rho}. \tag{3.89}$$

In the Pascal's conception of mixtures ("partial pressure conception")

$$\frac{p}{\rho} = p \sum w_\alpha v_\alpha \quad [\mathrm{J \cdot kg^{-}1}], \tag{3.90}$$

where $p$ is pressure and $v_\alpha$ is a partial volume of component $\alpha$. This concept is sufficient for a mixture of fluids, however, for a mixture of solids Amagat's conception ("partial volume conception") based on the assumption

$$\mathbf{t}_{\mathrm{el}} \mathbf{e} = \mathbf{t}_{\mathrm{el}} \sum \mathbf{e}_\alpha \quad [\mathrm{J \cdot m^{-3}}], \tag{3.91}$$

is more acceptable. Let us recall

$$\mathbf{e}_\alpha = \xi_\alpha \mathbf{e}, \quad \xi_\alpha = \frac{V_{m\alpha}}{M_\alpha}\rho w_\alpha. \tag{3.92}$$

To realize the Amagat's concept we apply the Legendre transformation to change the independent variables (see [11], for instance)

$$u, \mathbf{e}, w_\alpha \Rightarrow T, \mathbf{t}_{\mathrm{el}}, \mu_\alpha, \tag{3.93}$$

and we introduce the Gibbs function $g$

$$g = u - \frac{\mathbf{t}_{\mathrm{el}}\mathbf{e}}{\rho} - Ts \quad \text{i.e.} \quad g = u - \frac{t^{ij}_{\mathrm{el}} e_{ij}}{\rho} - Ts \tag{3.94}$$

and

$$g = \sum w_\alpha \mu_\alpha. \tag{3.95}$$

Material derivative implies

$$\dot{g} = \dot{u} - \frac{t^{ij}_{\mathrm{el}}}{\rho}\dot{e}_{ij} - e_{ij}\overline{\left(\frac{t^{ij}_{\mathrm{el}}}{\rho}\right)^{\cdot}} - T\dot{s} - s\dot{T} \tag{3.96}$$

and

$$\dot{g} = \sum (w_\alpha \dot{\mu}_\alpha + \mu_\alpha \dot{w}_\alpha) \tag{3.97}$$

The right-hand side of (3.96) can be expanded using (3.70):

$$\dot{g} = -s\dot{T} - \frac{e_{ij}\overline{\dot{t^{ij}_{\mathrm{el}}}}}{\rho} + \frac{e_{ij}t^{ij}_{\mathrm{el}}}{\rho^2}\dot{\rho} + \frac{t^{ij}_{\mathrm{el}}}{\rho}(d_{ij} - \dot{e}_{ij}) - T\dot{s}_{\mathrm{N}} + \sum \mu_\alpha \dot{w}_\alpha \tag{3.98}$$

Let us assume the non-equilibrium part of the entropy of mixture in the form

$$\dot{s}_{\mathrm{N}} = \sum w_\alpha \dot{s}_{\mathrm{N},\alpha}. \tag{3.99}$$

Then, after some algebra, by comparison of equations (3.96) and (3.97) we obtain to so called Gibbs-Duham equation for substance $\alpha$ (recall (3.89)):

$$\dot{\mu}_\alpha = -s_\alpha \dot{T} - \frac{e_{ij,\alpha}\overline{\dot{t^{ij}_{\mathrm{el}}}}}{\rho_\alpha} + \frac{e_{ij,\alpha}t^{ij}_{\mathrm{el}}}{\rho_\alpha}\frac{\dot{\rho}}{\rho} + \frac{t^{ij}_{\mathrm{el}}}{\rho_\alpha}(d_{ij,\alpha} - \dot{e}_{ij,\alpha}) - T\dot{s}_{\mathrm{N},\alpha} \tag{3.100}$$

If we neglect non-equilibrium entropy (rapid irreversible processes) in (3.70), the entropy of a mixture of solid materials can be calculated by the equation

$$\dot{s} = \frac{\dot{u}}{T} - \frac{t^{ij}_{\mathrm{el}} d^{ij}}{\rho T} - \sum \frac{\mu_\alpha \dot{w}_\alpha}{T}. \tag{3.101}$$

This equation holds for a mixture (both in equilibrium states and in non-equilibrium states) where equilibrium processes are running, e.g. phase transition processes. These processes are driven by the differences of chemical potentials (3.100) for different $\alpha$.

Consider thermodynamical equilibrium in the mixture, i.e.

$$\dot{s} = 0, \tag{3.102}$$

when system adiabatically isolated and no external forces act

$$T(t) = \text{const.},\ t^{ij}(t) = \text{const.},\ \ i,j = 1,2,3. \tag{3.103}$$

Then (3.101) implies

$$\sum \mu_\alpha \dot{w}_\alpha = 0. \tag{3.104}$$

In the special case of phase transition with 2 components a decrease of one phase must be substituted by an increase of the other, i.e.

$$\mathrm{d}w_1 = \mathrm{d}w_2, \tag{3.105}$$

therefore

$$\mu_1 = \mu_2. \tag{3.106}$$

and for slow isothermal changes (equilibrium process) also holds

$$\dot{\mu}_1 = \dot{\mu}_2. \tag{3.107}$$

With respect to the subject of this thesis, let us consider one-dimensional case of solid-to-solid phase transition between martensite, denoted by $M$, and austenite, denoted by $A$, i.e.

$$\mathbf{e}_\alpha = \begin{pmatrix} \varepsilon_\alpha & 0 & 0 \\ 0 & -\upsilon_\alpha\varepsilon_\alpha & 0 \\ 0 & 0 & -\upsilon_\alpha\varepsilon_\alpha \end{pmatrix}, \quad \mathbf{d}_\alpha = \begin{pmatrix} d_\alpha & 0 & 0 \\ 0 & -\upsilon_\alpha \mathrm{d}_\alpha & 0 \\ 0 & 0 & -\upsilon_\alpha \mathrm{d}_\alpha \end{pmatrix}, \tag{3.108}$$

$$\mathbf{t} = \begin{pmatrix} \sigma & 0 & 0 \\ 0 & 0 & 0 \\ 0 & 0 & 0 \end{pmatrix}, \tag{3.109}$$

$\alpha = M, A$, ($\upsilon_\alpha$ is the Poisson ratio of a component $\alpha$). Then modified (3.100) implies

$$\dot{\mu}_\alpha = -s_\alpha \dot{T} - \frac{\dot{\sigma}\varepsilon_\alpha}{\rho_\alpha} + \frac{\sigma}{\rho_\alpha}\left(d_\alpha - \dot{\varepsilon}_\alpha + \frac{\dot{\rho}}{\rho}\dot{\varepsilon}_\alpha\right) \quad \alpha = M, A. \tag{3.110}$$

The change in density ($\dot{\rho}$) is usually negligible for solids, therefore equation (3.107) takes the form

$$\dot{T}(s_A - s_M) = \dot{\sigma}\left(\frac{\varepsilon_M}{\rho_M} - \frac{\varepsilon_A}{\rho_A}\right) + \sigma\left(\frac{d_A - \dot{\varepsilon}_A}{\rho_A} - \frac{d_M - \dot{\varepsilon}_M}{\rho_M}\right). \tag{3.111}$$

In the case of small deformations, i.e. $\dot{\varepsilon}_\alpha = d_\alpha,\ \alpha = M, A$, we obtain so called Clusius-Clapeyron equation for solid-to-solid phase transition

$$\frac{\mathrm{d}\sigma}{\mathrm{d}T} = \frac{s_A - s_M}{\frac{\varepsilon_M}{\rho_M} - \frac{\varepsilon_A}{\rho_A}}. \tag{3.112}$$

The difference between density of martensite and density of austenite is very small ($< 1\%$), but martensitic phase transition induces great transformation strains, since the crystallographic lattice is deformed (see section 2.1). Hence, for martensitic phase transformation the Clusius-Clapeyron equation has the form

$$\frac{\mathrm{d}\sigma}{\mathrm{d}T} = \frac{\rho\Delta s}{\Lambda}, \tag{3.113}$$

where $\sigma$ denotes (one-dimensional) stress, $\rho$ is density of martensite, $\Delta s := s_A - s_M$ denotes entropy change due to phase transition and $\Lambda = \varepsilon^M - \varepsilon^A$ is (maximum) transformation strain. For experimental reasons, the usual form is

$$\frac{\mathrm{d}\sigma}{\mathrm{d}T} = \frac{\rho h}{T\Lambda}. \tag{3.114}$$

Both transformation heat, $h := T\Delta s$, and transformation strain, $\Lambda$, are well-measurable quantities.

In SMA studies, the Clausius-Clapeyron equation is used to approximate the value of the critical stress inducing the phase transition. From now on, let us assume the entropy change $\Delta s$ is *temperature independent* (at least for reasonable temperature ranges it is well-satisfied assumption). We define

$$s := \frac{\rho\Delta s}{\Lambda} \tag{3.115}$$

and call this value *critical transformation slope*. Critical transformation stress for tensile martensite is then defined

$$\sigma^{\mathrm{cr}}(T) := M_{\mathrm{s}} + s(T - M_{\mathrm{s}}), \quad T \geq M_{\mathrm{s}} \tag{3.116}$$

This equation reflects the experimental observations, in which the uniaxial stress required to induce the martensitic transformation in SMA is (approximately) linearly dependent on the temperature $T$.

Thermodynamical driving force of transformation is usually defined (see next chapters):

$$\varphi := \frac{\sigma}{s} - T + C^{\varphi}, \tag{3.117}$$

where $C^{\varphi}$ is arbitrary constant, stress- and temperature-independent. Thus, driving force is constant for critical stresses. The value of this driving force is further considered to express the actual state (phase composition) of material. The process of reverse transformation from tensile martensite to austenite occurs to some extent also in negative stresses (and similarly for compressive martensite). Hence, the equation (3.116) can be defined even for $T < M_{\mathrm{s}}$ deliberately.

Interesting fact is the tension-compression asymmetry. In compression different value of maximum transition strain $\Lambda$ influence the form of (3.113) and thus the value of parameter $s$ and definition of driving force. That is why in SMAs models driving force for tensile and compressive martensite differs (see chapter 5).

## 3.5 Hysteresis and Return Point Memory in Shape Memory Alloys

As mentioned in chapter 2, an important property of martensitic transformation is hysteresis. From the thermodynamical point of view, hysteretic systems are not in thermodynamic equilibrium. They behave like systems with a rugged free-energy landscape, in which thermal fluctuations are not sufficient to reach the absolute free-energy minimum. Instead, under the external driving, they pass from one relative minimum to another, in a sequence of metastable equilibria. The energy dissipation occurs in the passage from one minimum to another, which often results in large variations of the system response.

Let us summarize the properties of hysteresis in SMAs as decsribed by Ortìn and Delaey in their work [13]. Many properties of hysteresis depend on the relation between two time scales. The intrinsic time scale of relaxation in the system (the typical time taken by the system to reach the nearest relative free-energy minimum) and the time scale at which the system is driven externally. When the time scale of relaxation is comparable to the time scale of driving, hysteresis is a dynamic phenomenon, in which the driving rate plays a major role. On the other extreme, when the time scale of relaxation is negligible in comparison with the time scale of driving, hysteresis is a static phenomenon: the system is almost all the time in a state of metastable equilibrium. In this limit, the driving rate has no influence on branching. The actual behavior of the majority of hysteretic systems, however, is somewhere in between these two limits. This represents an additional difficulty in the theoretical description of hysteresis.

A generic energy balance applies to the macroscopic evolution of the system under an external driving. The balance reads:

$$\frac{\mathrm{d}}{\mathrm{d}t}E_{\mathrm{exin}} = \frac{\mathrm{d}}{\mathrm{d}t}E_{\mathrm{stored}} + \frac{\mathrm{d}}{\mathrm{d}t}E_{\mathrm{dis}}, \tag{3.118}$$

where $E_{\mathrm{exin}}$ is an excess of energy input externally in the system, $E_{\mathrm{stored}}$ represents energy stored in the system and $E_{\mathrm{dis}}$ is energy dissipated. The first term in the equation originates from the driving, and it is positive or negative depending on the direction of driving. The second term is the time rate at which energy is stored or released in the system, and again has no definite sign. In SMA, energy is stored as the elastic strain energy between domains, strain energy due to the interaction with lattice defects, and interfacial energy of the multiple interfaces of the two-phase microstructure. Along a monotonous driving, the energy stored changes non-monotonously, in general, as the multi-domain structure of the material changes. Associated with the changes in stored energy there is energy dissipation, whose rate of change is represented by the third term in the balance. This term is responsible for hysteresis, and it must be always non-negative.

When a cyclic driving is considered, no matter its extension, the closed-contour integration of the first term in the balance gives the area of the hysteresis cycle. That

of the second term is identically zero (since the same multi-domain microstructure is recovered after the cycle), and that of the third term is non-negative. The result is that the cycle can be contoured only in one sense, not in the other, and the area enclosed by the cycle (in the proper coordinates) measures the energy dissipated in the cycle. It implies, the evolution of the energy dissipation as the transformation proceeds in SMA can be derived from the area enclosed by partial cycles. This kind of experiments shows that the energy dissipated increases monotonously with the volume fraction of martensite, $\xi$, approximately as $\xi^2$. The amount of energy dissipated in thermally induced transformations is always small compared to the latent heat of transformation.

The preceding example of cycling dealt with static hysteresis in SMAs, i.e. with dissipative behaviors, which appeared to be independent of time. Although static approximation of hysteresis in SMA is most useful and appropriate in the majority of situations, it should not be forgotten that it corresponds to a limiting case. Time-dependent phenomena associated with ageing, intensive cycling, or large driving rates (unavoidable in certain applications) lead to non-static hysteresis, i.e. to hysteresis cycles which evolve in time, in SMA. However, this phenomena is out of interest of this work and it not considered next.

Lastly, given a physical system or a model displaying hysteresis, Sethna and coworkers have shown rigorously that the RPM effect will hold when the following conditions are fulfilled [14]:

i. The possible states of the system admit a (partial) ordering. The ordering may be only partial because many states do not admit mutual comparison.

ii. The ordering of states is preserved by the dynamics. By this we mean that, from a given initial condition, any monotonous excursion of the driving makes the system go through the same ordered sequence of states.

iii. The dynamics are independent of driving rate, i.e. there is no influence of driving rate on the behavior of the system.

The first condition establishes an ordering of the different possible two-phase microstructures and it is a rather natural condition for domain-forming systems. The second condition is the most restrictive. The behavior of the system must be such that the possible microstructures are obtained in the right order, always the same, upon monotonous drivings. This kind of deterministic and reproducible behavior at the microstructural level has been observed in SMA, both directly through microscopic observations, and indirectly through the reproducibility of the associated acoustic emissions, for example. The third condition emphasizes that thermal fluctuations must be irrelevant, so that the evolution of the system is governed entirely by the driving values, independent of the time rate at which these values are reached. This is the case for SMA which operate via a thermoelastic martensitic transformation, since this transformation is athermal.

# Chapter 4

# Models of Structure Evolution in Shape Memory Alloys

## 4.1 Overview of Modelling Approaches

Mathematical and computational modelling of SMAs represents a certain tool of theoretical understanding of transformation processes and may both complete experimental results and predict response of new materials or applications in engineering workpieces even before made. Effective description of the microstructure in SMAs can be done, depending on a purpose and on available data as well as on computational abilities, at various levels compromising rigor with phenomenology. One of possible classification as proposed by Roubíček in [15] is following:

I. Atomic level: the description counts barycenter of particular atoms and interatomic potentials

II. Microscopic level: continuum mechanics is used to describe deformation, stress, strain, etc. at material points

III. Mesoscopic level: microstructure is described by volume fractions which mix deformation gradients of particular phases, while an averaged deformation is treated by tools of continuum mechanics

IV. Transient level: macroscopic deformation with volume fractions are used to describe configuration at given material point but no specific orientation or anisotropy is recorded (the geometric interaction between grains is often counted)

V. Macroscopic level: all detailed information about the microstructure and spatial dependence of variables are suppressed (lumped parameters approach)

With respect to internal structure, the second and the third levels are appropriate for single crystals modelling, whereas the last two are used in polycrystalline models. Describing the complex characteristics involved in the phase transitions in polycrystalline SMAs have been a significant challenge to researchers. These include modelling

the hardening during phase transition; the asymmetric response that SMAs exhibit in tension and compression; the modelling of detwinning of martensite; complicated thermomechanical paths beyond isobaric or isothermal ones; one-way shape memory effect; the effect of reorientation; the accumulation of plastic strains during cyclic loading; etc. The applications of shape-memory alloys and the need for a design tool have motivated a number of macroscopic constitutive models for these materials. Although the results of the microscopic and mesoscopic approaches give us valuable information how much correct our understanding of the physical principles of involved processes is, from the practical point of view, macroscopic models with several well-defined and well-measurable material variables appear to be the most powerful and successful tools for SMA-products behavior description so far. Their main advantages over other modelling approaches are usually simple numerical implementation, less time-consuming calculations or possibility to simulate wide range of materials and situations (by change of material and fitting parameters) for macroscopic objects.

Macroscopic modeling approaches involve the following two important aspects:

- constitutive relation between stress, strain and temperature,
- the driving force and evolution of phase transformation.

Some models take a thermodynamically consistent approach wherein using the concept of free energy both the constitutive relations and evolution kinetics are derived. However, to arrive at simpler models an independent assumption in the nature of evolution kinetics is sometimes made based on empirical data. An alternative to using internal variables and defining evolution equations not discussed thereinafter are the energy minimization methods.

In general, *thermodynamics based models* use some form of free energy (Gibbs, Helmholtz, etc.) that depends on state and internal variables used to describe the degree of phase transition. The free energy is composed of two parts, temperature dependent chemical part dealing with the entropies of volume fraction of the individual phases and the mechanical part dealing with the stress/strain field due to external loading and the interaction between the various phases. The interaction is due to the strains associated with the phase transformations and can be determined. Thus, using this approach evolution of phase boundaries can be determined. The driving force for the transformation is equated to dissipative terms from interfacial energy and internal friction. This approach is briefly summarized in the next section. (Thermodynamics based models for modelling of polycrystalline SMAs are reviewed in papers by Bo and Lagoudas [16]–[19] in detail.)

A closely related group of models, often referred as *phenomenological* in the literature, separates out the two aspects of modeling mentioned above. The phase evolution and transformation conditions are incorporated using empirically determined $\sigma$-$T$ phase diagram (as used in section 2.2). Subsequently, a constitutive relation that uses the phase fraction derived out of the explicit evolution kinetic is used to describe the ther-

momechanical behavior. This leads to simplified models facilitating their use as design tools.

The macroscopic models do not directly depend on material parameters at the microscopic level, but on a set of parameters at the macroscopic level which are determined by experimental observations. With respect to the topic of this thesis, we will focus on some of these models designed in one-dimensional form.

## 4.2 Macroscopic Models – General Thermodynamic Framework

In this section the general thermodynamic framework developed by Bo and Lagoudas in [16] is briefly reviewed. We restrict ourselves to one-dimensional case without plasticity effects, which correspond to the context of present work.[1]

The main idea is to formulate the mass-specific Gibbs free energy of the SMA polycrystalline material as a weighted sum of the free energies of the austenitic and the martensitic phases plus the free energy of mixing:

$$g(\sigma, T, \xi, \varepsilon^{tr}) = g^A(\sigma, T) + \xi(g^M(\sigma, T) - g^A(\sigma, T)) + g^{\text{mix}}(\sigma, T, \xi, \varepsilon^{\text{tr}}), \tag{4.1}$$

where $g^A$ and $g^M$ are the specific Gibbs free energy of austenite and martensite, respectively, and $g^{\text{mix}}$ is the specific free energy of mixing. $\sigma$ denotes the stress, $T$ the temperature, $\xi$ the volume fraction of martensite and $\varepsilon^{\text{tr}}$ is transformation strain. The following form for the Gibbs energy for both phases is assumed:

$$g^i(\sigma, T) = -\frac{1}{2\rho}\frac{\sigma^2}{E^i} - \frac{1}{\rho}\sigma\alpha^i(T - T_0) + c^i\left[(T - T_0) - T\ln\left(\frac{T}{T_0}\right)\right] - s_0^i T + u_0^i \tag{4.2}$$

with the superscript $i = A$ for austenitic and $i = M$ for martensitic phases, respectively. Here, $\alpha$ is the (linear) coefficient of thermal expansion, $E$ the Young's modulus, $c$ is the specific heat capacity, $s_0$ and $u_0$ denote the specific heat and specific entropy at the reference temperature $T_0$, respectively. Since the martensitic phase transformation is approximately volume conserving, the mass density $\rho$ is supposed to be the same for both phases.

Let us note the definition (4.2) correspond to relation (3.94), if internal energy and entropy are divided to the reference values $u_0, s_0$ and the increment due to specific heat $c$. Moreover, the thermoelastic part of strain is assumed to be linearly dependent on stress (Hook's law) and on temperature (linear thermal expansion).

A wide range of models can be presented within this formulation if the following assumption is made on the mixing term:

$$g^{\text{mix}} = -\frac{1}{\rho}\sigma\varepsilon^{\text{tr}} + f(\xi), \tag{4.3}$$

[1] For a three-dimensional formulation see [20], for instance.

where $f(\xi)$ is a generic function. Combining previous equations, the free energy reduces to the following equation:

$$\begin{aligned} g(\sigma, T, \xi, \varepsilon^{\mathrm{tr}}) = \; & -\frac{1}{2\rho} S(\xi)\sigma^2 - \frac{1}{\rho}\sigma\left[\alpha(\xi)(T - T_0) + \varepsilon^{\mathrm{tr}}\right] \\ & + c(\xi)\left[(T - T_0) - T\ln\left(\frac{T}{T_0}\right)\right] - s_0(\xi)T + u_0(\xi) + f(\xi). \end{aligned} \tag{4.4}$$

Effective material properties $S(\xi), \alpha(\xi), c(\xi), s_0(\xi), u_0(\xi)$ were calculated in terms of the martensitic volume fraction using the rule of mixtures:

$$S(\xi) := \frac{1}{E^A} + \xi\left(\frac{1}{E^M} - \frac{1}{E^A}\right) = \frac{1}{E^A} + \xi\Delta S \tag{4.5}$$

$$\alpha(\xi) := \alpha^A + \xi(\alpha^M - \alpha^A) = \alpha^A + \xi\Delta\alpha \tag{4.6}$$

$$c(\xi) := c^A + \xi(c^M - c^A) = c^A + \xi\Delta c \tag{4.7}$$

$$s_0(\xi) := s_0^A + \xi(s_0^M - s_0^A) = s_0^A + \xi\Delta s_0 \tag{4.8}$$

$$u_0(\xi) := u_0^A + \xi(u_0^M - u_0^A) = u_0^A + \xi\Delta u_0 \tag{4.9}$$

Note that (4.5) corresponds to the so-called *Reuss formula* for elastic modulus

$$\frac{1}{E} = \frac{\xi}{E^M} + \frac{1 - \xi}{E^A}. \tag{4.10}$$

This expression is used when it is assumed the phase transformations occur by nucleation and growth of platelet inclusions, mainly directed in the imposed stress direction. In this conception each part of wire is either in martensitic or austenitic phase in the whole cross section. Another formula, *Voigt expression*, can be obtained regarding the material as composed by strips of austenite and martensite parallel to the direction of the stress:

$$E = \xi E^M + (1 - \xi)E^A. \tag{4.11}$$

However, experimental evidence shows that the assumption of strips parallel to the stress direction is not quite realistic (in the case of uniaxial loading).

Further, general flow rule for transformation strain is usually assumed to have the type:

$$\varepsilon^{\mathrm{tr}}(\xi) = \Lambda\xi, \tag{4.12}$$

where $\Lambda$ is one-dimensional $\xi$- and time-independent transition tensor (i.e. scalar) corresponding to maximal transformation strain, thus the Gibbs free energy is a function of three independent state variables: $\sigma, T$ and $\xi$.

The evolution equation for martensitic volume fraction can be obtained systematically by introducing a dissipation potential in conjunction with the second law of thermodynamics. By performing standard calculations, the strong form of the second law of thermodynamics can be written in the following form for the local internal dissipation rate:

$$T\dot{\eta} = -\left(\varepsilon + \rho\frac{\partial g}{\partial \sigma}\right)\dot{\sigma} - \rho\left(s + \frac{\partial g}{\partial T}\right)\dot{T} - \rho\frac{\partial g}{\partial \xi}\dot{\xi} \geq 0, \tag{4.13}$$

where $\varepsilon$ is the total strain, $s$ is the total entropy, and $\dot{\eta}$ is the local dissipation rate which does not include the entropy production rate due to heat conduction.

Next, standard thermodynamics arguments (as used in section 3.3) are employed to obtain the following set of constitutive equations by identically satisfying inequality (4.13):

$$\varepsilon = -\rho\frac{\partial g}{\partial \sigma}, \tag{4.14}$$

$$s = -\frac{\partial g}{\partial T}, \tag{4.15}$$

$$-\rho\frac{\partial g}{\partial \xi}\dot{\xi} \geq 0. \tag{4.16}$$

Usually the thermodynamic force $\pi$ conjugate to $\xi$ is introduced

$$\pi := -\rho\frac{\partial g}{\partial \xi}. \tag{4.17}$$

The flow rule (4.12) then implies:

$$\begin{aligned}\pi = \ & \frac{1}{2}\Delta S\sigma^2 + \sigma\left[\Delta\alpha(T-T_0)+\Lambda\right] \\ & -\rho\Delta c\left[(T-T_0) - T\ln\left(\tfrac{T}{T_0}\right)\right] + \rho\Delta s_0(T-T_0) - \rho\Delta u_0 - \rho f'(\xi).\end{aligned} \tag{4.18}$$

Note if we neglect some less significant terms in the last equation (Hook's elasticity, thermal expansion, heat capacity, derivative of generic function) we obtain

$$\pi \approx \Lambda\sigma + \rho\Delta s_0 T + C, \tag{4.19}$$

where $C$ is stress- and temperature-independent constant. This after rescaling leads to definition of driving force $\varphi$ (3.117).

By evaluating (4.14) we obtain constitutive equation with three contributions to the total strain – elastic, thermal and transformation:

$$\begin{array}{rcccccc}\varepsilon & = & S(\xi)\sigma & + & \alpha(\xi)(T-T_0) & + & \Lambda\xi \\ & = & \varepsilon^{\mathrm{el}} & + & \varepsilon^{\mathrm{th}} & + & \varepsilon^{\mathrm{tr}}.\end{array} \tag{4.20}$$

The phase transformation criterion can be written using the following Kuhn-Trucker conditions (see [21] for details)

$$\Phi \leq 0, \tag{4.21}$$

$$\Phi\dot{\xi} = 0, \tag{4.22}$$

where the transformation function $\Phi$, which separates the thermoelastic response region from the transformation region, is given by

$$\Phi = \begin{cases} \pi - Y, & \dot{\xi} > 0, \\ -\pi - Y, & \dot{\xi} < 0. \end{cases} \tag{4.23}$$

The non-negative material constant $Y$ is a measure of the internal dissipation due to microstructural changes during the phase transformation. Since $\dot{\xi} \neq 0$ during the transformation process, equation (4.22) implies

$$\Phi = 0, \tag{4.24}$$

when transition proceeds. Next, (4.23) and (4.24) give

$$\dot{\Phi} = \pm\dot{\pi} = 0 \tag{4.25}$$

during the transition, which is used by some authors for determination of martensite evolution laws.

Using equations (4.13) and (4.24), the total internal dissipation (hysteresis) during a complete forward and reverse phase transformation cycle is given by term

$$\oint T \,\mathrm{d}\eta = \oint \pi \,\mathrm{d}\xi = \int_0^1 Y \,\mathrm{d}\xi + \int_1^0 (-Y) \,\mathrm{d}\xi = 2Y. \tag{4.26}$$

To complete the constitutive model, the generic function of mixing $f(\xi)$ in the term (4.3) needs to be defined. The most general assumption is that it is different for the forward and reverse transformation

$$f(\xi) = \begin{cases} f^M(\xi), & \dot{\xi} > 0, \\ f^A(\xi), & \dot{\xi} < 0. \end{cases} \tag{4.27}$$

and the particular choice of $f(\xi)$ is governed by experimental observations. Depending on the chemical composition, heat treatment, mechanical training, etc., different choices have been made in literature.

Review of the existing thermodynamic and free energy based models can be found in paper [20] (see also [22]), some of the most significant ones are briefly introduced in section 4.4.

## 4.3 Macroscopic Models – Hysteresis Subloops

Although a transition hysteresis mechanism must be involved in each SMA model, the way it simulates partial cycles and internal subloops may be inaccurate or even incorrect, since in these cases RPM effect plays the major role.

The dissipative mechanisms responsible for hysteresis are operative at many different spatial scales [13]: at a *microscopic scale*, both the nucleation of the new phase and the interaction of interfaces with defects (dislocations, vacancies) contribute to hysteresis; at a *mesoscopic scale*, sources of hysteresis are the formation, annihilation and rearrangement of elastically interacting domains; at a *macroscopic scale*, the problem of heat transfer within the material, and between the material and the surroundings, has an effect on hysteresis. At the present stage of knowledge, the procedures to go from one scale of description to the next one are not well established. Here, we will

focus on a phenomenological approach to modeling of hysteresis aiming to macroscopic description of the thermomechanical behavior of SMA, including dissipative effects, and briefly summarize three often referred hysteresis models. More extensive review can be found in [19] for instance.

From now on the partial cycles and internal subloops are termed as *minor (hysteresis) loops*, whereas the hysteresis loop established by completed forward and reverse transformation is referred as *major (hysteresis) loop*.

The principle of mathematical models is shown for the case the driving variable is thermodynamic driving force $\varphi$, the driven variable is volume fraction $\xi$, i.e. "$\varphi$-$\xi$ process". However, this can be easily transformed to other hysteresis cases, e.g. "$T$-$\xi$ process" ($\sigma$ kept constant) or "$\sigma$-$\varepsilon$ process" ($T$ kept constant).

### 4.3.1 Thermomechanics-Based Models

This group of models is based on the theory of continuum thermomechanics. It covers most of existing constitutive models for polycrystalline SMAs, at least all described in the next section. These models emphasize the transformation hardening behavior of SMAs during major loop phase transformation. The thermomechanical response under minor hysteresis loops is not studied in detail. It is usually assumed in these models that the transformation criterion, such as the one given by equation (4.22), remains the same for both major and minor hysteresis loops. Consequently, a minor hysteresis loop will be part of the major one, the segment being decided by the loading path. The results indicate that the assumption of minor hysteresis loops being part of the major one is not valid and thus this model do not simulate the minor hysteresis loops appropriately.

An attempt to modify this approach was done by Bo and Lagoudas in [19]. Their paper reveals that the macroscopic energy dissipation per unit volume of transforming SMA is the average energy dissipation of all single crystals that transform in the same loading step and it is concluded that the amount of energy dissipation during minor loop phase transformation cycles should be variable (compare with (4.26)). An evolution equation of that energy dissipation is proposed. (The wiping out property for the model is similar to that of the Preisach model.)

### 4.3.2 Duhem-Madelung Hysteresis Model

A simple way to improve the minor loop predictions, given by the thermomechanical model discussed above, is to introduce the Duhem-Madelung hysteresis model into the present formulation. This model was introduced to model minor hysteresis loops of SMAs by Ivshin and Pence in [23]. In their paper the state equation of martensitic volume fraction for minor hysteresis loops is related to the expression of the martensitic volume fraction for the major hysteresis loop. If $t_k$ indicate the last $\varphi$-reversal time for forward transition, then $\varphi(t)$ is non-increasing after $t_k$ (until a new reversal in $\varphi(t)$

evolution) and:

$$\xi(\varphi(t)) = \frac{\xi(t_k)}{\xi_{\max}(\varphi(t_k))}\xi_{\max}(\varphi(t)), \tag{4.28a}$$

If $t_j$ indicate the last $\varphi$-reversal time for reverse transition, then $\varphi(t)$ is non-decreasing after $t_j$ (until a new reversal in $\varphi(t)$ evolution) and:

$$\xi(\varphi(t)) = 1 - \left\{\frac{1-\xi(t_j)}{1-\xi_{\min}(\varphi(t_j))}\right\}[1-\xi_{\min}(\varphi(t))]. \tag{4.28b}$$

In the above, $\xi_{\min}$ and $\xi_{\max}$ ($\xi_{\min}(\varphi) \leq \xi_{\max}(\varphi)\ \forall\varphi$) are the martensite volume fraction for the lower branch of the major hysteresis loop and the upper branch of the major hysteresis loop, respectively. Both $\xi_{\max}$ and $\xi_{\min}$ are functions of driving force $\varphi$. A geometric interpretation of (4.28a) and (4.28b) is that the current minor hysteresis loop curve $\xi$ is self-similar to the major hysteresis loop with the scaling factor $\xi(t_k)/\xi_{\max}(\varphi(t_k))$ and $[1-\xi(t_j)]/[1-\xi_{\min}(\varphi(t_j))]$, respectively.

Note that both Duhem-Madelung hysteresis model as introduced by Ivshin and Pence and the thermomechanical hysteresis model discussed in the previous subsection have local memory, i.e., the behavior of the current minor loop depends only on the latest reversal point, and the loading history prior to the reversal point has no influence on the present minor hysteresis loop. It means these models do not capture the RPM effect. In the case of Duhem-Madelung model the internal subloops are not usually closed, which reminds time-dependent hysteresis (described in section 3.5). On the other side, this model succeeds in partial cycles modeling, especially when minor hysteresis loops are located at the middle of the major hysteresis loop. A possible extension covering the RPM effect was introduced by Bouvet et al. in a superelasticity model [24]. When establishing internal subloop, model of Bouvet does not projects the whole major loop (as in (4.28)), but only its part with respect to the nearest return point. This useful concept is adopted by iRLOOP model and thus described in chapter 5 rigorously.

### 4.3.3 Preisach Hysteresis Model

The main idea for the Preisach model is that the material to be modeled is assumed to be composed of an infinite number of simple hysteresis relays. Each hysteresis relay is represented mathematically by a hysteresis operator, $\gamma_{\alpha\beta}$. There is a weighting distribution function, $\mu(\varphi_\alpha, \varphi_\beta)$, associated with each hysteresis relay. The input can be taken to be the transition driving force, $\varphi(t)$, where $t$ is time. The output is volume fraction, $\xi$, in that case. Since $\xi$ can only take a value between 0 and 1, the hysteresis operator $\gamma_{\alpha\beta}$ is selected to have two states either 0 or 1 (in usual definition it takes a value either $-1$ or 1). Given an input history $\varphi(t)$, the output $\xi(t)$ can be obtained by counting how many relays are in state 1. Mathematically, this counting process can be written in the limit by the following integral

$$\xi[\varphi(t)] = \int\int_{\varphi_\alpha \geq \varphi_\beta} \mu(\varphi_\alpha, \varphi_\beta)\gamma_{\alpha\beta}\varphi(t)\,\mathrm{d}\varphi_\alpha\,\mathrm{d}\varphi_\beta. \tag{4.29}$$

In the above, the square brackets indicate that $\xi$ is a functional of the temperature history. A key issue for the application of the model to describe a specific material is to determine the distribution function $\mu(\varphi_\alpha, \varphi_\beta)$. A systematic way to obtain it numerically has been established using experimental data (see [6], for instance). However, the process of distribution function determination needs a relatively great number of experiments.

## 4.4 Macroscopic Models – Examples

Following several models were developed in one dimension and capture the main characteristics of SMAs.

Prominent among them is the model developed by Tanaka in 1986, who was among the first to use phenomenological approach for SMA to study superelasticity with martensitic fraction $\xi$ as an internal variable. In his work [25], he used strain and temperature as the control variables and derived a simple constitutive relation similar to equation (4.20). The generic function of mixing was defined as follows:

$$\begin{aligned} f^M(\xi) &= k_1^{\mathrm{T}}[(1-\xi)\ln(1-\xi)+\xi] + c_1^{\mathrm{T}}\xi, \\ f^A(\xi) &= k_2^{\mathrm{T}}[\xi\ln(\xi)-\xi] + c_2^{\mathrm{T}}\xi, \end{aligned}$$

where $k_1^{\mathrm{T}}, k_2^{\mathrm{T}}, c_1^{\mathrm{T}}$ and $c_2^{\mathrm{T}}$ are material parameters dependent constants. Using equation (4.25), the exponential hardening rule for martensite evolution was deduced.

Cycling, transformation induced plasticity and effect of the prior incomplete transformation on the subloops were the topics to be further investigated by Tanaka and co-workers with this model in [26] or [27]. (The local residual stress, local residual strain and the volume fraction of the martensite phase which takes no part in the subsequent transformations, were introduced as the internal variables there, in order to characterize the microscopic processes occurring in the alloys during cyclic loading.)

Tanaka's model was also adapted by Liang and Rogers in [28] and Brinson in [29]. To obtain a better fit to the experimental data, Liang and Rogers modified the phase kinetic to a cosine based function, which means the generic function is chosen as follows:

$$\begin{aligned} f^M(\xi) &= \int_0^\xi (-k_1^{\mathrm{LR}})[\pi - \arccos(2\zeta-1)]\,\mathrm{d}\zeta + c_1^{\mathrm{LR}}\xi, \\ f^A(\xi) &= \int_0^\xi (-k_2^{\mathrm{LR}})[\pi - \arccos(2\zeta-1)]\,\mathrm{d}\zeta + c_2^{\mathrm{LR}}\xi, \end{aligned}$$

where $k_1^{\mathrm{LR}}, k_2^{\mathrm{LR}}, c_1^{\mathrm{LR}}$ and $c_2^{\mathrm{LR}}$ are material dependent constants. However, since reorientation processes are not concerned, this model does not properly capture the material response at temperatures below the martensite start temperature.

Based on the broad framework of Tanaka and Liang and Rogers, Brinson proposed a modified model to also account for the shape memory effect [29]. The essential difference in Brinson's model is splitting the martensitic phase fraction into two parts, temperature induced twinned fraction ($\xi^{\mathrm{t}}$) and stress induced detwinned fraction ($\xi^{\mathrm{d}}$), which

contributes to the transformation strain. This differentiation of the phase fractions is necessary to capture recovery stress/strain. To describe the constitutive behavior, Brinson derived the constitutive model with non-constant elastic stiffness during MT, which has been further refined by Bekker and Brinson (see [2], [30]). The phase diagram is divided into "active zones", where transitions occur, and "dead zones", where martensite fraction does not change. Every loading process is represented by a trajectory in the diagram and the intensity of transition process depends on the tangential vector of the path. The driving equation is chosen in "switching points", where transformation process starts or finishes. The generic mixing term function $f(\xi)$ has similar form as was used by Liang and Rogers and lead to a simple cosine hardening law. When cyclic partial loading simulated (Duhem-Madelung hysteretic model incorporated), staircase transformation paths that lie outside of major loop are obtained. This behavior is inconsistent with the RPM effect. Although the Brinson's constitutive model was used extensively in the literature to model SMA material and devices ([2], [30] and others), recently Buravalla and Khandelwal highlighted an inconsistency in it (see their work [22]).

The similar approach to the one presented by Bekker and Brinson could be found in the model proposed by Govindjee and Kasper in [31]. It is assumed that during the martensitic phase transformation two different "martensitic variants" (corresponding volume fractions denoted as $\xi^+$ and $\xi^-$) may form, depending on the sign and magnitude of the applied loading (tension/compression asymmetry). In addition, if the material is cooled in stress-free condition, both variants form simultaneously, resulting in zero macroscopic transformation strain. Further mechanical loading will result in growth of one martensitic variant at the expense of the other, thus producing observable macroscopic transformation strain in the direction of the loading. The modified constitutive relation (4.20) involves plasticity strain. This model can be classified as a phase diagram based. For each involved transition the start and finish boundary lines $\sigma$-$T$ phase diagram are established and the value of martensitic volume fraction in these "transformation zones" is driven by linear evolution rule. Thanks to dividing martensite to two parts ("tension and compression variants"), effects of detwinning and reorientation, pseudoplasticity as well as one-way shape memory effect could be simulated. (Moreover, plasticity effects are considered by introducing irreversibly deformed part of $\xi$ inactive in further processes.)

One of often referred models based on $\sigma$-$T$ phase diagram is that developed by Auricchio in [32]. There are three different phases (austenite, single-variant martensite and multiple-variant martensite) introduced and mutual transformations (including reorientation process) in the "transformation zones" are driven with exponential flow rule similar to the one used by Tanaka. Superelasticity and one-way shape memory effect are modeled in one dimension, but the model was also extended to three dimensions. Auricchio's model was implemented in finite element method algorithm and a lot of favorable simulations were conducted (e.g. [33], [34], etc.).

One of the latest model was suggested by Sadjadpour [35] in 2006 and it is pre-

sented both in one-dimensional and in three-dimensional version. Since only $\xi$ can not differentiate microstructures of martensite, the second internal variable, effective transformation strain of the martensite $\varepsilon^M$, is introduced. Although Sadjadpour uses basic principles of thermodynamics, the evolution law for $\xi$ is empirical and does not correspond to the concept described in the previous section. The effective transformation strain increment is linearly dependent on stress $\sigma$. Since the rate dependent non-proportional loading, tension-compression asymmetry, influence of texture in polycrystals and general plasticity are concerned, the model becomes rather complex.

As an example of a (phenomenological) one-dimensional model let us summarize the RLOOP algorithm for simulation of rate independent hysteretic responses of SMA in cyclic uniaxial thermomechanical loads developed by Šittner et. al. in 2000 and described in [36]. The algorithm is proposed in a compact differential form that uses ten well defined material parameters and is adjustable to a particular alloy by fitting a single experimental pseudoelastic loop. It has been developed as a tool for predictions of history dependent uniaxial $\sigma$-$\varepsilon$-$T$ responses of SMA elements to be embedded into the smart structures and composites.

The material parameters characterizing the SMA element are elastic modulus of martensite, $E^{\mathrm{M}}$, and elastic modulus of austenite, $E^{\mathrm{A}}$, measured at reference temperatures $T^{\mathrm{M}}_{\mathrm{ref}}$ and $T^{\mathrm{A}}_{\mathrm{ref}}$; temperature- and phase-independent coefficient of linear thermal expansion, $\alpha$; (maximum) transformation strain, $\Lambda$; martensite and austenite start temperature, $M_{\mathrm{s}}$, $A_{\mathrm{s}}$ respectively; slope $s$ of the temperature dependence of transformation start stresses, $\sigma^{\mathrm{tr}}$, in tensile pseudoelastic tests above austenite finish temperature, $A_{\mathrm{f}}$; reorientation stress, $\sigma^{\mathrm{re}}$, observed as yield stress in tensile tests below martensite finish temperature, $M_{\mathrm{f}}$. The Young's modulus of the SMA, $E(\xi, T)$, is calculated from the martensite and austenite moduli, each of them linearly dependent on the temperature with characteristic rates $RE^{\mathrm{M}}$ and $RE^{\mathrm{A}}$ (compare with equation (4.11)):

$$E(\xi, T) = \xi[E^{\mathrm{M}} + RE^{\mathrm{M}}(T - T^{\mathrm{M}}_{\mathrm{ref}})] + (1 - \xi)[E^{\mathrm{A}} + RE^{\mathrm{A}}(T - T^{\mathrm{A}}_{\mathrm{ref}})]. \tag{4.30}$$

Complex hysteretic SMA behavior is supposed to be derived from the knowledge of the evolution function for martensite phase fraction $\xi = \xi(\sigma, T, history)$ as a function of stress, temperature and history. The evolution function is assumed to be rate independent in agreement with the approximation of the rate independence of energy dissipation in SMAs.

Šittner and co-workers assumed an existence of a general thermomechanical driving force on the MT when constructing a governing kinetics equation for the evolution martensite phase fraction $\xi$. The martensite phase fraction rate, $\dot{\xi}$, is supposed to be a function of an internal variable $\varphi$:

$$\varphi = T - \frac{\sigma}{s}, \tag{4.31}$$

and its rate

$$\dot{\varphi} = \dot{T} - \frac{\dot{\sigma}}{s}, \tag{4.32}$$

combining the effects of temperature and applied uniaxial stress on the MT in accord with the Calusius-Clapeyron equation (compare with (3.117)). An equilibrium between austenite and martensite phases under stress is assumed to exist when

$$T - \frac{\sigma}{s} - T_0(\xi) = 0. \tag{4.33}$$

$T_0(\xi)$ denotes an "effective equilibrium temperature", which is assumed to be linearly dependent on the martensite volume fraction $\xi$ according to equation

$$T_0(\xi) = (1-\xi)M_\mathrm{s} + \xi A_\mathrm{s}. \tag{4.34}$$

(Equation (4.33) correspond with (4.18) if some less significant terms except of derivative of generic function $f'(\xi)$ (connected with $T_0(\xi)$) are neglected and equation is rescaled. Also (4.25) with this rescaled driving force is satisfied.)

Term $\varphi - T_0$ quantifies the thermomechanical driving force both on the forward transformation (i.e. when austenite transforms into martensite) and on the reverse transformation. The equilibrium exists when driving forces on forward and reverse MT are equal, i.e. only if $\varphi - T_0 = 0$ as given by (4.33). Note that, according to this definition, the forward transformation may proceed equally well upon cooling or heating. Such defined thermomechanical driving force depends on the uniaxial stress, temperature and history and does not differentiate between the stress-induced and thermally-induced martensitic transformations.

The unknown evolution function $\xi = \xi(\varphi)$ is searched as a solution of two proposed differential equations governing the kinetics of the forward ($\dot{\varphi} < 0$) and reverse ($\dot{\varphi} > 0$) transformations:

$$\dot{\varphi} < 0: \quad \dot{\xi} = c\frac{G}{s}\xi^l(1-\xi)^{m+n}\mathrm{e}^{-G(\varphi - T_0)}\dot{\varphi}, \tag{4.35a}$$

$$\dot{\varphi} > 0: \quad \dot{\xi} = c\frac{G}{s}\xi^{l+n}(1-\xi)^{m}\mathrm{e}^{G(\varphi - T_0)}\dot{\varphi}, \tag{4.35b}$$

(Note the evolution is not driven by (4.25) with rescaled driving force (4.33) in this case.) In addition to the four material parameters $(M_\mathrm{s}, A_\mathrm{s}, s, \sigma^\mathrm{re})$, there are five fitting constants $G, c, n, l$ and $m$ introduced. Their values are determined by fitting the algorithm to a single experimental $\sigma$-$\varepsilon$ pseudoelastic curve to yield solutions featuring correct hysteresis width and further features of the simulated thermomechanical responses.

Equations (4.35a) and (4.35b) are mutually switched on/off whenever the rate of the thermomechanical driving force $\dot{\varphi}$ changes its sign. There is a discontinuity of the $\dot{\xi}, \dot{\varphi}$ time derivatives in the return points, therefore $\dot{\xi}$ is arbitrarily set to zero there. Current values of the $\xi$ at the return points are taken over by the newly activated differential equation, whose solution contains the previous RP. This roughly constitutes the unique memory mechanism built in the algorithm, which is different from the ones summarized in the previous section, but specific for proposed governing equations.

Besides, the ideal transformation deformability is supposed, which means that any deformation mechanisms considered are rate independent and that other deformation

mechanisms as the plastic strains due to dislocation slip, fracture and/or any time dependent phenomena are neglected. The macroscopic uniaxial strain of the transforming SMA element hence consists of its elastic, $\varepsilon^{\mathrm{el}}$, thermal, $\varepsilon^{\mathrm{th}}$, and transformation, $\varepsilon^{\mathrm{tr}}$, strain parts, respectively, according to constitutive equation (compare with (4.20))

$$\dot{\varepsilon} = \frac{\dot{\sigma}}{E(\xi, T)} + \alpha \dot{T} + \Lambda \tanh\left(k_1 \frac{\sigma}{\sigma^{\mathrm{re}} - k_2}\right) \dot{\xi}. \tag{4.36}$$

The transformation strain $\varepsilon^{\mathrm{tr}}$ sharply decreases towards zero if the simulated transformation proceeds at stresses $\sigma < \sigma^{\mathrm{re}}$. This is achieved by including the hyperbolic tangent function fitted by coefficients $k_1$ and $k_2$ into the third term of equation (4.36). The hyperbolic tangent function was picked up just because it can be well parametrized by the $\sigma^{\mathrm{re}}$ to reach the required effect. The transformation strain $\varepsilon^{\mathrm{tr}}$ thus vanishes, even if the martensite fraction $\xi = 1$, when MT is induced only thermally ($\sigma = 0$).

Although the algorithm has been primarily designed to simulate the inelastic strains due to the thermomechanically induced MT, the inelastic strains appearing upon tensile loading in the martensitic state and thermal loading under very low stresses $\sigma < \sigma^{\mathrm{re}}$ are formally considered by observing special boundary conditions on the internal variable $\varphi$ in the case $T \leq M_{\mathrm{s}}$. Then the mathematical formalism developed for martensitic transformation is applied to the description of pseudoplastic deformation at low temperatures $T \leq M_{\mathrm{s}}$, where physically different deformation processes take place. Such approach, although useful for quantitative results, is incorrect in terms of the physical principles.

In numerical implementation (e.g. finite element method) the actual temperature of the SMA wire element and its actual strain instead of imposed stress is prescribed. Also in various experiments and practical applications "strain driven" process is involved. In that case implicit formula (4.36) for $\sigma$ must be solved with respect to equations (4.31) and (4.35). The model RLOOP was numerically implemented and various simulations (uniaxial superelastic tests, cyclic thermal load tests, one-way SME tests, recovery stress tests, etc.; see [36], [8]) for SMA wires were conducted. In work [37] the model was upgraded (the version called RCLOOP) to capture SMA-polymer composites thermomechanical behavior.

Although RLOOP is successful in thin wires thermomechanical tests modelling, some difficulties significant for its further development have revealed. Since differential formulas (4.35a) and (4.35b) are not analytically integrable, numerical solution is needed. The argument of exponential function may vary in a wide range of values dependent on actual $\sigma$ and $T$, which can make error control problematic. In the strain driven process discretized algorithm is unable to meet integration tolerances without reducing the step size to the smallest value allowed. In more complex geometrical structures enormous computational time would be spend and modelling would be ineffective. As mentioned above, the pseudoplasticity modelling is covered incorrectly by the algorithm and the system becomes hardly expandable to complex $\sigma$-$\varepsilon$-$T$-space description to be able to capture compression behavior, R-phase transition or one-way SME. All these problems have lead to development of program iRLOOP.

# Chapter 5

# iRLOOP

In the first chapter the unique properties of shape memory alloys were described. Since invention of NiTiNOL there has been considerable effort to utilize these properties in applications. Thin wires are especially suitable for significant part of possible applications as intervascular stents, medical devices or actuators; they can be easily incorporated to textile fibres or embedded in composites, etc. They are easy to be produced at reasonable price and their metallurgical production and processing is quite well established. However, development of new products by repeated production and testing of prototypes could be expansive and time-consuming, thus quite ineffective. That is why for proper post-processing treatment and design purposes robust and stable computational model capable of reliable reproducing the complex SMA behavior, which could be easily implemented to finite element models, is highly desired.

First of all, model must be capable to simulate superelasticity, because it is of great importance for most of thin wires applications. In fact, practically used SMA elements work typically in partial cycles, so it is a very good test of the engineering applicability of any SMA model, to inspect, whether it is capable to reproduce the hysteresis and partial subloops features in thermal, mechanical and particularly in thermomechanical loads. Since strain connected with R-phase transition affects mechanical behavior of SMAs, incorporating of multiple transition mechanisms including R-phase is necessary for modelling products operating in R-phase transition temperatures. Next important step is to involve martensite reorientation process, which enables us to simulate pseudoplasticity and one-way shape memory effect. The above described processes occur in also compression (negative stress values), which is involved in bending of wires, thus it tension-compression asymmetry must be concerned for correct finite element method implementation. Since shape memory alloys are functional materials, made for the functions they do, instability and fatigue of their functional properties is important for safe design of structures containing them.

## 5.1 Introduction

Although the earlier elaborated uniaxial RLOOP model captures well the mechanical behavior of straight NiTi wires in tensile thermomechanical tests including partial internal cycles, it is fairly unsuitable for further development particularly since it could not have been easily numerically implemented in FEM codes. This lead to the idea to develop a new model inspired by integral form of the RLOOP model.

The new model should:

- keep the concept of thermodynamic force linking stress and temperature, which drives the transformation processes,
- reliably describe both entire and partial martensite to austenite and reverse transformation processes with partial cycles and internal subloops equally well as RLOOP model,
- capture the strains due to multiple deformation mechanisms taking place in NiTi transforming through austenite $\rightarrow$ R-phase $\rightarrow$ martensite sequence,
- capture reorientation processes taking place in martensite phase,
- capture asymmetric behavior in tension and compression,
- be able to be driven by prescribed evolution of strain and temperature of a wire,
- be able to adapt to particular material by changing several experimentally well-measurable input parameters,
- be implementable into finite element models by a relatively simple way.

The most important SME found by experiments – superelasticity, pseudoplasticity, one-way SME, RPM (hysteretic subloops) and R-phase transition, all both in the case of tension and compression – are based on these requirements, thus fulfilling them ensure the effects are included in the model. On the other side, fatigue, stability of mechanical properties and cyclic training are connected with plasticity effects, thus could not be simulated when only above requirements are concerned.

With intension to satisfy the requirements, a new phenomenological one-dimensional model was developed at Institute of Thermomechanics and Institute of Physics, Academy of Sciences of the Czech Republic. It was called iRLOOP and it is extensively described in this chapter. Thermomechanical behavior is rather complex, so the model was constructed gradually, each stage expanded the previous one. First, superelastic behavior with R-phase contribution, partial cycles and return point memory effect were modeled. Next, pseudoplasticity, reorientation process and thus also one-way SME in tension were added. So far latest proposed model connects all previous effects to complex tension-compression algorithm. Each step is described in its own section.

As emphasized in previous text, the evolution of SMA element is not determined only by actual values of state variables, but strongly depends on thermomechanical history of material. The proposed algorithm follows this experimental fact and we suppose the initial conditions including history and the trajectory in $\sigma$-$T$ plane uniquely determine the evolution of state of SMA material at any point of the curve. Let us define an internal time $t$, which is a non-negative real variable

$$t \in \mathbb{R}_0^+ := \langle 0, +\infty). \tag{5.1}$$

The algorithm is rate independent, which means computed values of strains are independent on time rescaling. The input is supposed to be prescribed evolution of state variables stress $\sigma(t)$ and temperature $T(t)$, where

$$\sigma(t) : \mathbb{R}_0^+ \to \mathbb{R}, \quad \sigma(t) \in \mathcal{C}^1(\mathbb{R}_0^+) \tag{5.2}$$

$$T(t) : \mathbb{R}_0^+ \to \mathbb{R}^+, \quad T(t) \in \mathcal{C}^1(\mathbb{R}_0^+) \tag{5.3}$$

(thermodynamically reachable temperature is a real positive value; $\mathcal{C}^1(\mathbb{R}_0^+)$ denotes (space of) continuously differentiable functions defined for non-negative real numbers). Time evolution of functions $\sigma(t), T(t)$ uniquely establishes a trajectory in $\sigma$-$T$ space. It remains to properly introduce initial conditions with respect to thermomechanical history of material. This could be rather problematic for states when the material is partially transformed (experimental determining of $\xi$, description of history). Thus, for simplicity we suppose the element of material is in pure austenitic state just after completed transition, no loading is imposed and material has "no thermomechanical history" (in the sense of RPs as defined next) at the beginning of computational process $t = 0$, i.e.

$$\begin{aligned} &T(0) = A_\mathrm{f}, \\ &\sigma(0) = 0, \end{aligned} \tag{5.4}$$

This assumption is not restrictive, since any other possible physical state of material can be reached by thermomechanical loading arising from this initial state.

Let us also define a real closed unit interval

$$I := \langle 0, 1\rangle. \tag{5.5}$$

## 5.2 Superelasticity Model

### 5.2.1 Physical Model

In this section we concentrate on the part of $\sigma$-$T$ phase space marked with yellow color on figure 5.1, we suppose $\sigma \geq 0$ and

$$T \geq S_\mathrm{s} := A_\mathrm{f} + \frac{\sigma^\mathrm{re}}{s}. \tag{5.6}$$

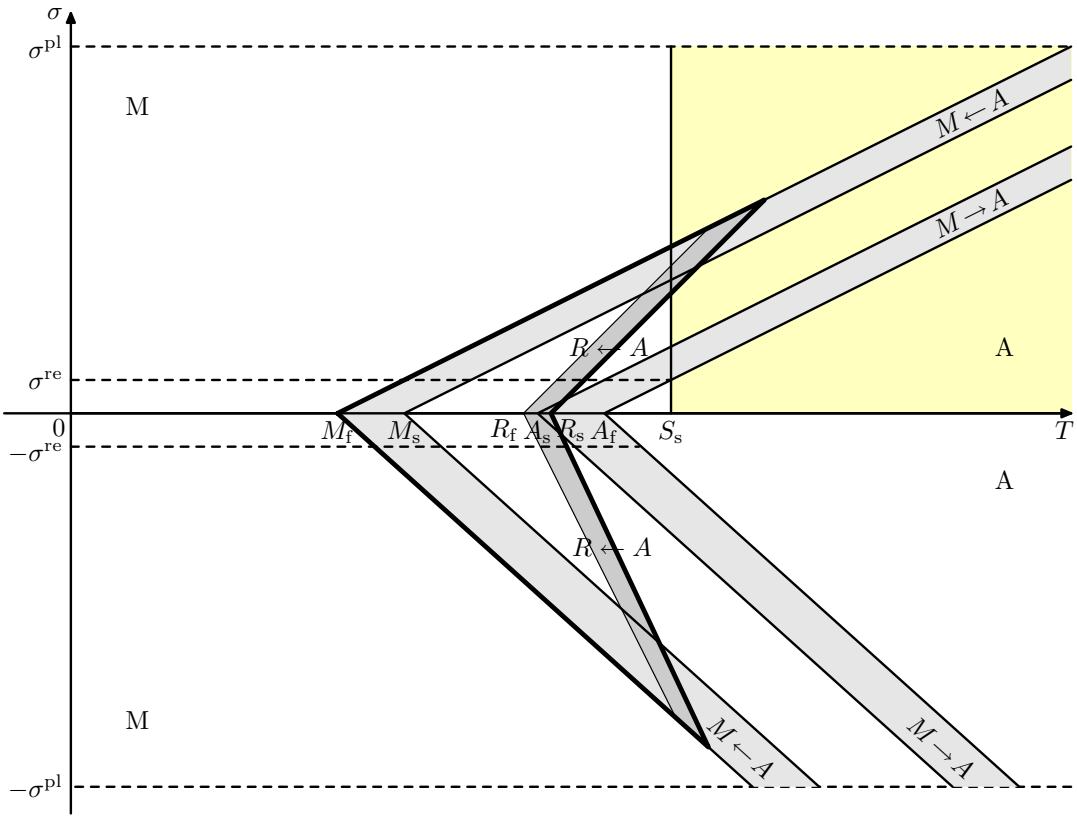


Figure 5.1: Stress-temperature space. Part considered in the superelasticity model marked with yellow color.

This condition ensures no martensite reorientation is involved in the processes and material is in pure austenite at the beginning. The grey area between lines starting at points $M_\mathrm{s}, M_\mathrm{f}$ marks points in $\sigma$-$T$ space where volume fraction of martensite increases, similarly for the area where martensite transforms to austenite (lines starting at points $A_\mathrm{s}, A_\mathrm{f}$) and for R-phase transformation strip. The area where R-phase is present is marked by thick line. Since R-phase can transform reversibly with negligibly small or no hysteresis, we assume austenite to R-phase transition is non-hysteretic. Transformation strain of R-phase is assumed to be stress-dependent with maximal value after reorientation stress level $\sigma^{R\mathrm{re}}$ is attained. The Young's modulus of R-phase is supposed to be the same as Young's modulus of austenite and the transformation strain for R-phase transforming to martensite is assumed to be the same as the transformation strain of austenite transforming to martensite at the same conditions.

We will neglect thermal expansion contribution to the total strain in equation (4.20), since $\varepsilon^\mathrm{th} \ll \varepsilon^\mathrm{el}, \varepsilon^\mathrm{th} \ll \varepsilon^\mathrm{tr}$ for considered magnitudes of stress and temperature, but it can be introduced to the model straightforwardly.

### 5.2.2 Algorithm

Inspired by previous models we define transformation driving force, which links stress $\sigma$ and temperature $T$ in accordance with Clausius-Clapeyron equation (see section 3.4). Each point in the $\sigma$-$T$ phase plane is assigned a value of martensitic phase transformation driving force

$$\varphi(t) := \frac{\sigma(t)}{s} - (T(t) - A_\mathrm{f}). \tag{5.7}$$

and a value of R-phase transformation driving force

$$\varphi^R(t) := \frac{\sigma(t)}{s^R} - T(t), \tag{5.8}$$

$s$ and $s^R$ are constants described below. The difference $T(t) - A_\mathrm{f}$ only change $\varphi$ values so they are equal to zero whenever the reverse transition is just finished. This "addition of a constant" has no influence on physical essence of the problem.

We introduce internal variables

| | |
|---|---|
| $\xi(t)$ | a real function representing volume fraction of martensite, $\xi(t) : \mathbb{R} \to I$ |
| $\xi^R(t)$ | a real function representing volume fraction of R-phase in austenite, $\xi^R(t) : \mathbb{R} \to I$ |
| $RP(t)$ | a set of ordered pairs of real variables representing set of return points in evolution of martensite, $RP(t) := \{[\varphi(t_1), \xi(t_1)], [\varphi(t_2), \xi(t_2)], \ldots, [\varphi(t_n), \xi(t_n)];\ \varphi(t_i) \in \mathbb{R}, \xi(t_i) \in I,\ 0 \le t_i \le t,\ \forall\, i = 1, 2, \ldots, n(t),\ n(t) \in \mathbb{N},\ n(t) \ge 2\}$ |

Let us note, due to this definition $\xi^R = 1$ when all austenite is transformed to R-phase, no matter what the volume fraction of austenite is. The volume fraction of R-phase in material is given by product $(1 - \xi)\xi^R$.

Next, we introduce following parameters corresponding to material properties:

| | |
|---|---|
| $A_\mathrm{f}$ | real constant, martensite to austenite finish temperature |
| $E^M$ | real constant, Young's elastic modulus of martensite |
| $E^A$ | real constant, Young's elastic modulus of austenite |
| $s$ | real constant, critical transformation slope of martensitic transition |
| $s^R$ | real constant, critical transformation slope of R-phase transition |
| $\Lambda$ | real constant, maximum transformation strain of martensitic transition |
| $e^R(\sigma)$ | real function, transformation strain of austenite to R-phase transition |
| $\xi_{A2M}(\varphi)$ | real function, completed martensite to austenite transition |
| $\xi_{M2A}(\varphi)$ | real function, completed austenite to martensite transition |
| $\xi_{A2R}(\varphi)$ | real function, completed austenite to R-phase transition |

$\xi_{A2M}(\varphi)$ and $\xi_{M2A}(\varphi)$ represent completed austenite (or R-phase) to martensite and

reverse transition, thus must fulfill following physically motivated conditions:

$$\begin{aligned}&\xi_{M2A}(\varphi):\mathbb{R}\to I \text{ is a non-decreasing continuously differentiable function,}\\&\{\varphi\le 0\Rightarrow\xi_{M2A}(\varphi)=0\}\wedge\{\varphi>0\Rightarrow\xi_{M2A}(\varphi)>0\},\\&\exists!\, A_{\mathrm{s}}\in\mathbb{R}:\{\varphi\ge A_{\mathrm{f}}-A_{\mathrm{s}}\Rightarrow\xi_{M2A}(\varphi)=1\}\wedge\{\varphi<A_{\mathrm{f}}-A_{\mathrm{s}}\Rightarrow\xi_{M2A}(\varphi)<1\}.\end{aligned}\tag{5.9}$$

$$\begin{aligned}&\xi_{A2M}(\varphi):\mathbb{R}\to I \text{ is a non-decreasing continuously differentiable function,}\\&\exists!\, M_{\mathrm{s}}\in\mathbb{R}:\{\varphi\le A_{\mathrm{f}}-M_{\mathrm{s}}\Rightarrow\xi_{A2M}(\varphi)=0\}\\&\qquad\qquad\wedge\{\varphi>A_{\mathrm{f}}-M_{\mathrm{s}}\Rightarrow\xi_{A2M}(\varphi)>0\},\\&\exists!\, M_{\mathrm{f}}\in\mathbb{R}:\{\varphi\ge A_{\mathrm{f}}-M_{\mathrm{f}}\Rightarrow\xi_{A2M}(\varphi)=1\}\wedge\{\varphi<A_{\mathrm{f}}-M_{\mathrm{f}}\Rightarrow\xi_{A2M}(\varphi)<1\},\end{aligned}\tag{5.10}$$

and

$$\xi_{A2M}(\varphi)\le\xi_{M2A}(\varphi)\quad\forall\varphi\in\mathbb{R}.\tag{5.11}$$

Real constants $M_{\mathrm{s}}, M_{\mathrm{f}}, A_{\mathrm{s}}, A_{\mathrm{f}}$ correspond to transition temperatures (introduced in section 2.2), thus they must satisfy one of relations:

$$A_{\mathrm{f}}<A_{\mathrm{s}}\le M_{\mathrm{s}}<M_{\mathrm{f}}\quad\text{or}\quad A_{\mathrm{f}}\le M_{\mathrm{s}}<A_{\mathrm{s}}\le M_{\mathrm{f}}.\tag{5.12}$$

Similarly, for completed austenite to R-phase transition we assume function (since no hysteresis is supposed, the reverse transition follows the same evolution reversely)

$$\begin{aligned}&\xi_{A2R}(\varphi):\mathbb{R}\to I \text{ is a non-decreasing continuously differentiable function,}\\&\exists!\, R_{\mathrm{f}}>0:\{\varphi^R\ge -R_{\mathrm{f}}\Rightarrow\xi_{A2R}(\varphi^R)=1\}\wedge\{\varphi^R\le -R_{\mathrm{f}}\Rightarrow\xi_{A2R}(\varphi^R)<1\},\\&\exists!\, R_{\mathrm{s}}>R_{\mathrm{f}}:\{\varphi^R\le -R_{\mathrm{s}}\Rightarrow\xi_{A2R}(\varphi^R)=0\}\wedge\{\varphi^R>-R_{\mathrm{s}}\Rightarrow\xi_{A2R}(\varphi^R)>0\},\end{aligned}\tag{5.13}$$

Real constant $R_{\mathrm{s}}$ corresponds to temperature when austenite starts to transform to R-phase, $R_{\mathrm{f}}$ to temperature when the process finishes.

Transformation strain of R-phase formed at constant stress $\sigma$ (i.e. at thermally induced transition) is described by input function $e^R(\sigma)$, which can be obtained experimentally. If $\sigma>\sigma^{R\mathrm{re}}$ ($\sigma^{R\mathrm{re}}$ denotes reorientation stress of R-phase), R-phase is fully oriented and and its transformation strain is maximal, if $\sigma=0$, R-phase is not oriented and it has no transformation strain. (Let us note for materials undergoing process of training, not considered in this work, R-phase transformation strain could develop during training.) Thus, function $e^R(\sigma)$ is assumed to fulfil following conditions:

$$\begin{aligned}&e^R(\sigma):\mathbb{R}\to\mathbb{R}_0^+ \text{ is a non-decreasing continuously differentiable function,}\\&e^R(\sigma)=-e^R(-\sigma)\quad\forall\sigma\in\mathbb{R}\text{ (odd function),}\\&e^R(\sigma)=\Lambda^R\quad\text{if}\quad\sigma>\sigma^{R\mathrm{re}},\end{aligned}\tag{5.14}$$

where positive constant $\Lambda^R$ represents maximum R-phase transformation strain. (Definition is extended $\forall\sigma\in\mathbb{R}$ with respect to further development of the model.)

To capture the history of thermomechanical loading of material a set of return points $RP(t)$ was introduced. (For evolution of return points see figure 5.2.) At the beginning of computational process, we define

$$RP(0)=\{[+\infty,1],[-\infty,0]\}.\tag{5.15}$$

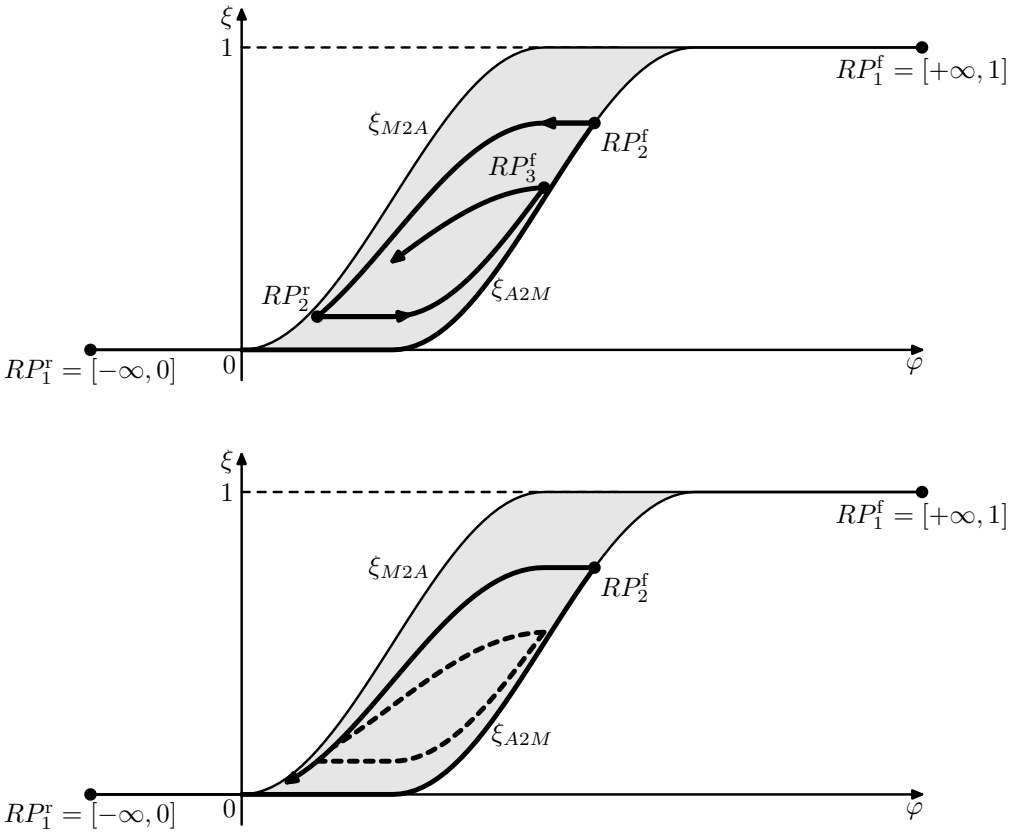


Figure 5.2: Return point memory mechanism. In the upper figure an internal loop is being closed, after which history of the closed loop is "forgotten" – evolution continues in a partial cycle in the lower figure. Area of possible internal trajectories of $\xi$-evolution is marked with grey color.

(Here $+\infty$ and $-\infty$ denotes a very large positive and negative numbers, respectively, which cannot be reached by physically reasonable values of stress and temperature. Reasonable values of stress are less than plasticity stress, reasonable values of temperature are positive less than melting point.)

Then, the actual values $\varphi(t), \xi(t)$ at time $t > 0$ are added to the set $RP$ if change in "direction" of $\varphi$ evolution has occurred, i.e.

$$\begin{aligned} &\exists\, t^* \in \mathbb{R}^+,\ t^* > t : \{\dot{\varphi}(\tau) < 0 \quad \forall\, \tau \in (t, t^*)\} \wedge \\ &\underline{\exists\, \tilde{t} \in \mathbb{R}_0^+,\ \tilde{t} < t : \{\dot{\varphi}(\tau) \geq 0 \quad \forall\, \tau \in (\tilde{t}, t);\ \dot{\varphi}(\tilde{t}) > 0\}} \\ &\Rightarrow\ RP(t) = RP(t) \cup [\varphi(t), \xi(t)], \end{aligned} \tag{5.16}$$

or

$$\begin{aligned} &\exists\, t^* \in \mathbb{R}^+,\ t^* > t : \{\dot{\varphi}(\tau) > 0 \quad \forall\, \tau \in (t, t^*)\} \wedge \\ &\underline{\exists\, \tilde{t} \in \mathbb{R}_0^+,\ \tilde{t} < t : \{\dot{\varphi}(\tau) \leq 0 \quad \forall\, \tau \in (\tilde{t}, t);\ \dot{\varphi}(\tilde{t}) < 0\}} \\ &\Rightarrow\ RP(t) = RP(t) \cup [\varphi(t), \xi(t)] \end{aligned} \tag{5.17}$$

(The above notation means the set of return points is upgraded at time $t$.) We can distinguish two subsets of each set of RPs depending on the change in sign of driving

force increment leading to addition of RPs. In the first group there are RPs added due to mechanism (5.16) (denoted by superscript 'f' next, because forward transition was interrupted), whereas RPs appearing when (5.17) are included in the second group (and denoted by superscript 'r' next, because reverse transition was interrupted):

$$RP(t) = RP^{\mathrm{f}}(t) \cup RP^{\mathrm{r}}(t). \tag{5.18}$$

It is clear that creation of a return point of the first group must be followed by creation of a new RP of the second group and vice versa and

$$RP^{\mathrm{f}}(t) \cap RP^{\mathrm{r}}(t) = \emptyset. \tag{5.19}$$

Conversely, a return point is removed from the set, if the actual value of driving force and martensite volume fraction is equal to values of the return point – loop has been closed, i.e.

$$\begin{array}{l} \underline{[\varphi(t_i), \xi(t_i)] \in RP(t) \ \wedge \ \varphi(t) = \varphi(t_i) \ \wedge \ \xi(t) = \xi(t_i)} \\ \Rightarrow \quad RP(t) = RP(t) \setminus [\varphi(t_i), \xi(t_i)] \end{array} \tag{5.20}$$

Furthermore, wiping out property (introduced in (2.2)) requires all the RPs established inside the just closed subloop must be removed too (system "forgets" this part of its evolution history). But which RPs should be wiped out depends on prescribed $\xi(\varphi(t))$ evolution, so let us describe the evolution first and return to this problem later on.

Since for computational mechanism is not important at which time RP appeared or disappeared, let us simplify notation:

$$\varphi_i = \varphi(t_i),$$

$$\xi_i = \xi(t_i).$$

If $\dot{\varphi}(t) = 0$, there is no evolution of variable $\xi(t)$. Else algorithm chooses the actual nearest appropriate return point $L_t$ (let us denote $t_l$ time, when it was formed). This is the RP in one of subsets $RP^{\mathrm{f}}, RP^{\mathrm{r}}$ in accord with the sign of $\dot{\varphi}$ ("direction of evolution"), whose $\varphi$-coordinate is the nearest to $\varphi(t)$, i.e.

$$\begin{array}{lll} \dot{\varphi}(t) > 0 & \Rightarrow & L_t := [\varphi_i^{\mathrm{f}}, \xi_i^{\mathrm{f}}] \in RP^{\mathrm{f}}(t) : \\ & & |\varphi(t) - \varphi_i^{\mathrm{f}}| = \min\limits_{1 \le j \le n^{\mathrm{f}}} |\varphi(t) - \varphi_j^{\mathrm{f}}|, \end{array} \tag{5.21a}$$

$$\begin{array}{lll} \dot{\varphi}(t) < 0 & \Rightarrow & L_t := [\varphi_i^{\mathrm{r}}, \xi_i^{\mathrm{r}}] \in RP^{\mathrm{r}}(t) : \\ & & |\varphi(t) - \varphi_i^{\mathrm{r}}| = \min\limits_{1 \le j \le n^{\mathrm{r}}} |\varphi(t) - \varphi_j^{\mathrm{r}}|. \end{array} \tag{5.21b}$$

($n^{\mathrm{f}}$ and $n^{\mathrm{r}}$ corresponds to the total number of RPs in $RP^{\mathrm{f}}$ and $RP^{\mathrm{r}}$, respectively.) And similarly the algorithm finds the actual nearest return point $K(t)$ (let us denote $t_k$

time, when it was formed) in the other subset, i.e. the nearest RP "behind" the actual one:

$$\begin{aligned}\dot{\varphi}(t) > 0 \quad \Rightarrow \quad & K_t := [\varphi_i^{\mathrm{r}}, \xi_i^{\mathrm{r}}] \in RP^{\mathrm{r}}(t) : \\ & |\varphi(t) - \varphi_i^{\mathrm{r}}| = \min_{1 \le j \le n^{\mathrm{r}}} |\varphi(t) - \varphi_j^{\mathrm{r}}|, \end{aligned} \tag{5.22a}$$

$$\begin{aligned}\dot{\varphi}(t) < 0 \quad \Rightarrow \quad & K_t := [\varphi_i^{\mathrm{f}}, \xi_i^{\mathrm{f}}] \in RP^{\mathrm{f}}(t) : \\ & |\varphi(t) - \varphi_i^{\mathrm{f}}| = \min_{1 \le j \le n^{\mathrm{f}}} |\varphi(t) - \varphi_j^{\mathrm{f}}|. \end{aligned} \tag{5.22b}$$

Then the algorithm assigns:

$$\begin{aligned}\dot{\varphi}(t) > 0 \quad \Rightarrow \quad & \text{if } \xi_{\mathrm{A2M}}(\varphi(t_k)) = \xi_{\mathrm{A2M}}(\varphi(t_l)) \text{ then } \xi(t) := \xi(\varphi(t_k)) \text{ else} \\ \xi(t) \quad := \quad & \frac{\xi(t_k) - \xi(t_l)}{\xi_{\mathrm{A2M}}(\varphi(t_k)) - \xi_{\mathrm{A2M}}(\varphi(t_l))} [\xi_{\mathrm{A2M}}(\varphi(t)) - \xi_{\mathrm{A2M}}(\varphi(t_l))] + \xi(t_l), \end{aligned} \tag{5.23a}$$

$$\begin{aligned}\dot{\varphi}(t) < 0 \quad \Rightarrow \quad & \text{if } \xi_{\mathrm{M2A}}(\varphi(t_k)) = \xi_{\mathrm{M2A}}(\varphi(t_l)) \text{ then } \xi(t) := \xi(\varphi(t_k)) \text{ else} \\ \xi(t) \quad := \quad & \frac{\xi(t_k) - \xi(t_l)}{\xi_{\mathrm{M2A}}(\varphi(t_k)) - \xi_{\mathrm{M2A}}(\varphi(t_l))} [\xi_{\mathrm{M2A}}(\varphi(t)) - \xi_{\mathrm{M2A}}(\varphi(t_l))] + \xi(t_l), \end{aligned} \tag{5.23b}$$

which corresponds to a projection of function $\xi_{A2M}(\varphi)$ or $\xi_{M2A}(\varphi)$ between points $K = [\varphi_K, \xi_K]$ and $L = [\varphi_L, \xi_L]$.

Properties of this modification of Duhem-Madelung model of hysteresis (compare with section (3.5)) and a restriction on envelope functions imposed by physics,

$$[\xi_{A2M}(\varphi) - \xi_{A2M}(\varphi_L)] \frac{\mathrm{d}\xi_{M2A}(\varphi)}{\mathrm{d}\varphi} \le [\xi_{M2A}(\varphi) - \xi_{M2A}(\varphi_L)] \frac{\mathrm{d}\xi_{A2M}(\varphi)}{\mathrm{d}\varphi} \quad \forall \varphi \in \mathbb{R}, \tag{5.24}$$

are further discussed later. Now note only, evolution of $\xi(t)$ keeps the monotonicity of $\varphi(t)$ evolution, for equations (5.23a), (5.23b) keep monotonicity of $\xi_{A2M}(\varphi), \xi_{M2A}(\varphi)$.

Now, it is easy to show, the sequence of RPs appearing in $RP^{\mathrm{f}}$ is non-increasing and the sequence of RPs appearing in $RP^{\mathrm{r}}$ is non-decreasing (in the sense $\xi(\varphi)$). For instance, let us consider the case of $RP^{\mathrm{f}}$. After formation of a return point $P$ (let us denote this time $t_P$) values of $\varphi(t)$ do not increase and thus values of $\xi(t)$ do not decrease until a next RP (belonging to $RP^{\mathrm{r}}$) is created. Only after that, when $\varphi$ is non-decreasing again, another RP (let us denote $t_Q$ time, when it has occurred) can appear in $RP^{\mathrm{f}}$. But then it must hold $\varphi(t_Q) < \varphi(t_P), \xi(t_Q) \le \xi(t_P)$ otherwise $P$ would be erased, when $\varphi(t) = \varphi(t_P) \Rightarrow \xi(t) = \xi(t_P)$ because of (5.23a), (5.23a). Hence, we can express RPs sets as follows:

$$\begin{aligned} RP^{\mathrm{f}} \quad = \quad & \big\{ [\varphi_1^{\mathrm{f}}, \xi_1^{\mathrm{f}}],\, [\varphi_2^{\mathrm{f}}, \xi_2^{\mathrm{f}}],\, \ldots,\, [\varphi_n^{\mathrm{f}}, \xi_{n^{\mathrm{f}}}^{\mathrm{f}}];\ \varphi_i^{\mathrm{f}} \in \mathbb{R},\ \xi_i^{\mathrm{f}} \in I,\ i = 1, 2, \ldots, n^{\mathrm{f}}; \\ & n^{\mathrm{f}} \in \mathbb{N};\ \varphi_j^{\mathrm{f}} > \varphi_{j+1}^{\mathrm{f}},\ \xi_j^{\mathrm{f}} \ge \xi_{j+1}^{\mathrm{f}},\ j = 1, 2, \ldots, n^{\mathrm{f}} - 1 \big\}, \end{aligned} \tag{5.25}$$

$$RP^{\mathrm{r}} = \{[\varphi_1^{\mathrm{r}}, \xi_1^{\mathrm{r}}], [\varphi_2^{\mathrm{r}}, \xi_2^{\mathrm{r}}], \ldots, [\varphi_{n^{\mathrm{r}}}^{\mathrm{r}}, \xi_{n^{\mathrm{r}}}^{\mathrm{r}}];\ \varphi_i^{\mathrm{r}} \in \mathbb{R},\ \xi_i^{\mathrm{r}} \in I,\ i = 1, 2, \ldots, n^{\mathrm{r}};$$
$$n^{\mathrm{r}} \in \mathbb{N};\ \varphi_j^{\mathrm{r}} < \varphi_{j+1}^{\mathrm{r}},\ \xi_j^{\mathrm{r}} \leq \xi_{j+1}^{\mathrm{r}},\ j = 1, 2, \ldots, n^{\mathrm{r}} - 1\}, \tag{5.26}$$

and

$$\varphi_{n^{\mathrm{f}}}^{\mathrm{f}} > \varphi_{n^{\mathrm{r}}}^{\mathrm{r}} \quad \wedge \quad \xi_{n^{\mathrm{f}}}^{\mathrm{f}} \geq \xi_{n^{\mathrm{r}}}^{\mathrm{r}}. \tag{5.27}$$

Moreover, as the sequences are monotonous, it is always easy to find the nearest RP as introduced in (5.20) – it is simply the last formed RP in the subset. Now, we can also specify the mechanism ensuring the wiping out property is involved. When the subloop is being closed and the last RP in the appropriate subset is erased, no other return points of both $RP^{\mathrm{f}}$ and $RP^{\mathrm{r}}$ can remain "inside it", since the sequences keep monotonous. Thus the only point which has to be wiped out is the nearest one of alternative subset (forming "the other end" of the subloop), which is, due to the monotonicity, the last created RP there again. In summary, RPs disappear in pairs, one is erased from $RP^{\mathrm{f}}$ and one from $RP^{\mathrm{r}}$.

This RPM mechanism was proposed in the work of Bouvet et al. [24]. Due to just proved properties, creation and disappearance of return points in each subset follows "last in, first out" rule.

Experimentally often observed fact is that thermomechanically induced internal transformation subloops are not uniquely determined by the hysteretic envelope for completed forward and reverse transition. Their shape can slightly change depending on type of material, manufacturing or thermomechanical history. One of many possibilities how to influence the shape of subloops to some extent, and thus fit the model to actual experimental data, is the following one.

Let us introduce two fitting parameters $k_{A2M},\ k_{M2A} \in \mathbb{R}$ modifying the $\xi_{A2M}(\varphi)$, $\xi_{M2A}(\varphi)$ functions and let points in $\xi$-$\varphi$ plane be transformed due to prescriptions

$$\begin{aligned} &\tilde{\kappa}_{A2M} : \mathbb{R} \times I \to \mathbb{R} \times I, \\ &[\varphi, \xi(\varphi)] \to [\tilde{\varphi}, \tilde{\xi}(\tilde{\varphi})] := [\varphi + k_{A2M}\xi(\varphi), \xi(\varphi)], \end{aligned} \tag{5.28}$$

$$\begin{aligned} &\bar{\kappa}_{M2A} : \mathbb{R} \times I \to \mathbb{R} \times I, \\ &[\varphi, \xi(\varphi)] \to [\bar{\varphi}, \bar{\xi}(\bar{\varphi})] := [\varphi + k_{M2A}\xi(\varphi), \xi(\varphi)]. \end{aligned} \tag{5.29}$$

Continuity and differentiability of transformed functions $\tilde{\xi}_{\mathrm{A2M}}(\tilde{\varphi}) := \tilde{\kappa}_{A2M}(\xi_{\mathrm{A2M}}(\varphi))$ and $\bar{\xi}_{\mathrm{M2A}}(\bar{\varphi}) := \bar{\kappa}_{A2M}(\xi_{\mathrm{M2A}}(\varphi))$ are preserved by these transformations. For forward transformation evolution equation (5.23a) is replaced by

$$\dot{\varphi} > 0 \quad \Rightarrow \quad \text{if} \quad \xi_{\mathrm{A2M}}(\varphi(t_k)) = \xi_{\mathrm{A2M}}(\varphi(t_l)) \ \text{ then } \ \xi(t) := \xi(\varphi(t_k)) \ \text{ else} \tag{5.30a}$$
$$\xi(t) := \frac{\xi(t_k) - \xi(t_l)}{\tilde{\xi}_{\mathrm{A2M}}(\tilde{\varphi}(t_k)) - \tilde{\xi}_{\mathrm{A2M}}(\tilde{\varphi}(t_l))}[\tilde{\xi}_{\mathrm{A2M}}(\tilde{\varphi}(t)) - \tilde{\xi}_{\mathrm{A2M}}(\tilde{\varphi}(t_l))] + \xi(t_l),$$

and for reverse transformation equation (5.23b) is replaced by

$$\dot{\varphi} < 0 \quad \Rightarrow \quad \text{if} \quad \xi_{\mathrm{M2A}}(\varphi(t_k)) = \xi_{\mathrm{M2A}}(\varphi(t_l)) \ \text{ then } \ \xi(t) := \xi(\varphi(t_k)) \ \text{ else} \tag{5.30b}$$
$$\xi(t) := \frac{\xi(t_k) - \xi(t_l)}{\bar{\xi}_{\mathrm{M2A}}(\bar{\varphi}(t_k)) - \bar{\xi}_{\mathrm{M2A}}(\bar{\varphi}(t_l))}[\bar{\xi}_{\mathrm{M2A}}(\bar{\varphi}(t)) - \bar{\xi}_{\mathrm{M2A}}(\bar{\varphi}(t_l))] + \xi(t_l).$$

Modified thermodynamics based condition (5.24) takes the form

$$[\bar{\xi}_{A2M}(\bar{\varphi}) - \xi_{A2M}(\bar{\varphi}_L)]\frac{\mathrm{d}\tilde{\xi}_{M2A}(\tilde{\varphi})}{\mathrm{d}\tilde{\varphi}} \leq [\tilde{\xi}_{M2A}(\tilde{\varphi}) - \tilde{\xi}_{M2A}(\tilde{\varphi_L})]\frac{\mathrm{d}\bar{\xi}_{A2M}(\varphi)}{\mathrm{d}\bar{\varphi}} \quad \forall\varphi \in \mathbb{R}, \quad (5.31)$$

where $\tilde{L} := [\tilde{\varphi}_L, \tilde{\xi}_L]$ and $\bar{L} := [\bar{\varphi}_L, \bar{\xi}_L]$ are projections of a return point $L := [\varphi_L, \xi_L]$ according to transformation functions $\tilde{\kappa}_{A2M}$ and $\bar{\kappa}_{M2A}$.

Next, for evolution of $\xi^R$ (no hysteresis assumed), algorithm simply assigns

$$\xi^R(t) := \xi_{\mathrm{A2R}}(\varphi^R(t)). \quad (5.32)$$

To establish constitutive equation, we consider elastic and transformation strains (thermal expansion neglected). The included processes are:

- linear deformation of austenite
- linear deformation of martensite
- non-linear hysteretic behavior representing forward and reverse transformations of austenite (or R-phase) to martensite
- non-linear non-hysteretic behavior of austenite to R-phase transformation

For determination of transformation strain the usual type of general flow rule (4.12) is used

$$\varepsilon^{\mathrm{trM}}(t) = \Lambda\xi(t), \quad (5.33)$$

for R-phase transition we define

$$\varepsilon^{\mathrm{trR}}(t) = (1 - \xi(t))\xi^R(t)e^R(\sigma(t)). \quad (5.34)$$

Hence, there are four terms contributing to the total strain (see also equation (4.20))

$$\varepsilon(t) = (1 - \xi(t))\frac{\sigma(t)}{E^A} + \xi(t)\frac{\sigma(t)}{E^M} + \Lambda\,\xi(t) + (1 - \xi(t))e^R(\sigma(t))\xi^R(t) \quad (5.35)$$

The last equation and following initial conditions reflecting (5.4) (and "no history") complete the algorithm:

$$\begin{aligned} &T(0) = A_{\mathrm{f}}, \\ &\sigma(0) = 0, \\ &RP^{+\mathrm{f}}(0) = \{[+\infty, 1]\}, \\ &RP^{+\mathrm{r}}(0) = \{[-\infty, 0]\}, \end{aligned} \quad (5.36)$$

To be more explicit let us recall

$$\xi(t) = \xi(\sigma(t), T(t), history(t)),$$

$$\xi^R(t) = \xi^R(\sigma(t), T(t)),$$

where parameter $history(t)$ stands for thermomechanical history of material represented by set of return points $RP(t)$ and the actual value of martensite volume fraction $\xi(t)$, in the algorithm.

Next natural aim is to expand proposed algorithm upon the case of compression loading, i.e. $\sigma < 0$, but still (5.6) holds. The extension of model should reflect the experimentally observed difference between the superelastic responses in tension and compression, i.e. tension-compression asymmetry. This means the different (negative) maximum transformation strain $\Lambda^-$, which (due to (3.113)) results in a different critical transformation slope $s^-$.

An important fact for extension of previous model is that tensile and compressive martensite never occur simultaneously in considered part of $\sigma$-$T$ space ($\sigma > 0, T \geq S_\mathrm{s}$), thus their evolution is mutually independent and for compressive martensite the same algorithm as for tensile one with different parameters is used. Furthermore, it is assumed the R-phase is formed and reioriented at negative values of stress in a symmetric way as at positive values, with critical transformation slope $-s^R$.

The new tension-compression superelastic algorithm could be divided to three parts. The first two are quite mutually independent subalgorithms, one for tensile and one for compressive loading, describing the evolution of martensite volume fraction and transformation strain. The last part algorithm computes evolution of volume fraction and transformation strain of R-phase and evaluate total volume fraction of martensite and total strain of material.

From now on, let us denote the original variables by superscript + (i.e. $\xi^+(t)$, $RP^+(t)$), whereas the new compression ones by superscript − (i.e. $\xi^-(t)$, $RP^-(t)$). Following procedure of previous section, we define driving force

$$\varphi^-(t) := \frac{\sigma(t)}{s^-} - (T(t) - A_\mathrm{f}), \tag{5.37}$$

we assume the same functions for completed compressive martensite transformation, $\xi_{\mathrm{A2M}}, \xi_{\mathrm{M2A}}$, the evolution of $\xi^+$ driven by (5.23a) and (5.23b) and obvious modification for $\xi^-$, the same RPM effect mechanism. Similarly, transformation strain

$$\varepsilon^{\mathrm{tr}-}(t) = \Lambda^- \xi^-(t), \tag{5.38}$$

where $\Lambda^- < 0$ is the maximum transformation strain for compressive martensite. The initial conditions (5.36) are appended with

$$\begin{aligned} RP^{-\mathrm{f}}(0) &= \{[+\infty, 1]\}, \\ RP^{-\mathrm{r}}(0) &= \{[-\infty, 0]\}. \end{aligned} \tag{5.39}$$

We define R-phase driving force as follows

$$\varphi^R(t) := \frac{|\sigma(t)|}{s^R} - T(t). \tag{5.40}$$

R-phase transformation strain function was already introduced in (5.14). Function $\xi_{\mathrm{A2R}}$ and equation (5.32) then fully determine the actual value of volume fraction of R-phase in austenite.

Since there is no interaction between tensile and compressive martensite in considered part of $\sigma$-$T$ space, at least one of variables $\xi^+$, $\xi^-$ is equal to zero at any point of it. We can define

$$\xi(t) := \max(\xi^+(t), \xi^-(t)) \tag{5.41}$$

and introduce constitutive equation for tension-compression superelastic algorithm

$$\varepsilon(t) = (1-\xi(t))\frac{\sigma(t)}{E^A} + \xi(t)\frac{\sigma(t)}{E^M} + \Lambda^+\,\xi^+(t) + \Lambda^-\,\xi^-(t) + (1-\xi(t))e^R(\sigma(t))\xi^R(t), \tag{5.42}$$

where the first two terms on the right are the elastic part, whereas the rest is the transformation part.

### 5.2.3 Extended Duhem-Madelung Model of Hysteresis

As mentioned in (4.3), in their paper [23] Ivshin and Pence adapted the Duhem-Madelung model of hysteresis for phase transitions. We will briefly summarize some of their results, propose an extension of this model respecting RPM effect and find a system of hysteresis envelope functions suitable for practical purposes.

Let us consider a hysteresis loop given by functions

$$\begin{aligned}
&\xi_{\min}(\varphi) : \mathbb{R} \to I \text{ is non-decreasing continuously differentiable function,}\\
&\exists!\, \varphi_{\min s} \in \mathbb{R} : \{\varphi \le \varphi_{\min s} \Rightarrow \xi_{\min}(\varphi) = 0\} \wedge \{\varphi > \varphi_{\min s} \Rightarrow \xi_{\min}(\varphi) > 0\},\\
&\exists!\, \varphi_{\min f} \in \mathbb{R} : \{\varphi \ge \varphi_{\min f} \Rightarrow \xi_{\min}(\varphi) = 1\} \wedge \{\varphi < \varphi_{\min f} \Rightarrow \xi_{\min}(\varphi) < 1\}.
\end{aligned} \tag{5.43}$$

and

$$\begin{aligned}
&\xi_{\max}(\varphi) : \mathbb{R} \to I \text{ is non-decreasing continuously differentiable function,}\\
&\exists!\, \varphi_{\max s} \in \mathbb{R} : \{\varphi \le \varphi_{\max s} \Rightarrow \xi_{\max}(\varphi) = 0\} \wedge \{\varphi > \varphi_{\max s} \Rightarrow \xi_{\max}(\varphi) > 0\},\\
&\exists!\, \varphi_{\max f} \in \mathbb{R} : \{\varphi \ge \varphi_{\max f} \Rightarrow \xi_{\max}(\varphi) = 1\} \wedge \{\varphi < \varphi_{\max f} \Rightarrow \xi_{\max}(\varphi) < 1\},
\end{aligned} \tag{5.44}$$

which satisfy

$$\xi_{\min}(\varphi) \le \xi_{\max}(\varphi) \quad \forall \varphi \in \mathbb{R}. \tag{5.45}$$

There are two possible cases of relations between just defined points (compare with (5.12)):

$$\varphi_{\max f} < \varphi_{\max s} \le \varphi_{\min s} < \varphi_{\min f}, \quad \varphi_{\max f} \le \varphi_{\min s} < \varphi_{\max s} \le \varphi_{\min f} \tag{5.46}$$

To describe the internal path algorithm, the given $\varphi(t)$ evolution ($t \ge 0$ is time) is divided into subintervals $\langle \varphi(t_k), \varphi(t_{k+1}) \rangle$ upon which is non-decreasing or non-increasing. This defines a sequence of return points at which the directionality of $\varphi(t)$ changes. In the event that $\varphi(t)$ is held constant over a time interval that mediates a in directionality, then the associated return point can be chosen arbitrarily within the interval. If

$\langle t_k, t_{k+1}\rangle$ is a time interval upon which $\varphi(t)$ is non-increasing, then $\xi(t)$ is to be given by

$$\xi(\varphi(t)) = \frac{\xi(t_k)}{\xi_{\max}(\varphi(t_k))}\xi_{\max}(\varphi(t)), \quad t \in \langle t_k, t_{k+1}\rangle, \tag{5.47a}$$

Conversely, if $\langle t_k, t_{k+1}\rangle$ is a time interval upon which $\varphi(t)$ is nondecreasing, then $\xi(t)$ is to be given by

$$\xi(\varphi(t)) = 1 - \left\{\frac{1-\xi(t_k)}{1-\xi_{\min}(\varphi(t_k))}\right\}[1-\xi_{\min}(\varphi(t))], \quad t \in \langle t_k, t_{k+1}\rangle. \tag{5.47b}$$

Formula (5.47a) defines a family of trajectories for decreasing $\xi(t)$ within the region enclosed by the two envelopes. These trajectories, as well as the corresponding trajectories for increasing $\xi(t)$ determined by (5.47b), fulfil

$$\xi_{\min}(\varphi(0)) \le \xi(0) \le \xi_{\max}(\varphi(0)) \Rightarrow \xi_{\min}(\varphi(t)) \le \xi(t) \le \xi_{\max}(\varphi(t)) \quad \forall t > 0. \tag{5.48}$$

The phase fraction evolution is rate-independent in the sense that a resealing of the time variable $t$ only alters the parametrization of the locus $[\varphi(t), \xi(t)]$ but does not change its graph in the $\xi$-$\varphi$ space.

Invshin and Pence show how algorithm (5.47), for envelope functions given by (5.43) and (5.44), follows from a Duhem-Madelung model for phase fraction evolution subjected to the following physically motivated requirements:

(A1) Phase transitions take place on a temperature range $\varphi_{\max f} \le \varphi \le \varphi_{\min f}$, in the sense that algorithm is required to ensure that

$$\xi(\varphi) = 0 \quad \forall \varphi \le \varphi_{\max f}; \qquad \xi(\varphi) = 1 \quad \forall \varphi \ge \varphi_{\min f}. \tag{5.49}$$

(A2) The phase fraction variable respectively increases, remains stationary or decreases as the driving variable respectively increases, remains stationary or decreases.

(A3) Phase transformations proceed at a pace that is proportional to the phase fraction of the parent phase (the phase that is being depleted) and is independent of the phase fraction of the daughter phase (the phase that the parent is transforming into).

Indeed, these conditions are fulfilled by definitions (5.43), (5.44) and (5.47). Next important physical condition is:

(A4) The maximum value of $\xi$ compatible with a given driving force $\varphi$ is attained by any temperature history that begins with $\varphi \ge \varphi_{\min f}$, (and therefore $\xi = 1$) which then subsequently decreases to the given $\varphi$. Conversely, the minimum value of $\xi$ compatible with a given driving variable $\varphi$ is attained by any temperature history that begins with $\varphi \ge \varphi_{\max f}$ (and therefore $\xi = 0$) which then subsequently increases to the given value $\varphi$.

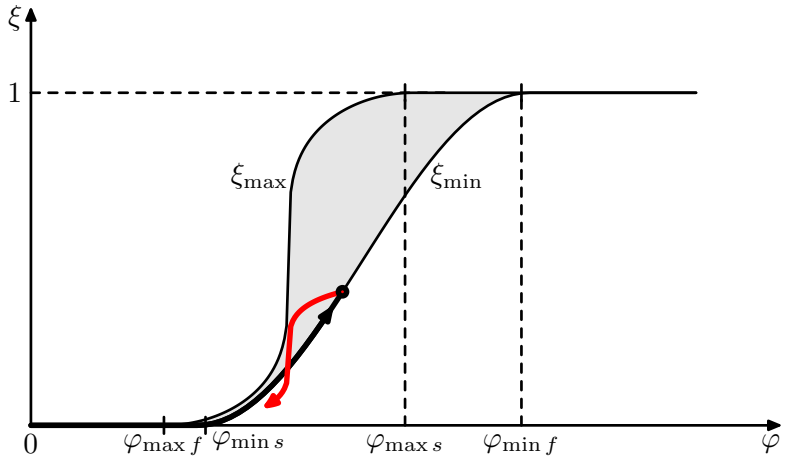


Figure 5.3: An example of internal trajectory (red line) piercing the envelope function $\xi_{\min}$.

The interpretation of (A4) could be that any decreasing/increasing trajectory in $\xi$-$\varphi$ plane representing the time evolution of martensite (and given by (5.47)) do not *pierce* function $\xi_{\min}(\varphi)/\xi_{\max}(\varphi)$, i.e. the trajectory remains just in one part of $\xi$-$\varphi$ plane, which is divided into two parts parts by the function (see figure 5.3).

As described in section 3.5, area enclosed by a cycle in $\xi$-$\varphi$ plane (i.e. area inside the loop) is equal to energy dissipated during the process, thus, due to the second law of thermodynamics, always non-negative (recall (4.26)):

$$\oint \varphi \, \mathrm{d}\xi \geq 0. \tag{5.50}$$

and each phase transformation cycle in $\xi$-$\varphi$ plane can be contoured only in one sense, not in the other. If the trajectory of a minor loop do pierce the major loop, then it is possible to find a closed cycle with negative dissipation. Thus, the condition (A4) could be also interpreted as an expression of the second law of thermodynamics.

However, as can be proven on examples (see figure 5.3), the form of evolution equations (5.47) is not sufficient to meet (A4), which means, there could be some possible evolutions which break the second law of thermodynamics.

In [23] it has been further proven the necessary and sufficient conditions for the algorithm (5.47) to satisfy the requirement (A4) are:

$$\xi_{\min}(\varphi)\frac{\mathrm{d}\xi_{\max}(\varphi)}{\mathrm{d}\varphi} \leq \xi_{\max}(\varphi)\frac{\mathrm{d}\xi_{\min}(\varphi)}{\mathrm{d}\varphi}. \tag{5.51}$$

$$[1-\xi_{\max}(\varphi)]\frac{\mathrm{d}\xi_{\min}(\varphi)}{\mathrm{d}\varphi} \leq [1-\xi_{\min}(\varphi)]\frac{\mathrm{d}\xi_{\max}(\varphi)}{\mathrm{d}\varphi}. \tag{5.52}$$

It is easy to realize equations (5.47) do not respect the RPM effect even though (5.51), (5.52) are satisfied (consider $\xi_{\max}$ and $\xi_{\min}$ are mutually independent and equations (5.47) do not concern the previously formed return point). In order to include

RPM effect in this hysteresis model (so it could be used in the iRLOOP model), the equations are changed to have the form as introduced in previous subsection, i.e.

$$\begin{aligned} \dot{\varphi}(t) > 0 \quad &\Rightarrow \quad \text{if} \quad \xi_{\min}(\varphi(t_k)) = \xi_{\min}(\varphi(t_l)) \quad \text{then} \quad \xi(t) := \xi(t_l) \quad \text{else} \quad (5.53a) \\ \xi(t) \quad &:= \quad \frac{\xi(t_k) - \xi(t_l)}{\xi_{\min}(\varphi(t_k)) - \xi_{\min}(\varphi(t_l))}[\xi_{\min}(\varphi(t)) - \xi_{\min}(\varphi(t_l))] + \xi(t_l), \end{aligned}$$

$$\begin{aligned} \dot{\varphi}(t) < 0 \quad &\Rightarrow \quad \text{if} \quad \xi_{\max}(\varphi(t_k)) = \xi_{\max}(\varphi(t_l)) \quad \text{then} \quad \xi(t) := \xi(t_l) \quad \text{else} \quad (5.53b) \\ \xi(t) \quad &:= \quad \frac{\xi(t_k) - \xi(t_l)}{\xi_{\max}(\varphi(t_k)) - \xi_{\max}(\varphi(t_l))}[\xi_{\max}(\varphi(t)) - \xi_{\max}(\varphi(t_l))] + \xi(t_l). \end{aligned}$$

(Subscripts $A2M$ and $M2A$ correspond now to subscripts 'min' and 'max', respectively.) The RP mechanism and return points $K = [\varphi(t_k), \xi(\varphi(t_k))]$, $L = [\varphi(t_l), \xi(\varphi(t_l))]$ are introduced in previous subsection, i.e. by (5.15)–(5.17), (5.20), (5.21a)–(5.22b) and (5.25)–(5.27). Let us call this extension "Extended Duhem-Madelung Model of Hysteresis" (EDM). It is worth noting model of Ivshin and Pence is a special case of the EDM, where the return point $L$ is chosen

$$\begin{aligned} L &:= [-\infty, 0] \quad \text{if} \quad \dot{\varphi} < 0, \\ L &:= [+\infty, 1] \quad \text{if} \quad \dot{\varphi} > 0. \end{aligned} \tag{5.54}$$

Now we would like the EDM to meet conditions (A1)–(A3) and the following generalization of (A4):

(A4+) Let $B, C$ be two *consecutively* formed return points so that:

$$B := [\varphi_B, \xi_B] \in RP^{\mathrm{r}},\ C := [\varphi_C, \xi_C] \in RP^{\mathrm{f}} \quad (\Rightarrow \varphi_B < \varphi_C). \tag{5.55}$$

The maximum value of martensite volume fraction $\xi(\varphi)$ within this loop compatible with a given driving force $\varphi_B \leq \varphi \leq \varphi_C$ is attained by the $\varphi$ history that begins with $\varphi_C$ which then subsequently decreases to the given $\varphi$. Conversely, the minimum value of $\xi(\varphi)$ within this loop compatible with a given driving variable $\varphi_B \leq \varphi \leq \varphi_C$ is attained by the $\varphi$ evolution that begins with $\varphi_B$, which then subsequently increases to the given value $\varphi$.

Let us realize the condition (A4) is a special case of (A4+) for major loop when $B = [-\infty, 0], C = [+\infty, 1]$. From thermodynamic point of view, (A4+) is an expression of the second law of thermodynamics, again.

It is easy to show EDM satisfies the conditions (A1), (A2) and (A3). For requirement (A4+) let us realize

$$\xi_B \leq \xi_C \tag{5.56}$$

due to (5.27). In the degenerated case $\xi_B = \xi_C$ the loop is just a segment and (A4+) is obviously satisfied.

Now let us consider

$$\xi_B < \xi_C. \tag{5.57}$$

To ensure (A4+) it is necessary and sufficient that both

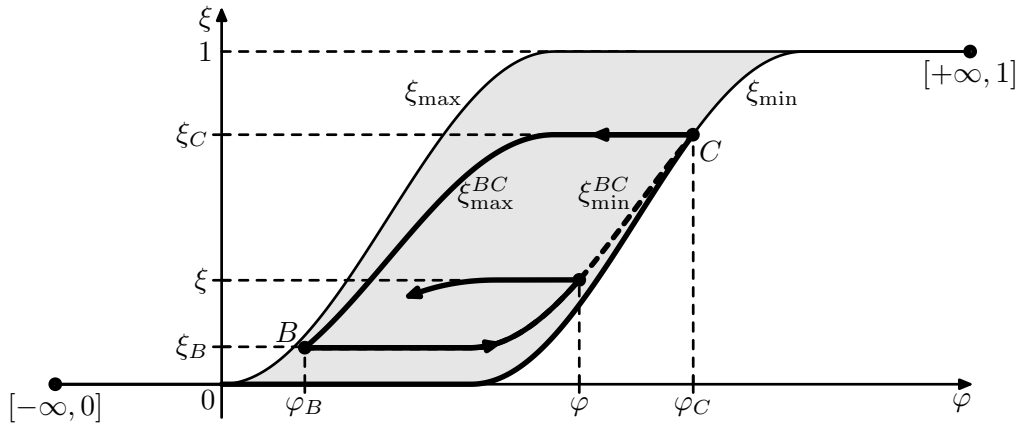


Figure 5.4: A system of trajectories inside a major loop, see text for notation.

(i) each trajectory starting at $\varphi_B < \varphi \leq \varphi_C$ and pointing to $B$ generated by (5.53b) with $K = C$, $L = B$ do not pierce the lower branch of loop $\xi^{BC}$, let us denote it by $\xi^{BC}_{\min}$ (see figure 5.4), and

(ii) each trajectory starting at $\varphi_C > \varphi \geq \varphi_B$ and pointing to $C$ generated by (5.53a) with $K = B$, $L = C$ do not pierce the upper branch of loop $\xi^{BC}$, let us denote it by $\xi^{BC}_{\max}$.

(There is no need to care if the trajectory in (i)/(ii) can pierce the nearest established "above"/"below" trajectory, since it is impossible due to RPM and "self-similar" $\xi$-evolution mechanisms.)

The first of the above requirements yields

$$\frac{\mathrm{d}\xi}{\mathrm{d}\varphi} \leq \frac{\mathrm{d}\xi^{BC}_{\min}}{\mathrm{d}\varphi} \tag{5.58}$$

where the left-hand side of (5.58) is to be calculated using the temperature decreasing algorithm (5.53b) with the condition that $\xi = \xi^{BC}_{\min}$ at the instant that the derivative is computed, i.e. at the arbitrary chosen point $\varphi$. Consequently one obtains

$$[\xi_{\min}(\varphi) - \xi_{\min}(\varphi_B)]\frac{\mathrm{d}\xi_{\max}(\varphi)}{\mathrm{d}\varphi} \leq [\xi_{\max}(\varphi) - \xi_{\max}(\varphi_B)]\frac{\mathrm{d}\xi_{\min}(\varphi)}{\mathrm{d}\varphi} \quad \forall\varphi > \varphi_B. \tag{5.59}$$

In a similar fashion, requirement (ii) leads to

$$[\xi_{\max}(\varphi_C) - \xi_{\max}(\varphi)]\frac{\mathrm{d}\xi_{\min}(\varphi)}{\mathrm{d}\varphi} \leq [\xi_{\min}(\varphi_C) - \xi_{\min}(\varphi)]\frac{\mathrm{d}\xi_{\max}(\varphi)}{\mathrm{d}\varphi} \quad \forall\varphi < \varphi_C. \tag{5.60}$$

(Note that due to definitions (5.53a), (5.53b) conditions (i) and (ii) are satisfied even for $\xi_{\max}(\varphi_B) = \xi_{\max}(\varphi_C)$ and $\xi_{\min}(\varphi_B) = \xi_{\min}(\varphi_C)$.) For special choice (5.54) we get (5.51) and (5.52).

For practical purposes, we would like to find a system of hysteresis envelope functions $\xi_{\min}, \xi_{\max}$ to which experimentally obtained data could be fitted with respect to (A1)–(A4+). Let (5.43),(5.44) and (5.45) hold and assume

$$\begin{aligned}
&\exists\, \varphi_{\min\inf} \in \mathbb{R}: \\
&\frac{\mathrm{d}\xi_{\min}(\varphi)}{\mathrm{d}\varphi} \text{ is non-decreasing (continuous) function } \forall \varphi < \varphi_{\min\inf} \\
&\frac{\mathrm{d}\xi_{\min}(\varphi)}{\mathrm{d}\varphi} \text{ is non-increasing (continuous) function } \forall \varphi \geq \varphi_{\min\inf},
\end{aligned} \tag{5.61}$$

$$\begin{aligned}
&\exists\, \varphi_{\max\inf} \in \mathbb{R}: \\
&\frac{\mathrm{d}\xi_{\max}(\varphi)}{\mathrm{d}\varphi} \text{ is non-decreasing (continuous) function } \forall \varphi < \varphi_{\max\inf} \\
&\frac{\mathrm{d}\xi_{\min}(\varphi)}{\mathrm{d}\varphi} \text{ is non-increasing (continuous) function } \forall \varphi \geq \varphi_{\max\inf}.
\end{aligned} \tag{5.62}$$

Experimentally obtained forms of envelope functions often well correspond to such type of functions in SMAs. There can be more than one point satisfying condition (5.61) or (5.62), but if so, then all such points form a line segment. Then we choose the greatest number satisfying (5.61) and denote it by $\varphi_{\min\inf}$ and we choose the smallest number satisfying (5.62) and denote it by $\varphi_{\max\inf}$.

Not concerning possible internal relations between two return points establishing a branch of hysteresis loop, we require conditions (5.60) and (5.59) would be satisfied for each pair $B, C$:

$$\varphi_B, \varphi_C \in \mathbb{R},\ \xi_{\min} \leq \xi_B \leq \xi_C \leq \xi_{\max}. \tag{5.63}$$

In that case we will show it is sufficient to demand

$$\varphi_{\max\inf} \leq \varphi_{\min s} \quad \wedge \quad \varphi_{\max s} \leq \varphi_{\min\inf}. \tag{5.64}$$

To prove that, we restrict ourselves to (5.60), the case (5.59) would be analogous. Remember both sides in the inequality are non-negative according to definitions. First let the left inequality in (5.46) hold. Then either

$$\frac{\mathrm{d}\xi_{\min}(\varphi)}{\mathrm{d}\varphi} = 0, \tag{5.65}$$

or

$$\xi_{\max}(\varphi_C) - \xi_{\max}(\varphi) = 0. \tag{5.66}$$

But right-hand side of (5.60) is non-negative, which completes the proof. (Note we have not even used (5.64).)

Now let us concern the right inequality in (5.46). If $\varphi \leq \varphi_{\min s}$ then (5.65) holds, if $\varphi \geq \varphi_{\max s}$ then (5.66) holds (since $\varphi < \varphi_C$). For $\varphi \in (\varphi_{\min s}, \varphi_{\max s})$ let us convert (5.60) to

$$\frac{\xi_{\max}(\varphi_C) - \xi_{\max}(\varphi)}{\varphi_C - \varphi} \frac{\mathrm{d}\xi_{\min}(\varphi)}{\mathrm{d}\varphi} \leq \frac{\xi_{\min}(\varphi_C) - \xi_{\min}(\varphi)}{\varphi_C - \varphi} \frac{\mathrm{d}\xi_{\max}(\varphi)}{\mathrm{d}\varphi} \quad \forall \varphi < \varphi_C \tag{5.67}$$

and consider two possibilities

(a) $\varphi_C \leq \varphi_{\max s}$,

(b) $\varphi_C > \varphi_{\max s}$.

Let us arbitrary choose $\varphi$, denote $\varphi^*$. For the (a) case the mean value theorem may be used. Since both $\xi_{\min}, \xi_{\max}$ are assumed to be continuously differentiable functions defined $\forall \varphi \in \mathbb{R}$, there exist some $m^\varphi, M^\varphi$ so:

$$m^\varphi \in \langle \varphi^*, \varphi_C \rangle \wedge \frac{\mathrm{d}\xi_{\min}(m^\varphi)}{\mathrm{d}\varphi} = \frac{\xi_{\min}(\varphi_C) - \xi_{\min}(\varphi^*)}{\varphi_C - \varphi^*}, \tag{5.68}$$

$$M^\varphi \in \langle \varphi^*, \varphi_C \rangle \wedge \frac{\mathrm{d}\xi_{\max}(M^\varphi)}{\mathrm{d}\varphi} = \frac{\xi_{\max}(\varphi_C) - \xi_{\max}(\varphi^*)}{\varphi_C - \varphi^*}. \tag{5.69}$$

Thus, we require

$$\frac{\mathrm{d}\xi_{\max}(M^\varphi)}{\mathrm{d}\varphi}\frac{\mathrm{d}\xi_{\min}(\varphi^*)}{\mathrm{d}\varphi} \leq \frac{\mathrm{d}\xi_{\min}(m^\varphi)}{\mathrm{d}\varphi}\frac{\mathrm{d}\xi_{\max}(\varphi^*)}{\mathrm{d}\varphi} \quad (\varphi^* < \varphi_C). \tag{5.70}$$

Because $\varphi_{\max \inf} \leq \varphi_{\min s} \leq \varphi^* < \varphi_C \leq \varphi_{\max s} \leq \varphi_{\min \inf}$ and (5.61), (5.62), it holds

$$\frac{\mathrm{d}\xi_{\min}(\varphi^*)}{\mathrm{d}\varphi} \leq \frac{\mathrm{d}\xi_{\min}(m^\varphi)}{\mathrm{d}\varphi} \tag{5.71}$$

and

$$\frac{\mathrm{d}\xi_{\max}(M^\varphi)}{\mathrm{d}\varphi} \leq \frac{\mathrm{d}\xi_{\min}(\varphi^*)}{\mathrm{d}\varphi}, \tag{5.72}$$

which imply (5.70) (all terms non-negative) and therefore (5.60) are satisfied.

To finish the proof it remains to solve the (b) case. Let us find a point $C'$ in $\xi$-$\varphi$ plane so that

$$\varphi_{C'} = \varphi_{\max s} \quad \wedge \quad \xi_{C'} = \xi_C \tag{5.73}$$

(It is always a point inside the major loop.) Then

$$\xi_{\min}(\varphi_{C'}) \geq \xi_{\min}(\varphi_C), \quad \xi_{\max}(\varphi_{C'}) = \xi_{\max}(\varphi_C) \tag{5.74}$$

Since minor loop with boundary points $\varphi^*$ and $C'$ satisfies (5.60) due to previous instance, it is possible to employ (5.74) and write

$$\begin{aligned} &[\xi_{\max}(\varphi_C) - \xi_{\max}(\varphi^*)]\frac{\mathrm{d}\xi_{\min}(\varphi^*)}{\mathrm{d}\varphi} = [\xi_{\max}(\varphi_{C'}) - \xi_{\max}(\varphi^*)]\frac{\mathrm{d}\xi_{\min}(\varphi^*)}{\mathrm{d}\varphi} \leq \\ &\leq [\xi_{\min}(\varphi_{C'}) - \xi_{\min}(\varphi^*)]\frac{\mathrm{d}\xi_{\max}(\varphi^*)}{\mathrm{d}\varphi} \leq [\xi_{\min}(\varphi_C) - \xi_{\min}(\varphi^*)]\frac{\mathrm{d}\xi_{\max}(\varphi^*)}{\mathrm{d}\varphi}. \end{aligned} \tag{5.75}$$

This concludes the whole proof.

To sum up, EDM introduced by (5.53a) and (5.53b) is a generalization of Duhem-Madelung model introduced by Ivshin and Pence. EDM capture RPM effect, condition

$$[\xi_{\min}(\varphi) - \xi_{\min}(\varphi_L)]\frac{\mathrm{d}\xi_{\max}(\varphi)}{\mathrm{d}\varphi} \leq [\xi_{\max}(\varphi) - \xi_{\max}(\varphi_L)]\frac{\mathrm{d}\xi_{\min}(\varphi)}{\mathrm{d}\varphi} \quad \forall \varphi \in \mathbb{R} \tag{5.76}$$

for any return point $L$ (given by (5.21a), (5.21b)) and definitions (5.43)–(5.45) ensure the physically based conditions (A1),(A2),(A3) and (A4+) are fulfilled. Note inequality (5.76) includes both (5.59) and (5.60). We have also proven the condition (5.64) is sufficient for a system of envelope functions (5.61), (5.62) to fulfil (5.76).

As an example lets consider the cosine function, which is usually regarded to best fit the experimental data [5]. One of possible form of envelope functions is:

$$\xi_{\min}(\varphi) := \begin{cases} 0 & \varphi \le \varphi_{\min s}, \\ \dfrac{1}{2}\left[\cos\left(\dfrac{\varphi - \varphi_{\min s}}{\varphi_{\min f} - \varphi_{\min s}}\pi + \pi\right) + 1\right] & \varphi_{\min s} < \varphi < \varphi_{\min f}, \\ 1 & \varphi \ge \varphi_{\min f} \end{cases} \tag{5.77}$$

$$\xi_{\max}(\varphi) := \begin{cases} 0 & \varphi \le \varphi_{\max f}, \\ \dfrac{1}{2}\left[\cos\left(\dfrac{\varphi - \varphi_{\max f}}{\varphi_{\max s} - \varphi_{\max f}}\pi + \pi\right) + 1\right] & \varphi_{\max f} < \varphi < \varphi_{\max s}, \\ 1 & \varphi \ge \varphi_{\max s} \end{cases} \tag{5.78}$$

Both functions fulfil the requirements for $\xi_{\min}, \xi_{\max}$ used in previous deliberations provided (simple computation with respect to (5.64))

$$\frac{\varphi_{\max s} + \varphi_{\max f}}{2} \le \varphi_{\min s} \quad \wedge \quad \frac{\varphi_{\min s} + \varphi_{\min f}}{2} \ge \varphi_{\max s}. \tag{5.79}$$

So, that are the sufficient conditions for cosine envelope functions (5.77) and (5.78) to respect (A1)–(A4+).

### 5.2.4 Inverse Problem Formulation; Existence and Uniqueness of a Solution

Let us return to superelasticity model for non-negative stresses. Whereas the superelasticity model computes time evolution of strain for prescribed stress and temperature evolution, for implementation to finite element method code the formulation must be converted to strain form, i.e. for input functions $T(t)$, $\varepsilon(t)$ we search for $\sigma(t)$ in order to satisfy (5.35). It leads to implicit relation

$$F(T(t), \sigma(t), \varepsilon(t)) = 0 \tag{5.80}$$

with initial conditions

$$\begin{aligned} &T(0) = A_{\mathrm{f}}, \\ &\varepsilon(0) = 0, \\ &RP(0) = \{[-\infty, 0], [+\infty, 1]\}. \end{aligned} \tag{5.81}$$

It is worth noting RPM mechanism depends on values of driving force $\varphi(\sigma(\tau), T(\tau))$ for $\tau$ in the close neighborhood of the actual time $t$ (see RPM mechanism (5.16), (5.17)).

Derivatives of volume fraction with respect to time (at actual time $t$) are

$$\dot{\xi} = \frac{\mathrm{d}\xi}{\mathrm{d}\varphi}\left(\frac{\dot{\sigma}}{s} - \dot{T}\right), \tag{5.82}$$

$$\dot{\xi}^R = \frac{\mathrm{d}\xi_{A2R}}{\mathrm{d}\varphi^R}\left(\frac{\dot{\sigma}}{s^R} - \dot{T}\right). \tag{5.83}$$

Employing (5.23a), (5.23b) one obtain either

$$\dot{\xi} = 0 \quad \text{if} \quad \left(\frac{\dot{\sigma}}{s} - \dot{T}\right) = 0. \tag{5.84}$$

or

$$\dot{\xi} = \underbrace{\frac{\xi(t_k) - \xi(t_l)}{\xi_{\mathrm{A2M}}(\varphi(t_k)) - \xi_{\mathrm{A2M}}(\varphi(t_l))}\frac{\mathrm{d}\xi_{\mathrm{A2M}}}{\mathrm{d}\varphi}}_{\frac{\mathrm{d}\xi}{\mathrm{d}\varphi}}\left(\frac{\dot{\sigma}}{s} - \dot{T}\right) \quad \text{if} \quad \left(\frac{\dot{\sigma}}{s} - \dot{T}\right) > 0, \tag{5.85}$$

$$\dot{\xi} = \underbrace{\frac{\xi(t_k) - \xi(t_l)}{\xi_{\mathrm{M2A}}(\varphi(t_k)) - \xi_{\mathrm{M2A}}(\varphi(t_l))}\frac{\mathrm{d}\xi_{\mathrm{M2A}}}{\mathrm{d}\varphi}}_{\frac{\mathrm{d}\xi}{\mathrm{d}\varphi}}\left(\frac{\dot{\sigma}}{s} - \dot{T}\right) \quad \text{if} \quad \left(\frac{\dot{\sigma}}{s} - \dot{T}\right) < 0, \tag{5.86}$$

Let us consider equation (5.35) and compute derivative of strain $\varepsilon(t)$ with respect to time. After some conversions we obtain:

$$\begin{aligned}
\dot{\varepsilon} \;=\; & \dot{\sigma}\left\{\frac{1}{E^A} + \Delta S\xi + \Delta S\frac{\sigma}{s}\frac{\mathrm{d}\xi}{\mathrm{d}\varphi} + (1-\xi)\frac{e^R(\sigma)}{s^R}\frac{\mathrm{d}\xi_{A2R}}{\mathrm{d}\varphi^R}\right. \\
& \left. + (1-\xi)\xi^R\frac{\mathrm{d}e^R(\sigma)}{\mathrm{d}\sigma} + \frac{1}{s}\frac{\mathrm{d}\xi}{\mathrm{d}\varphi}[\Lambda - \xi^R e^R(\sigma)]\right\} \\
& + \dot{T}\left[\Delta S\sigma\frac{\mathrm{d}\xi}{\mathrm{d}\varphi} + (1-\xi)e^R(\sigma)\frac{\mathrm{d}\xi_{A2R}}{\mathrm{d}\varphi^R} + \frac{\mathrm{d}\xi}{\mathrm{d}\varphi}[\Lambda - \xi^R e^R(\sigma)]\right],
\end{aligned} \tag{5.87}$$

where the sign of time-dependence, "$(t)$", was omitted for brief notation. We recall definition (4.5)

$$\Delta S := \left(\frac{1}{E^M} - \frac{1}{E^A}\right). \tag{5.88}$$

Let us show the value of the term in the curly brackets is always positive. Indeed, one can employ previous definitions of functions and parameters to obtain:

$$E^A, E^M, s, s^R, \Lambda, \Lambda^R > 0, \tag{5.89}$$

$$\xi(t), \xi^R(t) \in \langle 0, 1\rangle, \tag{5.90}$$

$$e^R(\sigma(t)) \in \langle 0, \Lambda^R\rangle, \tag{5.91}$$

$$\frac{\mathrm{d}e^R}{\mathrm{d}\sigma} \in \langle 0, D^{eR}\rangle \tag{5.92}$$

$$\frac{\mathrm{d}\xi_{A2R}}{\mathrm{d}\varphi^R} \in \langle 0, D^{A2R}\rangle, \tag{5.93}$$

$$\frac{\mathrm{d}\xi_{A2M}}{\mathrm{d}\varphi} \in \langle 0, D^{A2M}\rangle, \tag{5.94}$$

$$\frac{\mathrm{d}\xi_{M2A}}{\mathrm{d}\varphi} \in \langle 0, D^{M2A} \rangle, \tag{5.95}$$

where $0 < D^{eR}, D^{A2R}, D^{A2M}, D^{M2A} < +\infty$ are time-independent constants. Let us now choose an arbitrary but fixed time $\theta \in \mathbb{R}^+$ and consider time interval $t \in \langle 0, \theta \rangle$. Then

$$\dot{\varepsilon}(t), \dot{T}(t) \in \mathcal{C}\langle 0, \theta \rangle. \tag{5.96}$$

And for time subinterval $t \in \langle t_i, t_j \rangle,\ t_i, t_j \in \mathbb{R}^+,\ 0 < t_i < t_j < \theta$ when no return point is formed in $(t_i, t_j)$ it is also

$$\frac{\mathrm{d}\xi}{\mathrm{d}\varphi} \in \langle 0, D^{RP} \rangle, \tag{5.97}$$

where constant $0 \leq D^{RP} < +\infty$ depends on values of martensite volume fraction at RPs due to (5.84), (5.85), (5.86).

Next, following conditions on material parameters of SMA

$$E^A \geq E^M \Rightarrow \Delta S \geq 0, \tag{5.98}$$

$$\Lambda > \Lambda^R \Rightarrow [\Lambda - \xi^R e^R(\sigma)] > 0. \tag{5.99}$$

can be assumed to be satisfied due to physical properties of martensite, austenite and R-phase (e.g. usually $\Lambda^R \leq 1\%, \Lambda \sim$ 6-8%). Thus one can see in that case all the terms in the curly brackets in (5.87) are always non-negative and the whole term is positive ($1/E^A$ is positive) and it is possible to covert (5.87) to the form of first order ordinary differential equation (ODE)

$$\dot{\sigma}(t) = \tilde{F}(t, \sigma(t)) := \frac{\dot{\varepsilon} + \dot{T}\tilde{f}(t, \sigma(t))}{\tilde{g}(t, \sigma(t))}, \tag{5.100}$$

where $\tilde{f}(t, \sigma(t)), \tilde{g}(t, \sigma(t))$ are continuous functions ($\tilde{f}$ corresponds to the term in curly brackets, $\tilde{g}$ to the term in large square brackets in (5.87)).

Since $\varepsilon(t), T(t) \in \mathcal{C}^1\langle 0, +\infty)$ we can find real constants bounding temperature and strain derivatives, i.e. $\exists\, C^{\dot{\varepsilon}}, C^{\dot{T}} < +\infty$ :

$$|\dot{\varepsilon}(t)| \leq C^{\dot{\varepsilon}}, \quad |\dot{T}(t)| \leq C^{\dot{T}}, \quad \forall t \in \langle 0, \theta \rangle \tag{5.101}$$

(This correspond to finite maximum driving speed in physical experiment.)

If we define auxiliary constant $\sigma^m$:

$$\sigma^m := -\frac{1}{2E^A}\frac{s}{\Delta S}(D^{RP})^{-1} \quad \text{if} \quad D^{RP} > 0, \tag{5.102}$$

$$\sigma^m := -\frac{1}{2E^A}\frac{s}{\Delta S} \quad \text{if} \quad D^{RP} = 0. \tag{5.103}$$

then $\sigma^m < 0$ and function (of one variable $\sigma$ at fixed $t$) $\tilde{g}(t, \cdot)$ is positive for every stress $\sigma \geq \sigma^m$.

Next, let us consider differential equation (5.100) at a time point $t^* \in (0, \theta)$ with initial condition $\sigma(t^*) = \sigma^*$, $RP(t^*)$ given and fixed (no time evolution of RPs!) and

prescribed $\varepsilon(t^*), T(t^*)$. We further suppose the computational process is stopped whenever $\sigma < 0$ or $\sigma = \sigma^{\mathrm{pl}} \in \mathbb{R}^+$, since then next evolution is not defined in the superelasticity model (compression or plastic slip, see the yellow area in figure 5.1). Hence $0 \leq \sigma^* < \sigma^{\mathrm{pl}}$.

Collecting all mentioned properties of considered parameters and functions, it holds

- $\tilde{F}(t,\sigma) : \Omega := \langle 0, \theta\rangle \times \langle \sigma^m, \sigma^{\mathrm{pl}}\rangle \to \mathbb{R}$ is continuous and bounded on a planar domain $\Omega$.

Indeed, $\dot{\varepsilon}(t), \dot{T}(t), \tilde{f}(t,\sigma), \tilde{g}(t,\sigma)$ are defined and continuous on a closed set $\Omega$ and $\tilde{g}(t,\sigma)$ is positive there.

Employing Peano's theorem in the form:

(PT) Let $\tilde{F}(t,y)$ be continuous function defined and bounded on a domain $\Omega$ of the $t$-$y$-plane. Let initial condition $[t_0, y_0]$ belong to the interior of $\Omega$. Then there is an $h > 0$ and a function $y(t)$ continuously differentiable on $|t - t_0| < h$ such that $[t, y(t)]$ remains in $\Omega$ for $|t - t_0| < h$ and $y(t)$ solves ordinary differential equation $\dot{y} = \tilde{F}(t,y)$, with an initial condition $y(t_0) = y_0$.

one obtains existence of a solution of the problem with fixed set of return points (we denote $t_0 = t^*, \sigma_0 = \sigma^*$).

Moreover, let us further assume

$$e^R(\sigma) \in \mathcal{C}^2(\mathbb{R}), \quad \xi_{A2R}(\varphi^R), \xi_{A2M}(\varphi), \xi_{M2A}(\varphi) \in \mathcal{C}^2(\mathbb{R}), \tag{5.104}$$

where $\mathcal{C}^2(\mathbb{R})$ denotes (space of) functions defined on real numbers with a continuous second derivative. Then the first derivative of function $\tilde{F}$ is defined and continuous on $\Omega$ and thus it holds

- $\tilde{F}(t,\cdot)$ is Lipschitz continuous function of variable $\sigma$ on domain $\Omega$.

(Recall differentiable functions on a closed set are Lipschitz continuous there.)

Now, let us recall Picard-Lindelöf theorem:

(PLT) Let $\tilde{F}(t,y)$ be bounded continuous function on a domain $\Omega$ of the $t$-$y$-plane and satisfy a Lipschitz condition in variable $y$ there. Let initial condition $[t_0, y_0]$ belong to the interior of $\Omega$. Then there is an $h > 0$ and a unique function $y(t)$ continuously differentiable on $|t - t_0| < h$ such that $[t, y(t)]$ remains in $\Omega$ for $|t - t_0| < h$ and $y(t)$ solves ODE $\dot{y} = \tilde{F}(t,y)$, $y(t_0) = y_0$.

Thus, (PLT) implies uniqueness of a solution of the problem with fixed RP set.

We can repeat all the arguments with a different set of return points $RP$ fixed at $(0,\theta)$ and prove the existence and uniqueness for such case. For $t = 0$ conditions of (PLT) are not disrupted by expansion the domain $\Omega$ to a small time neighborhood of $t = 0$, i.e. $\Omega = (-\epsilon, \theta\rangle \times \langle \sigma^m, \sigma^{\mathrm{pl}}\rangle$, $\epsilon > 0$, if we define $\dot{\varepsilon}(t), \dot{T}(t)\ \forall t \in (-\epsilon, 0)$ to be continuously differentiable (recall it holds $\dot{\varepsilon}(t), \dot{T}(t) \in \mathcal{C}^1\langle 0, +\infty\rangle$, thus it is possible).

If $\dot{\varphi}(t) = 0$ at any time $t \in (0, \theta\rangle$, process is stopped, conditions (5.16), (5.17) are checked, return point set $RP$ is upgraded if needed, and in that case computational process starts with the same values of stress, temperature and strain, but with the new RP set as initial conditions. It means solutions between return points are joined to form the global solution at $\langle 0, \theta\rangle$. This global solution is continuous, but generally not continuously differentiable in return points.

Finally, since time $\theta$ was chosen arbitrarily, we can expand the time interval to any finite length and repeat the above procedures to obtain existence and uniqueness of solution at that time interval (only constants $C^{\dot{\varepsilon}}, C^{\dot{T}}$ are changing with $\theta$ in the proof).

Let us summarize. If conditions (5.98), (5.99) and (5.104) are satisfied, then there exists one unique continuous solution of the problem (5.80) at $\langle 0, +\infty\rangle$ with initial conditions (5.81).

### 5.2.5 Numerical Implementation and Comparison with Experimental Results

In numerical implementation, we discretize prescribed time evolution of strain and temperature to finite number of time points $t_i : 0 = t_0 < t_1 < \ldots < t_i < t_{i+1} < \ldots < t_N = \theta$. At actual time point $t_i$ we suppose input parameters and solution are known, i.e. $\varepsilon(t_i), T(t_i), RP(t_i), \sigma(t_i) (\Rightarrow \xi(t_i))$ are given, and strain and temperature increments are prescribed, i.e. $\varepsilon(t_{i+1}), T(t_{i+1})$ are known. Then we search for a stress increment $\Delta\sigma$ in order to value $\sigma(t_{i+1}) = \sigma_i + \Delta\sigma$ satisfies equation

$$\varepsilon(t_{i+1}) = (1-\xi(t_{i+1}))\frac{\sigma(t_{i+1})}{E^A} + \xi(t_{i+1})\frac{\sigma(t_{i+1})}{E^M} + \Lambda\,\xi(t_{i+1}) + (1-\xi(t_{i+1}))e^R(\sigma(t_{i+1}))\xi^R(t_{i+1}) \tag{5.105}$$

where $\xi(t_{i+1}) = \xi(\sigma(t_{i+1}), T(t_{i+1}), RP(t_i), \xi(t_i))$. This implicit discrete relation is solved iteratively by interior-reflective Newton method (minimization). After each step, the algorithm checks if a change in driving force direction ($\operatorname{sign}\Delta\varphi$) has occurred. If so, a new return point is formed provided the discretized form of above described conditions (5.16), (5.17) for establishing a new RP are satisfied. If a hysteresis loop has been closed in the step, then redundant RP are erased. Lastly, initial conditions are upgraded and algorithm is prepared to compute a new step.

If time step is decreased, the discretization of input functions $\varepsilon(t), T(t)$ and return points localization are more precise, which leads to improvement of solution accuracy. To formulate the total discretization error, the influence of "wrong RP formation" must be considered ("wrong formation" means a RP which is formed in discrete computation is not formed in continuous computation process or vice versa). Generally, it can be shown, the error depends on the actual number of RPs. If hysteretic loops are closed, error of further stress evolution is lesser than before. Mathematical formulation and a deeper numerical analysis is the subject of further research.

To fit the model to experimental data material parameters $A_{\mathrm{f}}, E^A, E^M, s, s^R, \Lambda$ and material functions $e^R(\sigma), \xi_{A2M}$, $\xi_{M2A}$, $\xi_{A2R}$ must be quantified. A possible way how to

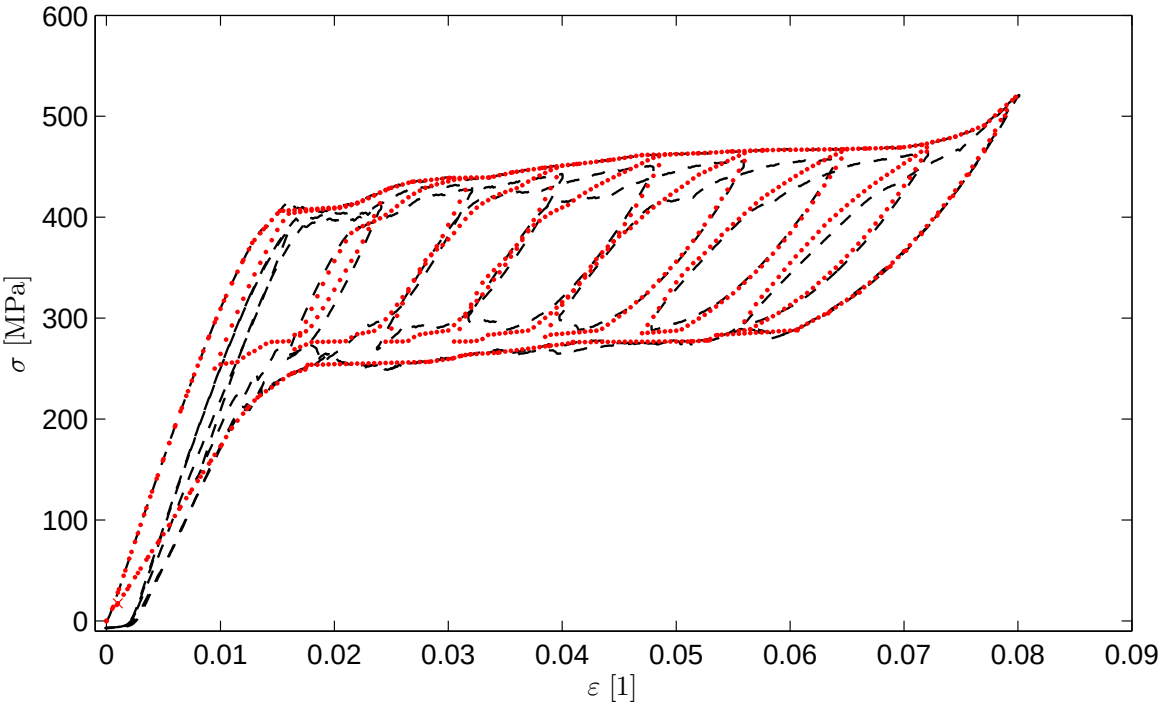


Figure 5.5: Comparison of results of an experiment and the model, internal loops. Experimental data denoted by dashed line, modeled data denoted by red points.

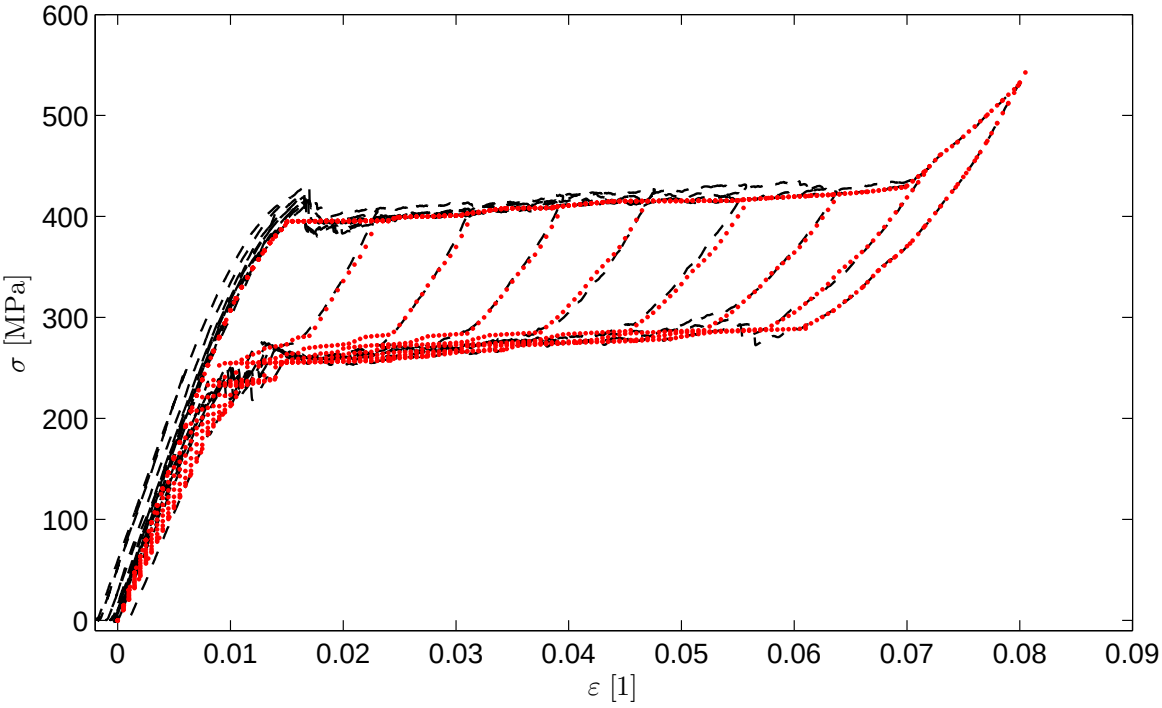


Figure 5.6: Comparison of results of an experiment and of the model, partial cycles. Experimental data denoted by dashed line, modeled data denoted by red points.

do so is described in the experimental part of section 5.3.

In figure 5.5 experimental results with computational model results are compared for mechanical loading at constant temperature. The major loop of the model was fitted to the major loop in the experiment and suitable values of coefficients $k_{A2M}$, $k_{M2A}$ were chosen in order to fit the internal loops. As can be seen, some experimental internal loops slightly violate the return point memory, which is probably caused by difficulties in evacuating or absorbing the transformation latent heat during the experiment. Some variations of experimental data in the austenite elastic range (low stress) indicate the wire undergoes process of training during cycling.

Based on the previous data fit, several partial cycles at constant temperature were modeled. Comparison with experimental results is in figure 5.6. Evidently, modeled partial cycles are in a very good agreement with experimental ones.

## 5.3 Pseudoplasticity Model

### 5.3.1 Physical Model

Now let us consider the part of $\sigma$-$T$ plane, where $\sigma \geq 0$, see figure 5.7. A new effect that must be further implemented in the algorithm is martensite reorientation processes (described in section 2.2). From a macroscopic point of view, reorientation is demonstrated by the fact, the transformation strain of an element of martensite (until it is transformed to austenite) depends on the value of the maximum stress to which it was subjected. This leads to hysteretic behavior of transformation strain. The critical stress required for full reorientation of martensite $\sigma^{\mathrm{re}}$ is assumed to be independent on temperature.

### 5.3.2 Algorithm

Since following algorithm is an extension of the previous one, definitions of driving force $\varphi^+(t)$, variables $\xi^+(t), RP^+(t)$, material parameters, RPM mechanism and $\xi^+(t)$ evolution mechanism do not differ from superelasticity model in tension and will not be repeated here. (Just change $\varphi$ to $\varphi^+$, $\xi$ to $\xi^+$ and $RP$ to $RP^+$ in definitions and equations.) A new internal variable representing transformation strain is defined in order to include reorientation processes:

$\varepsilon^+(t,\zeta)$ a real function of two variables representing the evolution of (non-negative) transformation strain of tensile martensite,
$\varepsilon^+(t,\zeta) : \mathbb{R}_0^+ \times I \to \mathbb{R}_0^+$.

We assume each infinitesimal amount of martensite "remembers" the maximum stress to which it has been subjected since it was formed. This stress determines the transformation strain of this element, which is experimentally demonstrated by different transformation strain for martensite formed at different stress. Whenever an element of martensite is exposed to stress $\sigma^*$ grater than the maximum stress in its own history,

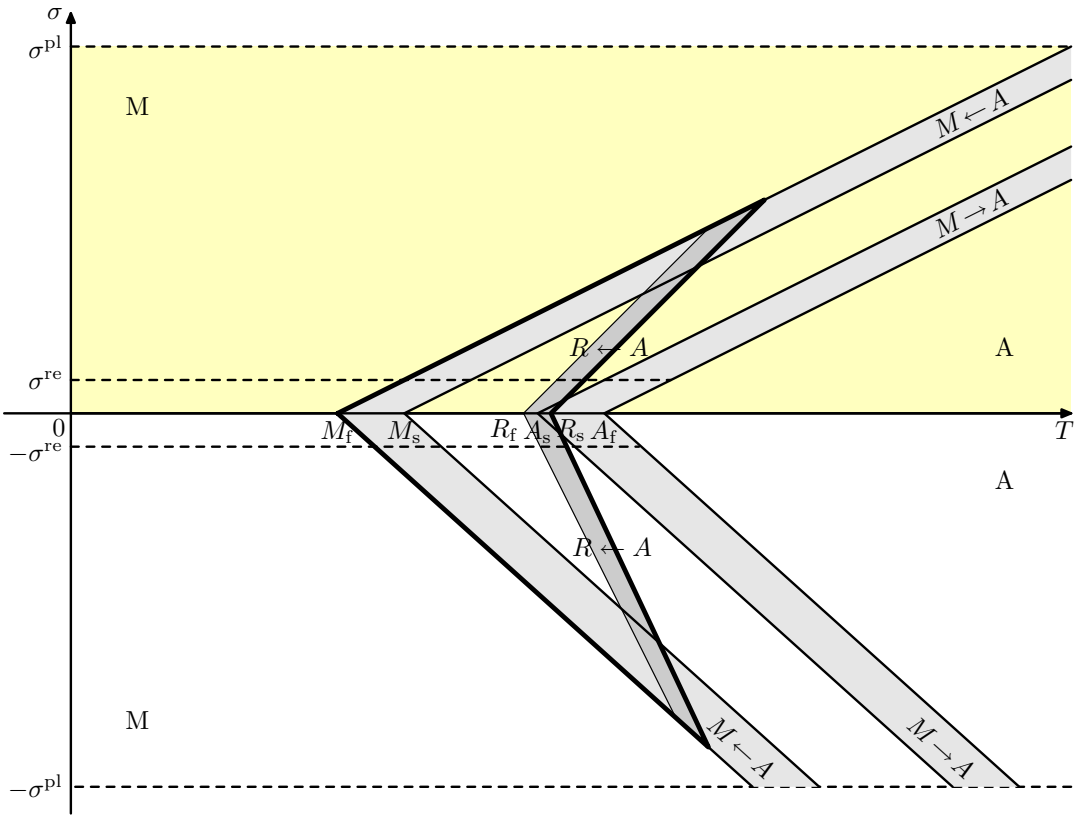


Figure 5.7: Stress-temperature space. Part considered in the pseudoplasticity model is marked with yellow color.

it is being "oriented" and finally increases its transformation strain up to $e^+(\sigma^*)$. If imposed stress is decreased afterwards, transformation strain of this element does not change until it is transformed back to austenite.

Transformation strain of martensite formed at constant stress (i.e. at thermally induced transition) $\sigma$ is described by input function $e^+(\sigma)$, which can be obtained experimentally. If $\sigma > \sigma^{\mathrm{re}}$, martensite is fully oriented and transformation strain is maximal, if $\sigma = 0$, self-accommodating (twinned) martensite is formed and macroscopical transformation strain equals zero, see section 2.2. (Let us note for materials undergoing process of training, not considered in this work, described strains could develop during training.) Thus function $e^+(\sigma)$ is assumed to fulfil following conditions:

$$\begin{aligned} &e^+(\sigma) : \mathbb{R} \to \mathbb{R}_0^+ \text{ is a non-decreasing continuously differentiable function,} \\ &e^+(\sigma) = 0 \quad \text{if} \quad \sigma \leq 0, \\ &e^+(\sigma) = \Lambda^+ \quad \text{if} \quad \sigma > \sigma^{\mathrm{re}}, \end{aligned} \tag{5.106}$$

where positive constant $\Lambda^+$ represents already introduced maximum strain in tension.

We introduce RPM effect in reorientation processes due to "last in, first out" rule. Algorithm "remembers" sequence in which the martensite increments has been formed

and when driving force $\varphi^+$ decreases, they are removed in the reverse order. (Detailed description of algorithm in the next paragraph will make the mechanism clearer.)

The evolution of the function $\varepsilon^+(t,\zeta)$ is determined by function $e^+(\sigma)$ and a reorientation mechanism. Next, the evolution of $\varepsilon^+(t,\zeta)$ is described. Because this function is discontinuous in variables $t,\zeta$, we introduce an infinitesimal increment of time $\mathrm{d}t$ and define infinitesimal time increment of real function $x(t)$ at time $t$ as

$$\mathrm{d}x = \mathrm{d}x(t) := x(t+\mathrm{d}t) - x(t). \tag{5.107}$$

This help us to clearly demonstrate the idea of the reorientation mechanism.

Time increment of $\varepsilon^+(t,\zeta)$ depends on increments of volume fraction $\mathrm{d}\xi$ and stress $\mathrm{d}\sigma$ (driving force for reorientation), therefore we distinct four possibilities of evolution depicted (in discretization case) in figure 5.8 and described in following list. Let us note, we suppose the same initial conditions as in previous algorithm, i.e. relations (5.36) and

$$\varepsilon^+(0,\zeta) = 0 \quad \forall\, \zeta \in I. \tag{5.108}$$

1. Martensite volume fraction is non-decreasing, stress is increasing
   ($\mathrm{d}\xi^+ \geq 0$, $\mathrm{d}\sigma > 0$):
   Value of strain function of formed martensite is equal to $e^+(\sigma(t+\mathrm{d}t))$. Martensite elements with lower transformation strain increase this strain up to $e^+(\sigma(t+\mathrm{d}t))$:

$$\varepsilon^+(t+\mathrm{d}t,\zeta) = \begin{cases} \max\{\varepsilon^+(t,\zeta), e^+(\sigma(t+\mathrm{d}t))\} & \zeta \in \langle 0, \xi^+(t)\rangle \\ e^+(\sigma(t+\mathrm{d}t)) & \zeta \in (\xi^+(t), \xi^+(t+\mathrm{d}t))\rangle \\ 0 & \zeta \in (\xi^+(t+\mathrm{d}t), 1\rangle \end{cases} \tag{5.109}$$

2. Martensite volume fraction is non-decreasing, stress is non-increasing
   ($\mathrm{d}\xi^+ \geq 0$, $\mathrm{d}\sigma \leq 0$):
   Since stress is non-increasing, previously formed martensite is not reoriented, its strain remains unchanged and value of strain function of formed martensite is uniquely determined by $e^+(\sigma)$. Thus:

$$\varepsilon^+(t+\mathrm{d}t,\zeta) = \begin{cases} \varepsilon^+(t,\zeta) & \zeta \in \langle 0, \xi^+(t)\rangle \\ e^+(\sigma(t+\mathrm{d}t)) & \zeta \in (\xi^+(t), \xi^+(t+\mathrm{d}t))\rangle \\ 0 & \zeta \in (\xi^+(t+\mathrm{d}t), 1\rangle \end{cases} \tag{5.110}$$

3. Martensite volume fraction is decreasing, stress is non-increasing
   ($\mathrm{d}\xi^+ < 0$, $\mathrm{d}\sigma \leq 0$):
   Stress is decreasing, no reorientation process occurs, thus:

$$\varepsilon^+(t+\mathrm{d}t,\zeta) = \begin{cases} \varepsilon^+(t,\zeta) & \zeta \in \langle 0, \xi^+(t+\mathrm{d}t)\rangle \\ 0 & \zeta \in (\xi^+(t+\mathrm{d}t), 1\rangle \end{cases} \tag{5.111}$$

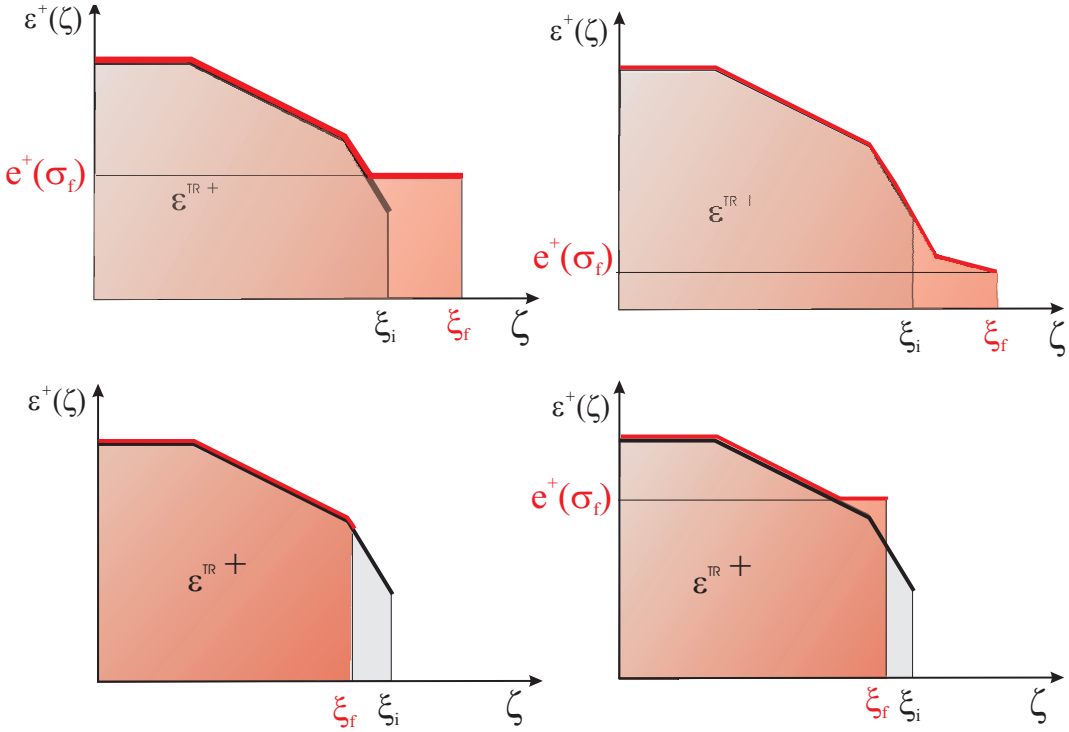


Figure 5.8: Four possible cases of $\varepsilon^+$ evolution before and after a time step, discrete approach. $\xi_\mathrm{i}/\xi_\mathrm{f}$ is the initial/final value of martensite volume fraction, $e^+(\sigma_\mathrm{f})$ denotes value of function $e^+(\sigma)$ at the final value of stress $\sigma_\mathrm{f}$. Function $\varepsilon^+(t,\zeta)$ before/after time step is marked with black/red line. Pictures correspond in turn to cases 1, 2, 3, 4.

4. Martensite volume fraction is decreasing, stress is increasing
   ($\mathrm{d}\xi^+ < 0$, $\mathrm{d}\sigma > 0$):
   Martensite elements with lower transformation strain (which have not transformed to austenite) increase this strain up to $e^+(\sigma(t+\mathrm{d}t))$:

$$\varepsilon^+(t+\mathrm{d}t,\zeta) = \begin{cases} \max\{\varepsilon^+(t,\zeta), e^+(\sigma(t+\mathrm{d}t))\} & \zeta \in \langle 0, \xi^+(t+\mathrm{d}t)\rangle \\ 0 & \zeta \in (\xi^+(t+\mathrm{d}t), 1\rangle \end{cases} \tag{5.112}$$

All cases in a more compact notation:

$$\varepsilon^+(t+\mathrm{d}t,\zeta) = \begin{cases} \max\{\varepsilon^+(t,\zeta), e^+(\sigma(t+\mathrm{d}t))\} & \zeta \in \langle 0, \min\{\xi^+(t), \xi^+(t+\mathrm{d}t)\}\rangle \\ e^+(\sigma(t+\mathrm{d}t)) & \zeta \in (\xi^+(t), \xi^+(t+\mathrm{d}t)\rangle \\ 0 & \zeta \in (\xi^+(t+\mathrm{d}t), 1\rangle \end{cases} \tag{5.113}$$

where we define

$$a, b \in \mathbb{R} : a \geq b \Rightarrow (a, b\rangle = \emptyset.$$

It is worth noting if martensite is formed at $\sigma > \sigma^{\mathrm{re}}$ then it is never "oriented" by the algorithm and the mechanism is equivalent to superelasticity algorithm.

Note also, for any fixed time $t^*$ the function of one variable $\varepsilon^+_{t^*}(\zeta) := \varepsilon^+(t^*, \cdot)$, $\zeta \in I$ is non-increasing and discontinuous. (For proof of the first property use contradiction and recall $\forall \zeta \in I : \varepsilon^+(0, \zeta) = 0$ at the beginning of computational process.)

The total transformation strain is a sum of transformation strains determined for each martensitic element by function $\varepsilon^+(t + \mathrm{d}t, \zeta)$. Mathematically expressed:

$$\varepsilon^{\mathrm{tr}+}(t) = \int_0^1 \varepsilon^+(t, \zeta)\, \mathrm{d}\zeta. \tag{5.114}$$

From the physical point of view, it is important, that the function $\varepsilon^{\mathrm{tr}+}(t)$, representing strain, is a continuous function, which is due to above described reorientation mechanism.

The slightly changed constitutive equation (5.35) can be written now:

$$\varepsilon(t) = (1 - \xi^+(t))\frac{\sigma(t)}{E^A} + \xi^+(t)\frac{\sigma(t)}{E^M} + (1 - \xi^+(t))e^R(\sigma(t))\xi^R(t) + \varepsilon^{\mathrm{tr}+}(t) \tag{5.115}$$

Let us recall again $\xi(t) = \xi(\sigma(t), T(t), history(t))$ and $\xi^R(t) = \xi^R(\sigma(t), T(t))$, where the parameter $history(t)$ is represented by the set of RPs and the actual value of $\xi^+(t)$.

Following similar procedures as in subsection 5.2.4 we can obtain differential equation in the form

$$\dot{\sigma}(t)^2 \bar{h}(t, \sigma(t), \operatorname{sign}\dot{\varphi}(t))\Theta(\dot{\sigma}(t)) + \dot{\sigma}(t)\bar{g}(t, \sigma(t)) - \dot{T}(t)\bar{f}(t, \sigma(t)) - \dot{\varepsilon}(t) = 0, \tag{5.116}$$

where $\bar{f}(t, \sigma(t)), \bar{g}(t, \sigma(t))$ are stress dependent functions, $\bar{h}(t, \sigma(t), \operatorname{sign}\dot{\varphi}(t))$ depends also on signum of driving force time derivative and Heaviside step function $\Theta : \mathbb{R} \to \{0, 1\}$ is defined as follows

$$\Theta(x) := \begin{cases} 0 & x < 0, \\ 1 & x \geq 0. \end{cases} \tag{5.117}$$

The first term in the equation corresponds to reorientation process. Properties of this differential equation, also existence and uniqueness of a solution of the inverse problem are subjects of further research.

### 5.3.3 Numerical Implementation and Comparison with Experimental Results

In numerical discretization we follow the procedure described in the superelasticity model. Function $\varepsilon^+(t, \zeta)$ must be discretized also in variable $\zeta$.

Now let us briefly describe the procedure enabling us to determine material parameters $A_{\mathrm{f}}, E^A, E^M$, $s, s^R$ and material functions $e^R(\sigma), e^+(\sigma), \xi_{A2M}$, $\xi_{M2A}$, $\xi_{A2R}$.

In described case, no R-phase transition has occurred during thermomechanical loading, which makes analysis easier. Experimentally, several thermal tests at constant load and mechanical (stress-strain) test at constant temperature were performed. As

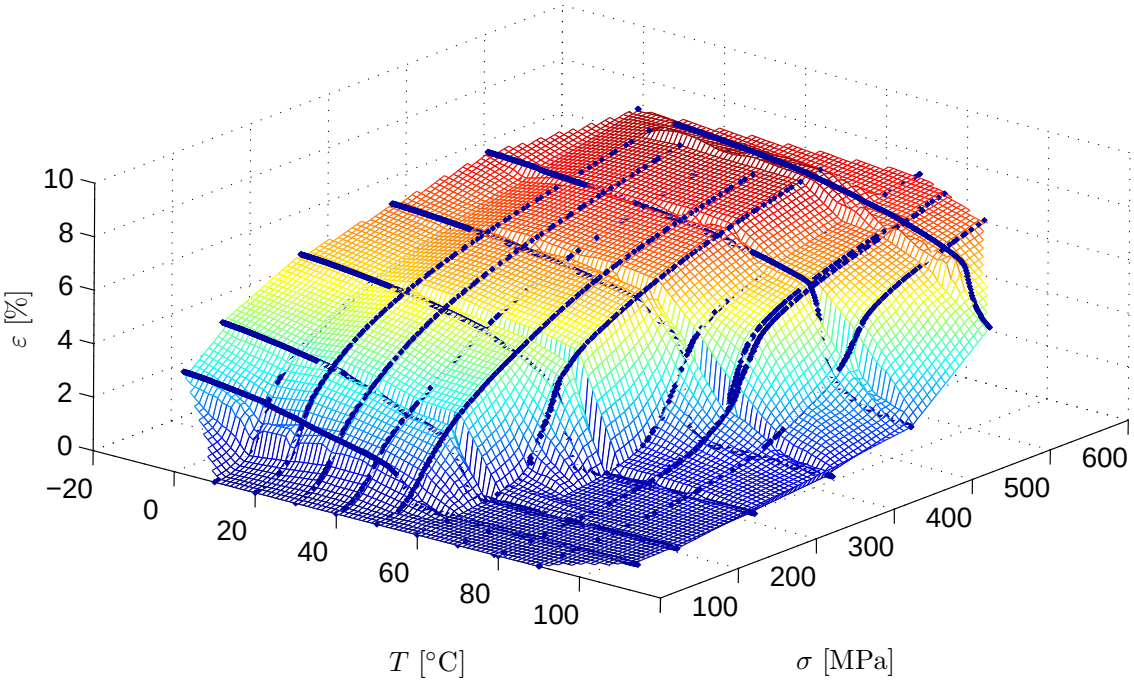


Figure 5.9: Experimental curves and interpolated strain surface.

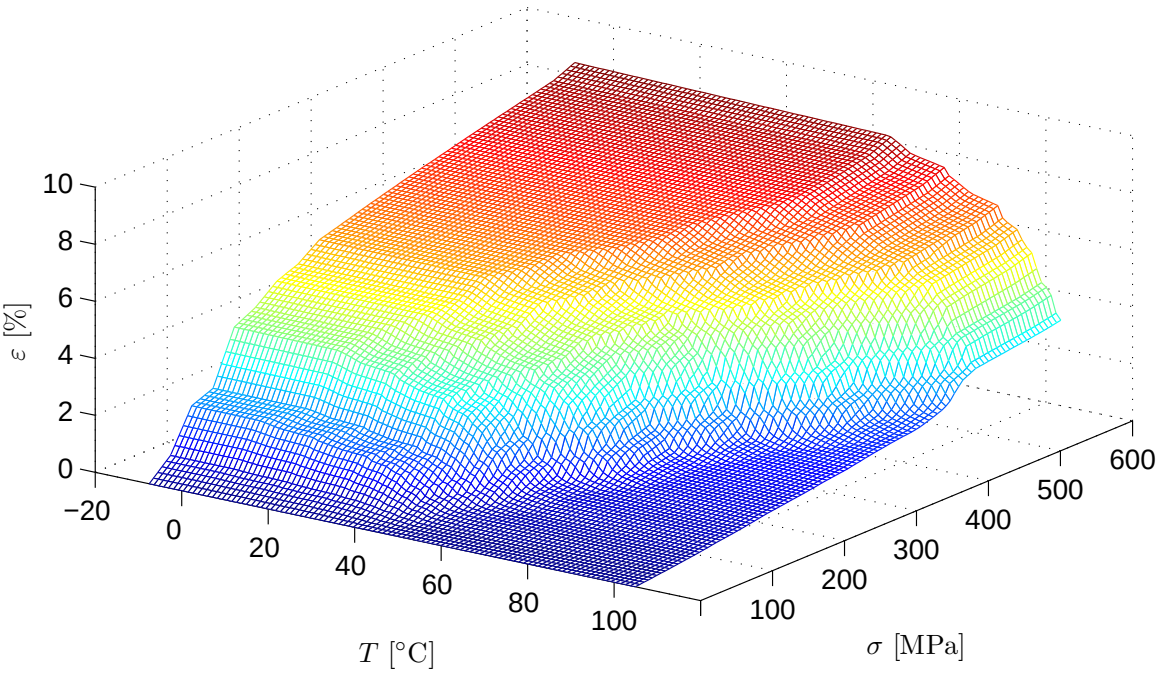


Figure 5.10: Fitted minimum strain surface.

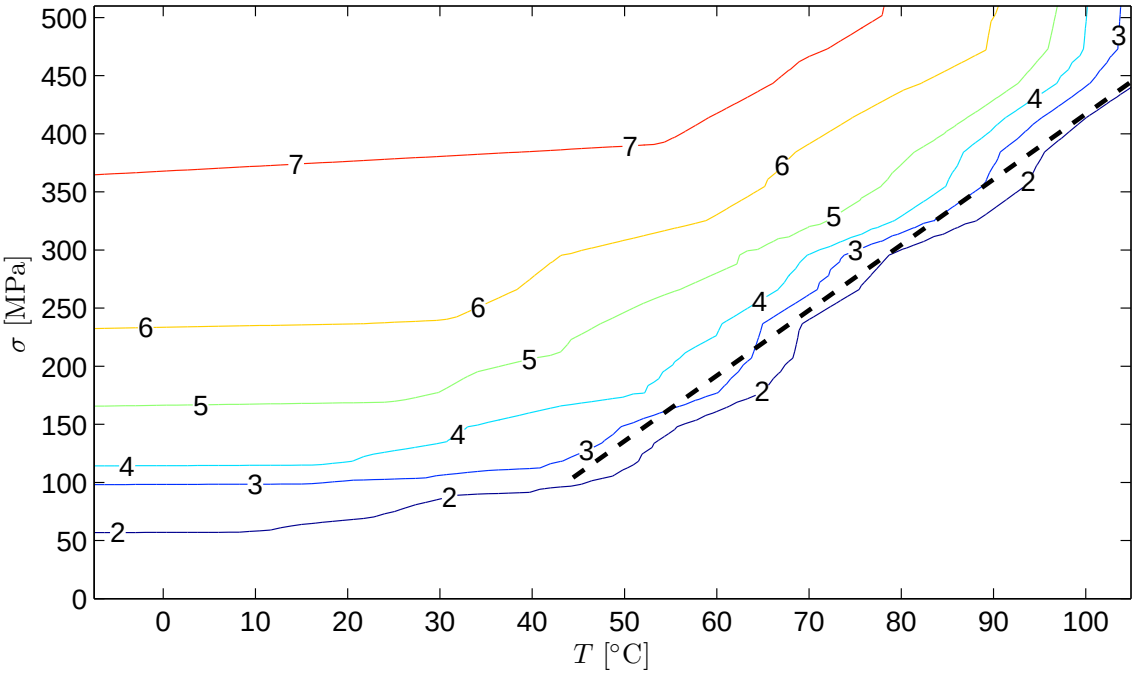


Figure 5.11: Isocurves of the minimum strain surface (values in percent). The critical transformation slope is tangent of the angle between dashed line (linear fit) and temperature axis.

a result one obtains several pairs of curves, one in a pair for forward and one for reverse martensitic transformation. For forward transition, each point in $\sigma$-$T$ plane can be assigned a value of the strain the material element has, if its initial strain at $T = A_\mathrm{f}, \sigma = 0$ equals zero and the point is achieved by a thermomechanical loading under monotonous driving force (so no RP has been formed during the loading). In other words, it can be assigned the minimum strain of the material element at that point. Values of minimum strain forms the "minimum strain surface", $\varepsilon^{\min}(\sigma, T)$. All curves for the forward transition are "slices" of the minimum strain surface in the stress-strain-temperature space.

In the first approximation we can neglect the contribution of elasticity and R-phase transition strain to the total strain with respect to martensite transformation strain in equation (5.115) for points in superelasticity part of $\sigma$-$T$ space near the critical transformation stresses (then $\varepsilon^{\mathrm{el}} \sim 0.5\%$, $\Lambda^R \sim 1\%$, $\Lambda \sim$ 6-8%). In that case values of total strain are approximately linearly proportional to martensite volume fraction, since $\varepsilon^{\min} = \varepsilon \sim \Lambda\xi$. The contour map of strain surface is thus a map of $\varphi$ isocurves due to $\xi(\varphi)$ dependence at superelasticity area.

The experimental curves ("slices" of strain surfaces) were fitted to obtain the minimum strain surface. In a fitting procedure values $\sigma, T, \varepsilon$ are prescribed by experiment and we search for the material parameters and functions in order to satisfy (5.115).

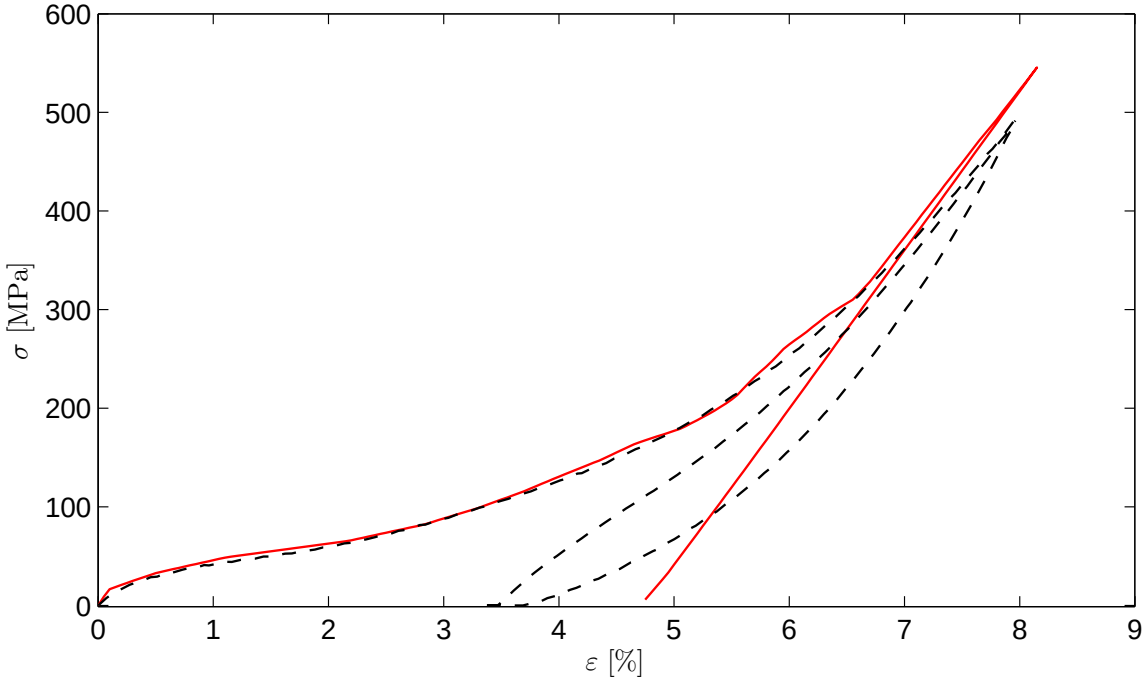


Figure 5.12: Comparison of results of an experiment and of the model, pseudoplastic cycle at 30 °C. Experimental data denoted by dashed line, modeled data denoted by red line.

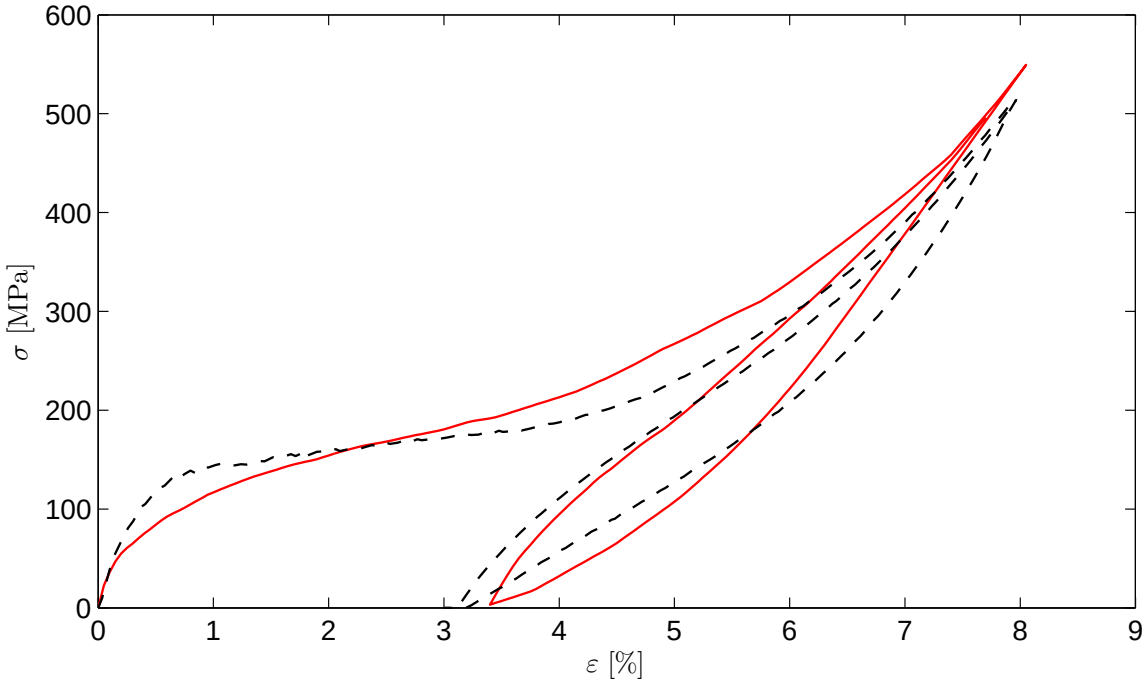


Figure 5.13: Comparison of results of an experiment and of the model, pseudoplastic cycle with internal subloop at 60 °C. Experimental data denoted by dashed line, modeled data denoted by red line.

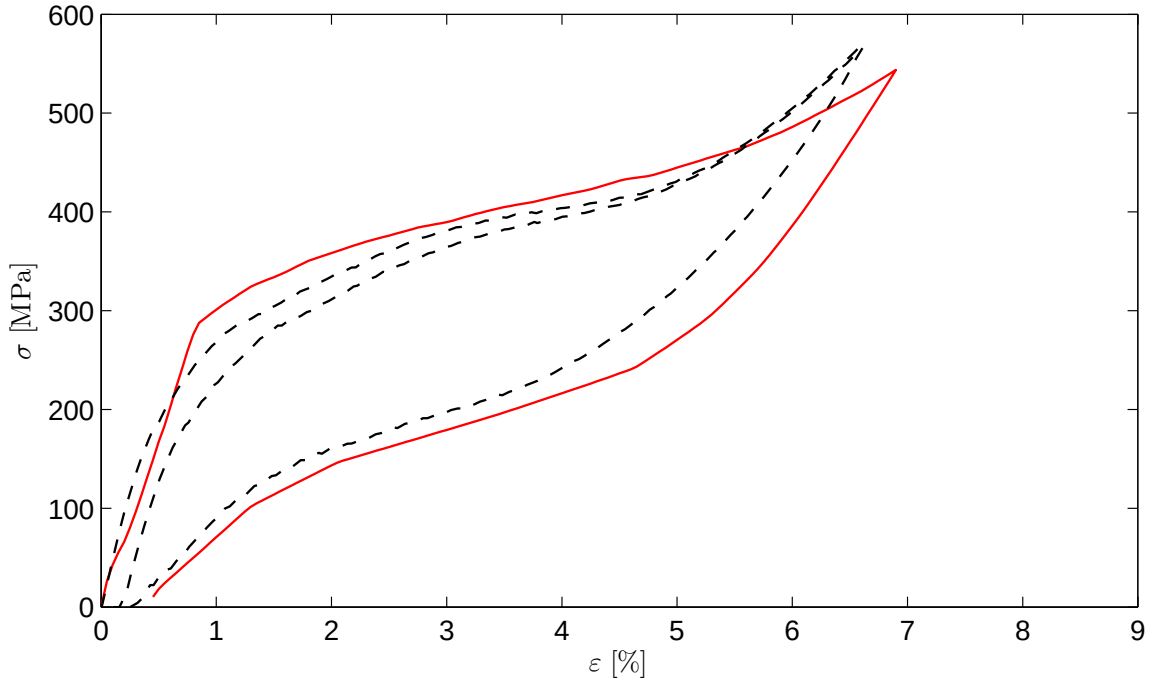


Figure 5.14: Comparison of results of an experiment and of the model, pseudoplastic cycle at 90 °C. Experimental data denoted by dashed line, modeled data denoted by red line.

Hence, we obtain material parameters and functions of a specimen except $\xi_{M2A}, A_\mathrm{f}$. Function $\xi_{M2A}$ can be determined from unloading paths, after rescaling this function also determines temperature $A_\mathrm{f}$.

The experimental curves (thick blue lines) and interpolated strains are depicted in figure 5.9. The fitted minimum transformation surface is in figure 5.10. As can be seen in figure 5.11, the $\varphi$ isocurves of fitted surface approximately correspond to be parallel lines with critical transformation slope supposed by Clausius-Clapeyron equation for higher temperatures (superelasticity area), whereas they tend to be temperature independent at lower temperatures which correspond to presence of martensite reorientation process.

As mentioned above, R-phase is not present in studied type of NiTiNOL wire. For evaluation of functions $e^R(\sigma), \xi_{A2R}$ it is important to strictly distinguish the area, where R-phase is present. Resistivity measurements and neutron diffraction are very helpful techniques [9]. Then the approach would be similar to the described one.

The obvious advantage of fitting approach compared to separate finding out the parameters (literature, single specialized measurements) is that the values reflect the real experimental data for concrete type of wire. A disadvantage is that more experiments are needed. Results of experimental and modeled data of thermal cycles at some temperatures are in figures 5.12, 5.13 and 5.14. Discrepancies occurring at reverse transitions are probably due to inaccurate fit of $\xi_{M2A}$ function.

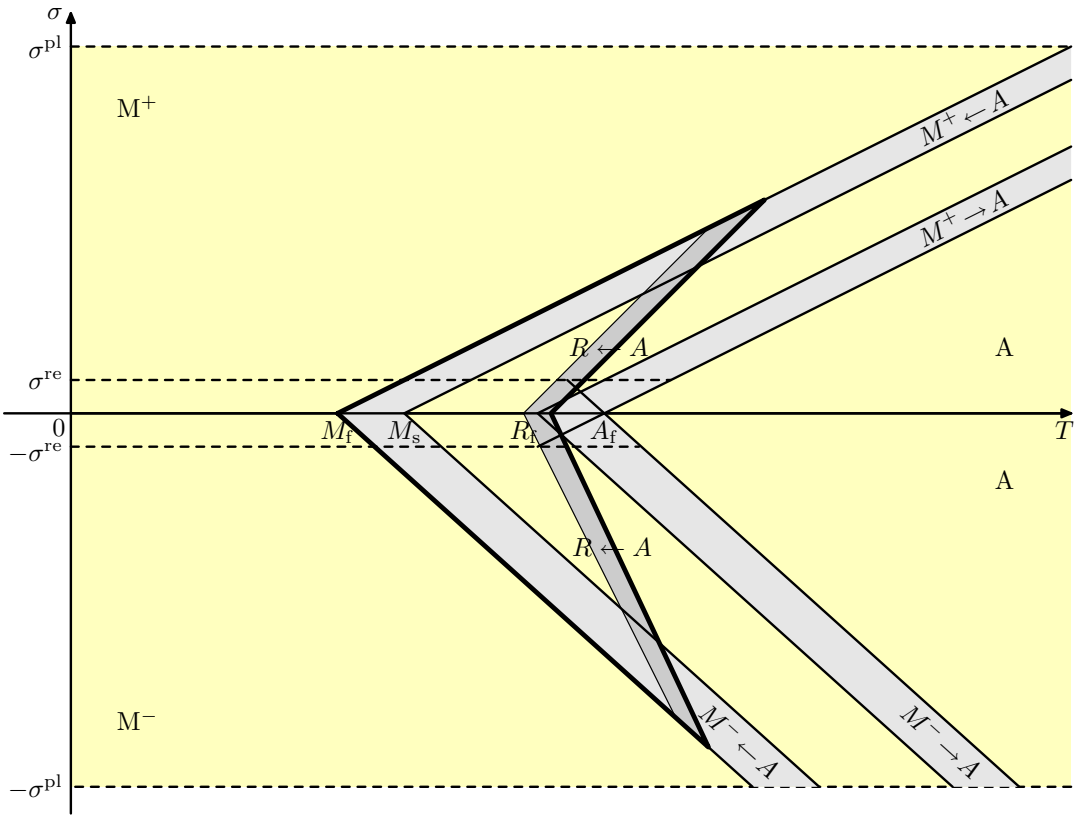


Figure 5.15: Stress-temperature space. The whole of it is considered in the thermomechanical model as marked with yellow color.

## 5.4 Thermomechanical Model

Next natural step is to expand pseudoplasticity-superelasticity model to negative values of stress. But, in contrast to the case of superelasticity model, tensile and compressive martensite may coexist and interact for $\sigma \in (-\sigma^{\mathrm{re}}, \sigma^{\mathrm{re}})$ and $T < A_{\mathrm{f}}$. The extension of just described algorithm is thus not straightforward. A possible way is sketched in this section, but the model is still under construction.

### 5.4.1 Physical Model

The phase diagram for this model is depicted in figure 5.15, main considered mechanisms are martensitic and R-phase transformations and reorientation process. $\sigma$-$T$ plane is divided into three main regions, where austenite phase (denoted by 'A') or tensile martensite phase ('M$^+$') or compressive martensite phase ('M$^-$') exists. The critical transformation stress required for forward and reverse transformations depends on temperature and thus strips separate these regions. The new physical phenomena is transformation between tensile and compressive martensite. This transformation oc-

curs in the stress interval $\langle -\sigma^{\mathrm{re}}, \sigma^{\mathrm{re}} \rangle$ and leads to existence of tensile martensite in compression and compressive martensite in tension. In compression tensile martensite disappears at stress level $-\sigma^{\mathrm{re}}$ at low temperatures or at critical transformation stress line prolonged from temperature $A_{\mathrm{f}}$ to negative values of stress as drawn in figure 5.15. Similarly, in tension compressive martensite disappears at stress level $\sigma^{\mathrm{re}}$ or when prolongation of critical transformation stress line from $A_{\mathrm{f}}$ to positive $\sigma$ half-space is reached.

### 5.4.2 Algorithm

The algorithm can be divided to three parts similarly to tension-compression superelasticity model. The first two are quite mutually independent subalgorithms describing the evolution of transformation strain of tensional and compressive martensite, respectively. In the last part algorithm computes evolution of volume fraction and transformation strain of R-phase, analyzes results and evaluate total volume fraction of martensite and total strain of material. To make the algorithm more lucid, all internal variables and parameters are summarized.

Let us introduce new driving forces for martensitic transition

$$\varphi^{+}(\sigma(t), T(t)) := \left[ \frac{\sigma(t)}{s^{+}} - (T(t) - A_{\mathrm{f}}) \right] f^{+}(\sigma(t)), \tag{5.118}$$

$$\varphi^{-}(\sigma(t), T(t)) := \left[ \frac{\sigma(t)}{s^{-}} - (T(t) - A_{\mathrm{f}}) \right] f^{-}(\sigma(t)), \tag{5.119}$$

where real functions $f^{+}(\sigma), f^{-}(\sigma)$ fulfil following conditions:

$$\begin{aligned} &f^{+}(\sigma) : \mathbb{R} \to I \text{ is a non-decreasing continuously differentiable function,} \\ &f^{+}(\sigma) = 0 \quad \text{if} \quad \sigma \leq -\sigma^{\mathrm{re}}, \\ &f^{+}(\sigma) = 1 \quad \text{if} \quad \sigma \geq 0, \end{aligned} \tag{5.120}$$

$$\begin{aligned} &f^{-}(\sigma) : \mathbb{R} \to I \text{ is a non-increasing continuously differentiable function,} \\ &f^{-}(\sigma) = 0 \quad \text{if} \quad \sigma \geq \sigma^{\mathrm{re}}, \\ &f^{-}(\sigma) = 1 \quad \text{if} \quad \sigma \leq 0, \end{aligned} \tag{5.121}$$

These additional functions were introduced in an effort to capture presence of tensile martensite under compression (and compressive martensite under tension). Low temperature stress induced formation of one type of martensite and simultaneous disappearing of the other one could be considered as a transformation with no (negligible) entropy change. With respect to this physical motivation, we define $\Delta s = 0$ in (3.113) and obtain $\mathrm{d}\sigma/\mathrm{d}T = 0$, which confirms temperature independence of $\sigma^{\mathrm{re}}$. In summary, tensile/compressive martensite disappears when critical stresses given by Clausius-Clapeyron equation or reorientation stresses $-\sigma^{\mathrm{re}}/\sigma^{\mathrm{re}}$ are attained. Introduction of function $f^{+}/f^{-}$ reflects both limiting cases.

An example of isocurves of driving forces $\varphi^{+}$, $\varphi^{-}$ (curves linking the points with the same value of driving force) in $\sigma$-$T$ space is depicted in figure 5.16.

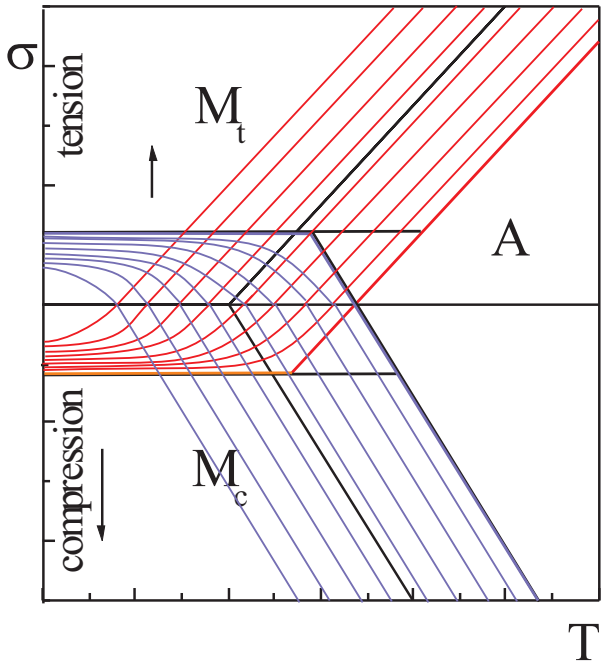


Figure 5.16: An example of some possible isocurves of driving forces $\varphi^+$ (red lines) and $\varphi^-$ (blue lines) in $\sigma$-$T$ space. $M_t$ denotes tensile martensite, $M_c$ denotes compressive martensite.

Next, we summarize internal variables for the first subalgorithm:

$\xi^+(t)$ a real function representing tensile martensite,
$\xi^+(t) : \mathbb{R} \to I$

$RP^+(t)$ a set of ordered pair of real variables representing set of return points in evolution of tensile martensite,
$RP^+(t) := \{[\varphi^+(t_1), \xi^+(t_1)], [\varphi^+(t_2), \xi^+(t_2)], .., [\varphi^+(t_n), \xi^+(t_n)];$
$\varphi^+(t_i) \in \mathbb{R}$, $\xi^+(t_i) \in I$, $0 \leq t_i < t$, $\forall\, i = 1, 2, .., n^+(t) \in \mathbb{N}$, $n^+(t) \geq 2\}$

$\varepsilon^+(t, \zeta)$ a real function of two variables representing the evolution of (non-negative) transformation strain of tensile martensite,
$\varepsilon^+(t, \zeta) : \mathbb{R}_0^+ \times I \to \mathbb{R}_0^+$.

and in a similar way for the second subalgorithm:

$\xi^-(t)$ a real variable representing compressive martensite,
$\xi^- : \mathbb{R} \to I$

$RP^-(t)$ a set of real variables representing set of return points in evolution of compressive martensite,
$RP^-(t) := \{[\varphi^-(t_1), \xi^-(t_1)], [\varphi^-(t_2), \xi^-(t_2)], .., [\varphi^-(t_n), \xi^-(t_n)];$
$\varphi^-(t_i) \in \mathbb{R}$, $\xi^-(t_i) \in I$, $0 \leq t_i < t$, $\forall\, i = 1, 2, .., n^-(t) \in \mathbb{N}$, $n^-(t) \geq 2\}$

$\varepsilon^-(t, \zeta)$ a real function of two variables representing the evolution of (non-positive) transformation strain of compressive martensite,
$\varepsilon^-(t, \zeta) : \mathbb{R}_0^+ \times I \to \mathbb{R}_0^-$.

Transformation strain of martensite created at constant stress $\sigma$ is described by two input functions $e^+(\sigma)$ and $e^-(\sigma)$ in the model, for tensile and compressive martensite, respectively. These functions are supposed to fulfil following conditions:

$$\begin{aligned} &e^+(\sigma) : \mathbb{R} \to \mathbb{R}_0^+ \text{ is a non-decreasing continuously differentiable function,} \\ &e^+(\sigma) = 0 \quad \text{if} \quad \sigma \leq 0, \\ &e^+(\sigma) = \Lambda^+ \quad \text{if} \quad \sigma > \sigma^{\mathrm{re}}, \end{aligned} \tag{5.122}$$

$$\begin{aligned} &e^-(\sigma) : \mathbb{R} \to \mathbb{R}_0^- \text{ is a non-increasing continuously differentiable function,} \\ &e^-(\sigma) = 0 \quad \text{if} \quad \sigma \geq 0, \\ &e^-(\sigma) = \Lambda^- \quad \text{if} \quad \sigma < -\sigma^{\mathrm{re}}. \end{aligned} \tag{5.123}$$

For R-phase transition it has already been introduced

$$\begin{aligned} &e^R(\sigma) : \mathbb{R} \to \mathbb{R}_0^+ \text{ is a non-decreasing continuously differentiable function,} \\ &e^R(\sigma) = -e^R(-\sigma) \quad \forall \sigma \in \mathbb{R}, \\ &e^R(\sigma) = \Lambda^R \quad \text{if} \quad \sigma > \sigma^{R\mathrm{re}}. \end{aligned} \tag{5.124}$$

Constants $\Lambda^+$, $\Lambda^-$ and $\Lambda^R$ represent the maximum strain of martensite in tension, compression and R-phase, respectively. Functions $e^+, e^-, e^R$ can be obtained experimentally (thermal lading at constant stress).

Recapitulation of material parameters:

| | |
|---|---|
| $A_{\mathrm{f}}$ | real constant, martensite to austenite transition finish temperature |
| $E^M$ | real constant, Young's elastic modulus of martensite |
| $E^A$ | real constant, Young's elastic modulus of austenite |
| $s^+$ | real constant, critical martensitic transformation slope (tension) |
| $s^-$ | real constant, critical martensitic transformation slope (compression) |
| $s^R$ | real constant, critical R-phase transformation slope |
| $e^+(\sigma)$ | real function, transformation strain evolution for tensile martensite |
| $e^-(\sigma)$ | real function, transformation strain evolution for compressive martensite |
| $e^R(\sigma)$ | real function, transformation strain of R-phase transformation |
| $f^+(\sigma)$ | real function, tensile to compressive martensite transformation |
| $f^-(\sigma)$ | real function, compressive to tensile martensite transformation |
| $\xi_{M2A}(\varphi)$ | real function, completed martensite to austenite transition |
| $\xi_{A2M}(\varphi)$ | real function, completed austenite to martensite transition |
| $\xi_{A2R}(\varphi)$ | real function, completed austenite to R-phase transition |

Functions are more specified above. Note transformation temperatures and maximum transformation strains are implicitly hidden in functions $\xi_{A2M}(\varphi), \xi_{M2A}(\varphi), \xi_{A2R}(\varphi)$ and $e^+, e^-, e^R$.

Lastly, recapitulation of input functions

$$\begin{aligned} &\sigma(t) : \mathbb{R}_0^+ \to \mathbb{R}, \quad \sigma(t) \in \mathcal{C}^1(\mathbb{R}_0^+), \quad (\text{must satisfy } \sigma(0) = 0), \\ &T(t) : \mathbb{R}_0^+ \to \mathbb{R}^+, \quad T(t) \in \mathcal{C}^1(\mathbb{R}_0^+), \quad (\text{must satisfy } T(0) = A_{\mathrm{f}}), \end{aligned} \tag{5.125}$$

and initial conditions:

$$\begin{aligned}
&T(0) = A_{\mathrm{f}},\\
&\sigma(0) = 0,\\
&RP^{+\mathrm{f}}(0) = \{[+\infty, 1]\},\\
&RP^{+\mathrm{r}}(0) = \{[-\infty, 0]\},\\
&RP^{-\mathrm{f}}(0) = \{[+\infty, 1]\},\\
&RP^{-\mathrm{r}}(0) = \{[-\infty, 0]\},\\
&\varepsilon^{+}(0,\zeta) = 0 \quad \forall \zeta \in I,\\
&\varepsilon^{-}(0,\zeta) = 0 \quad \forall \zeta \in I.
\end{aligned} \tag{5.126}$$

The evolution of the functions $\varepsilon^{+}(t,\zeta)$ was described in previous section, the evolution of $\varepsilon^{-}(t,\zeta)$ is determined by function $e^{-}(\sigma)$ and "reorientation mechanism" fairly similarly to $\varepsilon^{+}(t,\zeta)$. Time increment of $\varepsilon^{-}(t,\zeta)$ depends on increments of functions $\xi^{-}(t)$ and $\sigma(t)$, therefore we distinct four possible cases (keep in mind the transformation strain is non-positive now):

1. Compressive martensite function is non-decreasing, stress is non-decreasing ($\mathrm{d}\xi^{-} \geq 0$, $\mathrm{d}\sigma \geq 0$):
   Since stress is non-decreasing, no reorientation process is involved and value of strain function of formed martensite is uniquely determined by $e^{-}(\sigma)$. Thus:

$$\varepsilon^{-}(t+\mathrm{d}t,\zeta) = \begin{cases} \varepsilon^{-}(t,\zeta) & \zeta \in \langle 0, \xi^{-}(t)\rangle \\ e^{-}(\sigma(t+\mathrm{d}t)) & \zeta \in (\xi^{-}(t), \xi^{-}t + \mathrm{d}t\rangle \\ 0 & \zeta \in (\xi^{-}t + \mathrm{d}t, 1\rangle \end{cases} \tag{5.127}$$

2. Compressive martensite function is non-decreasing, stress is decreasing ($\mathrm{d}\xi^{-} \geq 0$, $\mathrm{d}\sigma < 0$):
   Value of strain function of formed martensite is equal to $e^{-}(\sigma(t+\mathrm{d}t))$. Martensite elements with higher transformation strain decrease their transformation strain up to $e^{-}(\sigma(t+\mathrm{d}t))$:

$$\varepsilon^{-}(t+\mathrm{d}t,\zeta) = \begin{cases} \min\{\varepsilon^{-}(t,\zeta), e^{-}(\sigma(t+\mathrm{d}t))\} & \zeta \in \langle 0, \xi^{-}(t)\rangle \\ e^{-}(\sigma(t+\mathrm{d}t)) & \zeta \in (\xi^{-}(t), \xi^{-}(t+\mathrm{d}t)\rangle \\ 0 & \zeta \in (\xi^{-}(t+\mathrm{d}t), 1\rangle \end{cases} \tag{5.128}$$

3. Compressive martensite function is decreasing, stress is decreasing ($\mathrm{d}\xi^{-} < 0$, $\mathrm{d}\sigma < 0$):
   Martensite elements with higher transformation strain (which have not transformed to austenite) decrease their transformation strain down to $e^{-}(\sigma(t+\mathrm{d}t))$:

$$\varepsilon^{-}(t+\mathrm{d}t,\zeta) = \begin{cases} \min\{\varepsilon^{-}(t,\zeta), e^{-}(\sigma(t+\mathrm{d}t))\} & \zeta \in \langle 0, \xi^{-}(t+\mathrm{d}t)\rangle \\ 0 & \zeta \in (\xi^{-}(t+\mathrm{d}t), 1\rangle \end{cases} \tag{5.129}$$

4. Compressive martensite function is decreasing, stress is non-decreasing ($\mathrm{d}\xi^- < 0$, $\mathrm{d}\sigma \geq 0$):
   Stress is non-decreasing, no reorientation process occurs, thus:

$$\varepsilon^-(t+\mathrm{d}t,\zeta) = \begin{cases} \varepsilon^-(t,\zeta) & \zeta \in \langle 0, \xi^-(t+\mathrm{d}t)\rangle \\ 0 & \zeta \in (\xi^-(t+\mathrm{d}t), 1\rangle \end{cases} \tag{5.130}$$

Recapitulation (in a more compact form):

$$\varepsilon^-(t+\mathrm{d}t,\zeta) = \begin{cases} \min\{\varepsilon^-(t,\zeta), e^-(\sigma(t+\mathrm{d}t))\} & \zeta \in \langle 0, \min\{\xi^-(t), \xi^-(t+\mathrm{d}t)\}\rangle \\ e^-(\sigma(t+\mathrm{d}t)) & \zeta \in (\xi^-(t), \xi^-(t+\mathrm{d}t)\rangle \\ 0 & \zeta \in (\xi^-(t+\mathrm{d}t), 1\rangle \end{cases} \tag{5.131}$$

and

$$\varepsilon^+(t+\mathrm{d}t,\zeta) = \begin{cases} \max\{\varepsilon^+(t,\zeta), e^+(\sigma(t+\mathrm{d}t))\} & \zeta \in \langle 0, \min\{\xi^+(t), \xi^+(t+\mathrm{d}t)\}\rangle \\ e^+(\sigma(t+\mathrm{d}t)) & \zeta \in (\xi^+(t), \xi^+(t+\mathrm{d}t)\rangle \\ 0 & \zeta \in (\xi^+(t+\mathrm{d}t), 1\rangle \end{cases} \tag{5.132}$$

Lastly, note again the evolution of variables representing tensile and compressive martensite is mutually independent in this algorithm, since there is no interaction between variables, driving forces or RPs of both subalgorithms.

Inspired by tension-compression superelastic model we define

$$\xi(t) = \xi(\sigma(t), T(t), history(t)) := \max(\xi^+(t), \xi^-(t)) \tag{5.133}$$

and

$$\varepsilon(t) = (1-\xi(t))\frac{\sigma(t)}{E^A} + \xi(t)\frac{\sigma(t)}{E^M} + \varepsilon^{\mathrm{tr}+}(t) + \varepsilon^{\mathrm{tr}-}(t) + (1-\xi(t))\varepsilon^{\mathrm{tr}R}(t) \tag{5.134}$$

where terms contributing to total strain are

$$\varepsilon^{\mathrm{tr}R}(t) = \xi^R(|\sigma(t)|, T(t))e^R(\sigma(t)), \tag{5.135}$$

$$\varepsilon^{\mathrm{tr}+}(t) = \int_0^1 \varepsilon^+(t,\zeta)\,\mathrm{d}\zeta, \tag{5.136}$$

$$\varepsilon^{\mathrm{tr}-}(t) = \int_0^1 \varepsilon^-(t,\zeta)\,\mathrm{d}\zeta. \tag{5.137}$$

Since tensile and compressive martensite can coexist and interact, definition (5.133) is useful but lack physical meaning in some possible thermodynamic states. However, more precise determination of martensite volume fraction could be obtained in parallel algorithm, which determines "true" driving forces

$$\varphi^+_{\mathrm{true}}(t) = \frac{\sigma(t)}{s^+} - T(t)$$

$$\varphi^{-}_{\text{true}}(t) = \frac{\sigma(t)}{s^{-}} - T(t)$$

and computes martensite volume fractions $\xi^{+}_{\text{true}}(t)$ and $\xi^{-}_{\text{true}}(t)$ due to equations (5.23a) and (5.23b) with $\varphi(t)$ replaced by $\varphi^{+}_{\text{true}}(t)$ and $\varphi^{+}_{\text{true}}(t)$, respectively.

The "true" martensite volume fraction representing the real volume fraction of martensite present in the system may be then determined as:

$$\xi_{\text{true}}(t) := \max\{\xi^{+}(t), \xi^{-}(t)\}. \tag{5.138}$$

### 5.4.3 Numerical Implementation and Comparison with Experimental Results

Since the complexity of considered processes requires deeper physical analysis, the proposed model must be considered as a first attempt to fulfil requirements set in section 5.1. Also mathematical formulation and numerical analysis are to be further developed.

# Chapter 6

# Conclusions

Let us summarize this thesis.

- The reversible martensitic phase transition was introduced, shape memory effects were extensively described and some specific properties of NiTiNOL were mentioned.
- The basics of extended non-equilibrium thermodynamics were outlined. The second law of thermodynamics was employed to obtain non-equilibrium entropy of mixtures, which was then applied to find the constitutive relation for homogenous isotropic thermo-visco-elastic material of Hookean type. Also, Clausius-Clapeyron equation for a solid-to-solid martensitic phase transition was derived.
- Shape memory effects modelling approaches were summarized and some one-dimensional SMEs models were discussed with respect to the general thermodynamic framework.
- A new phenomenological model was introduced. The model, developed at the AS CR and called iRLOOP, was mathematically formalized, each stage of development was described in detail. The pseudoplasticity model is capable to simulate superelasticity, R-phase transition, cyclic isothermal loading with incomplete martensitic phase transition, return point memory effect, pseudoplasticity, reorientation process and thus also one-way SME, all in the case of tensional loading of a NiTiNOL wire.
- The Duhem-Madelung model of hysteresis was extended with respect to the return point memory effect and restrictions on functions forming the hysteresis major loop (fitting functions of the model) were derived from the second law of thermodynamics.
- Employing Picard-Lindelöf theorem the existence and uniqueness of the solution of an initial problem were proven in the case of superelasticity model.

- A possible fitting procedure for material parameters were described and experimental results were compared with results of pseudoplasticity model implemented to MATLAB programming language.
- A possible way how to involve the majority of shape memory effects and their interactions in a complex thermomechanical tension-compression model was sketched (plasticity, training and ageing not covered).

# Bibliography


[1] Roytburd, A. L.: *Kurdjumov and His School in Martensite of the 20th Century*, Mat. Sci. Eng. A **273–275** (1999), 1–10.

[2] Bekker, A., Brinson, L. C.: *Temperature-Induced Phase Transformation in a Shape Memory Alloy: phase diagram based kinetics approach*, J. Mech. Phys. Solids **45** (1997), 949–988.

[3] Porter, D. A., Easterling, K. E.: *Phase Transformations in Metals and Alloys*, CRC Press, Cheltenham, 2001.

[4] Enkovaara, J., Ayuela, A., Zayak, A. T., Entel, P., Nordström, L., Dube, M., Jalkanen, J., Impola, J., Nieminen, R., M.: *Magnetically Driven Shape Memory Alloys*, Mat. Sci. Eng. A **378** (2004), 52–60.

[5] Ford, D. S., White, S. R.: *Thermomechanical Behavior of 55Ni45Ti NITINOL*, Acta Mater. **44** (1996), 2295–2307.

[6] Ortín, J.: *Preisach Modeling of Hysteresis for Pseudoelastic Cu-Zn-Al Single Crystal*, J. Appl. Phys. **71** (1992), 1454–1461.

[7] Šittner, P., Takakura, M., Tokuda, M.: *Shape Memory Effects Under Combined Forces*, Mat. Sci. Eng. A **234–236** (1997), 216–219.

[8] Šittner, P., Vokoun, D., Dayananda, G. N., Stalmans, R.: *Recovery Stress Generation in Shape Memory $Ti_{50}Ni_{45}Cu_5$ Thin Wires*, Mat Sci Eng A **286** (2000), 298-–311.

[9] Šittner, P., Sedlák, P.,Landa, M., Novák, V., Lukáš, P.: *In Situ Experimental Evidence on R-phase Related Deformation Processes in Activated NiTi Wires*, Mat. Sci. Eng. A **438–440** (2006), 579–584.

[10] Maršík, F.: *Termodynamika kontinua*, Academia, Praha 1999.

[11] Maršík, F., Dvořák, I.: *Biotermodynamika*, Academia, Praha 1998.

[12] Jou, D., Casas-Vazques, J., Lebon, G.: *Extended Irreversible Thermodynamics*, Springer-Verlag, Berlin 1996.

[13] Ortín, J., Delaey, L.: *Hysteresis in Shape-Memory Alloys*, Int. J. Nonlinear Mech. **37** (2002), 1275–1281.

[14] Sethna, J. P., Dahmen, K., Kartha, S., Krumhansl, J. A., Roberts, B. W., Shore, J. D.: *Hysteresis and Hierarchies: Dynamics of Disorder-Driven First-Order Phase Transformations*, Phys. Rev. Lett. **70** (1993), 3347–3350.

[15] Roubíček, T.: *Models of Microstructure Evolution in Shape Memory Alloys.* In: Casteneda P. P., Telega, J., Gambin, B. (Eds.): *Nonlinear Homogenization and its Application*, NATO Science Series II: Mathematics, Physics and Chemistry **170** (2004), 269–304.

[16] Bo, Z., Lagoudas, D., C.: *Thermomechanical modeling of polycrystalline SMAs under cyclic loading, Part I: theoretical derivations*, Int. J. Eng. Sci. **37** (1999), 1089–1140.

[17] Bo, Z., Lagoudas, D. C.: *Thermomechanical modeling of polycrystalline SMAs under cyclic loading, Part II: material characterization and experimental results for a stable transformation cycle*, Int. J. Eng. Sci. **37** (1999), 1141–1173.

[18] Bo, Z., Lagoudas, D., C.: *Thermomechanical modeling of polycrystalline SMAs under cyclic loading, Part III: evolution of plastic strains and two-way shape memory effect*, Int. J. Eng. Sci. **37** (1999), 1175–1203.

[19] Bo, Z., Lagoudas, D., C.: *Thermomechanical modeling of polycrystalline SMAs under cyclic loading, Part IV: modeling of minor hysteresis loops*, Int. J. Eng. Sci. **37** (1999), 1205–1249.

[20] Lagoudas, D. C., Entchev, P. B., Popov, P., Patoor, E., Brinson, L. C., Gao, X.: *Shape Memory Alloys, Part II: Modeling of Polycrystals*, Mechanics of Materials **38** (2006), 430–462.

[21] Qidwai M. A., Lagoudas, D. C.: *On Thermomechanics and Transformation Surfaces of Polycrystalline NiTi Shape Memory Alloy Material*, Int. J. Plasticity **16** (2000), 1309–1343.

[22] Buravalla, R. V., Khandelwal, A.: *Differential and Integrated Form Consistency in 1-D Phenomenological Models for Shape Memory Alloy Constitutive Behavior*, Int J Solids Struct **44** (2007), 4369-–4381.

[23] Ivshin, Y., Pence, T. J.: *A Constitutive Model for Hysteretic Phase Transition Behavior*, Int. Eng. Sci. **32** (1994), 681–704.

[24] Bouvet, Ch., Calloch, S., Lexcellent, Ch.: *A Phenomenological Model for Pseudoelasticity of Shape Memory Alloys Under Multiaxial Proportional and Nonproportional Loading*, Eur. J. Mech. A-Solid **23** (2004), 37–61.

[25] Tanaka, K.: *A Thermomechanical Sketch of Shape Memory Effect: One Dimensional Tensile Behavior*, Res. Mech. **18**, 251–263.

[26] Tanaka, K., Nishimura, F., Hayashi, T., Tobushi, H., Lexcellent, C.: *Phenomenological Analysis on Subloops and Cyclic Behavior in Shape Memory Alloys Under Mechanical and/or Thermal Loads*, Mech. Mater. **19** (1995), 281–292.

[27] Tanaka, K., Hayashi, T., Itoh, Y., Tobushi, H.: *Analysis of Thermomechanical Behavior of Shape Memory Alloys*, Mech. Mater. **13** (1992), 207–215.

[28] Liang, C., Rogers, C. A.: *One-dimensional Thermomechanical Constitutive Relations for Shape Memory Materials*, J. Intel. Mat. Syst. Str. **l** (1990), 207–234.

[29] Brinson, L. C.: *One Dimensional Constitutive Behavior of Shape Memory Alloys: Thermomechanical Derivation with Non-Constant Material Functions*, J. Intel. Mat. Syst. Str. **4**, 229–242.

[30] Bekker, A., Brinson, L. C.: *Phase Diagram Based Description of The Hysteresis Behavior of Shape Memory Alloys*, Acta Mater. **46** (1998), 3649–3665.

[31] Govindjee, S., Kasper, E. P.: *Computational Aspects of One-Dimensional Shape Memory Alloy Modeling with Phase Diagrams*, Comput. Methods Appl. Mech. Engrg. **171** (1999), 309–326.

[32] Auricchio, F.: *Shape Memory Alloys: Applications, Micromechanics, Macromodelling and Numerical Simulations*, PhD. Thesis, University of California at Berkley, Berkley, 1995.

[33] Auricchio, F., Sacco, E.: *A Temperature-Dependent Beam for Shape-Memory Alloys: Constitutive Modelling, Finite-Element Implementation and Numerical Simulations*, Comput. Methods Appl. Mech. Engrg. **174** (1999), 171–190.

[34] Auricchio, F., Sacco, E.: *A One-Dimensional Model for Superelastic Shape-Memory Alloys with Different Elastic Properties Between Austenite and Martensite*, Int. J. Non-Linear Mechanics. **32** (1997), 1101–1114.

[35] Sadjadpour, A.: *A Micromechanics-Inspired Three-Dimensional Constitutive Model for the Thermomechanical Response of Shape-Memory Alloys*, PhD. Thesis, California Institute of Technology, Pasadena, 2006.

[36] Šittner, P., Stalmans, R., Tokuda, M.: *An Algorithm for Prediction of the Hysteretic Responses of Shape Memory Alloys*, Smart Mater. Struct. **9** (2000), 452-465.

[37] Šittner, P., Michaud, V., Schrooten, J.: *Modelling and Material Design of SMA-Polymer Composites*, Mater. T. JIM, **43** (2002), Special Issue on Smart Materials-Fundamentals and Applications (2002), The Japan Institute of Metals, 984–993.